Study of Hydrodynamic and Mixing Behaviour of Continuous Stirred Tank Reactor Using CFD Tools

Thesis submitted in partial fulfillment
of the requirement for the degree of

Master of Technology (Research)

in

Chemical Engineering

by

Divya Rajavathsavai
(Roll No – 609CH306)

Under the guidance of

Prof. (Dr.) Basudeb Munshi

Department of Chemical Engineering
National Institute of Technology
Rourkela, Odisha – 769008
January 2012

NATIONAL INSTITUTE OF TECHNOLOGY, ROURKELA

(ORISSA), INDIA

CERTIFICATE

This is to certify that the dissertation report entitled**, "Study of Hydrodynamic and Mixing Behaviour of Continuous Stirred Tank Reactor Using CFD Tools"** is submitted by Divya Rajavathsavai, Roll No. 609CH306 for Dissertation (CH 692) course. It is required in partial fulfillment for the award of M. Tech. (Research) Degree in Chemical Engineering. The matter embodies original work done by her under my supervision.

Signature in full of the Supervisor _____

Name in capital block letters **Prof. BASUDEB MUNSHI**

Designation Assistant Professor

Department of Chemical Engineering

National Institute of Technology, Rourkela

Date:

Acknowledgments

I would like to acknowledge how much I have learned from the guidance of Prof. B. Munshi in my project. I continually benefitted from the technical discussions I had with Prof. B. Munshi, which were an invaluable addition to my knowledgebase. I am really indebted to him for sharing his wealth of knowledge with me. He was always available despite his busy schedule for clarification of my doubts, even the smallest ones. His encouragement and efforts enabled the successful completion of my project.

I also owe a debt of thanks to all the staff and faculty members of Chemical Engineering Department, National Institute of Technology, Rourkela for their constant encouragement.

I am also thankful for all the support that I had received from Mr. Akhilesh khapre. I also would like to thank all my friends who encouraged me in every aspect during the project.

Finally, I am forever indebted to my parents for their understanding, endless patience and encouragement from the beginning.

Divya Rajavathsavai

Roll No. 609CH306

Abstract

The effect of fluid flow and impeller characteristics on the mixing and hydrodynamic behaviour of a continuous stirred tank reactor (CSTR) has been studied using computational fluid dynamics software, Ansys Fluent 12.0. Various mathematical models like equation of continuity, momentum, volume of fluid method, laminar and the turbulent equations have been used to describe the flow behaviour in the reactor. The hydrodynamic behaviour was understood by velocity and pressure profiles and also by the vorticity plots. There are different ways to understand mixing phenomena in the reactor. In the present work, residence time distribution (RTD) method was used to observe the fluid flow in the reactor with and without stirrer and baffles. RTDs are evaluated by the swept volume of the impeller and also by tracer injection method where concentration of tracer (KCl) was determined at the exit of the reactor. The computed values of KCl concentration at the outlet were used to find out the age distribution function $I(\theta)$. The laminar flow and MRF model were used to solve the moving stirrer case. The present RTD data were compared with the available experimental values in the open literature. The simulated results were found in good agreement with the experimental data. Along with RTD, the mixing characteristics were also studied in terms of number of ideal CSTR in series, $N_{cstr,}$ hold back, segregation, mean residence time, τ_m and variance, σ^2. The effect of RPM of the impeller, tank Reynolds number, viscosity and density of the liquid on the mixing efficiency was found. The mixing behaviour was changed from dispersion to ideal mixing state with the increase of impeller rpm and tank Reynolds Number. The hydrodynamic behaviour of CSTR with water-air interface were also studied in presence of different kinds of impellers, baffles etc. The volume of fluid method was used to capture air-water interface. The realizable $k-\varepsilon$ turbulence model has been adopted to describe the flow behaviour of each phase, where water and air are treated as different continua, interpenetrating and interacting with each other everywhere in the computational domain. The results show that the air-water interface was disturbed by the inflow to the tank, and level of water was also increased with time.

Key Words: Mixing, Swept Volume, CFD, Dispersion, Ideal flow, Reynolds Number, CSTR

Contents

List of Figures

List of Tables

NOMENCLATURE:

a	Length of the impeller blade, mm/m
A	Cross sectional area, m^2/mm^2
b	height of the impeller blade, mm/m
b_w	baffle width, mm/m
C_0^+	Concentration of a tracer fed into a reactor after a step-wise change, mole/l
C_0^-	Initial concentration of a tracer in a reactor, mole/l
$C(t)$	Concentration of a tracer at an outlet from a reactor at the moment t, mole/l
D	Tank diameter, mm/m
d	Inlet tube diameter, mm/m
d_m	Impeller diameter, mm/m
H	Height of liquid tank, mm/m
N	Impeller speed, rotation per min/sec
Q	Impeller pumping capacity, cm^3/min
Re	Tank Reynolds number
Re_m	Impeller reynolds number
Re_{in}	Inlet Reynolds number
t	Time, min/sec
u	Velocity, m/sec
V	Tank volume, l/m^3
V^*	Volumetric flow rate, $(l/hr)/(m^3/sec)$
Greek Symbols	
τ	Time constant
μ	Viscosity, cP
ρ	Density, Kg/m^3
θ	Dimensionless time
σ	Variance of a residence time distribution

Chapter 1

INTRODUCTION

A Chemical reaction is a process that results in the conversion of chemical substances. Chemical reactions may be of different nature depending on the type of reactants, type of product desired, conditions and time of the reaction, for example, synthesis, decomposition, displacement, precipitation, isomerization, acid-base, redox or organic reactions.

Chemical reactors are vessels designed to contain chemical reactions. It is the site of conversion of raw materials into products and is also called the heart of a chemical process. Many of the materials that are used for clothing, housing, automobiles, appliances, construction, electronics, and healthcare come form processes that utilize reactors. Reactors are important even in the food and beverage industries, where farm products are processed. The production of ammonia, pesticides and herbicides we use on crop fields and orchards aid in the advances of modern agriculture. The drugs in the pharmaceutical industries are produced in the reactor. Thus, our modern society, for better or worse, makes extensive use of chemicals. Since it is a very vital step in the overall design of a process, designers ensure that the reaction proceeds with the highest efficiency towards the desired output, producing the highest yield of product in the most cost effective way.

1.1 CLASSIFICATION OF REACTORS

Reactors are classified based on features like mode of operation or types of phases present or the geometry of reactors. They are thus called (Levenspiel, 1999):

• Batch or Continuous depending on the mode of operation.

• Homogeneous or Heterogeneous depending upon the phases present.

They may also be classified as:

• Continuous Stirred Tank Reactor (CSTR), or

• Tubular or Plug Flow Reactor, or

• Packed Bed Reactor, or

• Fluidized Bed Reactor,

depending upon the flow pattern and manner in which the phases make contact with each other.

A batch reactor has neither inflow nor outflow of reactants or products while the reaction is being carried out. The resulting general mole balance on species *j* is $\frac{dN_j}{dt} = \int^{V} r_j dV$, where r_j is the volumetric rate of reaction of j^{th} component.

CSTR consists of a vessel with an agitator for mixing, a jacketed that surrounds the vessel for heating or cooling, feed lines entering the vessel and a liquid product stream exiting from the bottom. The liquid in the reactor is assumed to be perfectly mixed, that is with non radial, axial, or angular gradients in properties (temperature and compositions. The product stream has the same temperature and compositions as the contents of the liquid in the vessel.

This characteristic of a CSTR immediately generates an inherent weakness of the CSTR type of reactor, which is the concentration of reactant is inversely related to conversion. The fractional conversion χ defined as $\chi = \frac{C_{A0} - C_A}{C_{A0}}$. The general mole balance equation for j^{th} component for the CSTR is $F_{j0} - F_j + \int^{V} r_j dV = \frac{dN_j}{dt}$; where F_{j0} and F_j are the inlet and outlet molar flow rates, r_j is the volumetric rate of reaction of jth reactant, V is the volume of the reactor, N_j is the number of moles inside the reactor at any moment, t. If there is no spatial variation of r_j, the steady state design equation of CSTR becomes $V = \frac{F_{j0} - F_j}{-r_j}$

The tubular reactor used in industry consists of a cylindrical pipe and is normally operated at steady state. There is no radial variation in concentration and the reactor is referred to as the plug-flow reactor (PFR). The general mole balance equation is $F_{j0} - F_j + \int^{V} r_j dV = \frac{dN_j}{dt}$.

1.2 IDEAL AND NON-IDEAL REACTORS, AND USE OF RTD

The CSTR and plug flow reactors can behave as ideal reactors. In ideal CSTR, the content inside the reactor is well mixed i.e. at any moment the concentration of any reactant everywhere inside the reactor is same and the concentration at the exit stream is equal to that of the fluid inside the reactor. In ideal PFR, there is no overtaking and no back mixing. But in reality, no reactors are ideal. The main reasons of the non-ideal behaviour are (i) residence time distribution (RTD), (ii) state of aggregation and (iii) earliness or lateness of mixing (Fogler, 1999). In ideal reactors it is assumed that all the reactants have the same residence

time equal to space time. It is possible when all molecules move with same velocity. In real reactors some molecule may move faster compared to the other, and it results in RTD. The presence of channeling may result in RTD. In ideal reactors all molecules are considered in micro level size and they all are free to move. In reality, group of molecules may combine together or getting aggregated produce macro molecules, which movement is slower that micro molecules. Thus, state of aggregation causes non ideal behaviour. In real reactors molecules might go for early stage or late stage of mixing unlike ideal reactors where molecules are uniformly mixed. The tracer can be injected into the reactor by pulse and step input. In the pulse input, a known amount of tracer is injected for very small duration. Whereas in step input, a known concentration of tracer is start to inject at time, t = 0 and then kept at the same level continuously. The concentration at the exit of the reactor is measured with time. A tracer should be easy to analyze, stable and inactive.

1.3 HARDWIRES OF CSTR

The CSTR is the most commonly used chemical reactor. This is due to its considerable flexibility as regards the flow conditions. The tank diameter is generally restricted to $D \leq 4.6\,\mathrm{m}$. A further increase in liquid volume is therefore only possible by an enlargement of the vessel height, *H*. This results in disadvantages like the requirement of larger sized stirrer and increase in residence time. For most operation the favorable H/D aspect ration is ≈ 1. The internal fittings of the CSTR include: stirrer, baffles, coils, probes (e.g. thermometer, level indicators) and feed and drain pipes. All of these fittings can influence the stirring process (Zlokarnik, 2001).

In the case of rapidly rotating stirrers and low viscosity liquids, the vortex can reach the stirrer head with the result that the stirrer entrains the gas in the liquid. This often leads to the destruction of the stirrer. Even when the vortex formation causes no gas entrainment, rotation of the liquid is always undesirable if a two-phase system with different densities is concerned, since the centrifugal force counteracts the stirring process.

The rotation of liquid in cylindrical tanks is prevented by the installation of baffles. So-called "complete baffling" is realized with four baffles (flow interrupting strips) *D/10* in width, where *D* is the inner diameter of the vessel, arranged along the entire vessel wall. Dead zones in the flow direction behind the baffles can be avoided by using baffles *D/12* in width, set at a clearance of *D/50* from the vessel wall. Baffles are usually attached to the vessel wall by means of welded brackets (Fig. 1.1a). Baffles are not necessary, if stirring is carried out in a

container with rectangular cross-section (e.g. basins or pits) or when the stirrer is mounted laterally in the tank wall.

There are many types of stirrers appropriate for particular stirring operations and particular material systems (Zlokarnik, 2001).

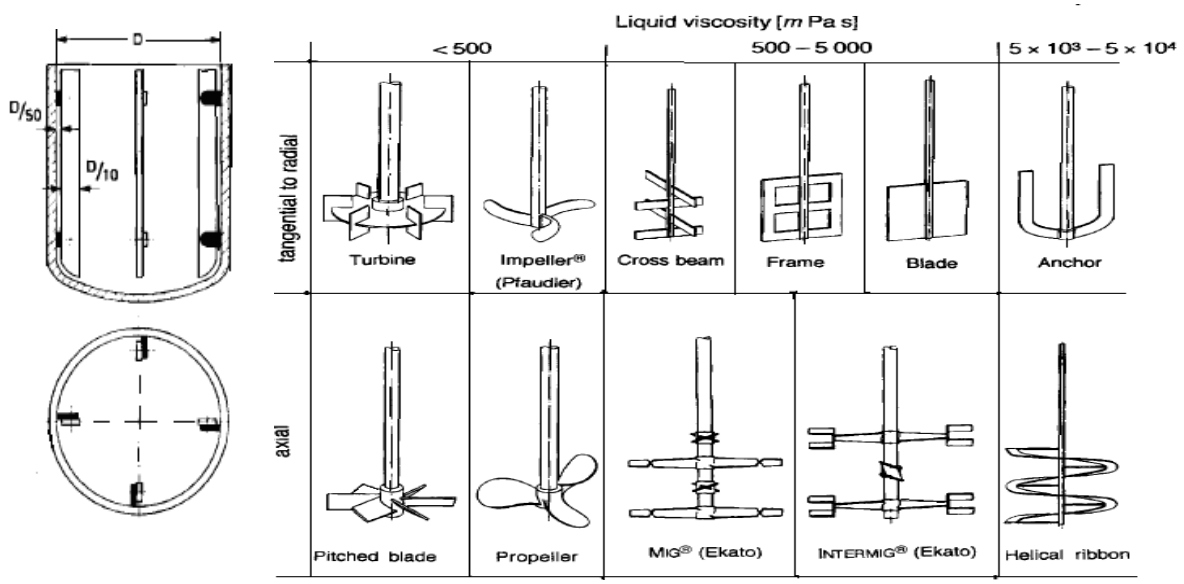

(a) (b)

Figure 1.1: (a) Standard Baffle design (b) different types of stirrer.

In Fig. 1.1b the different types of stirrer are arranged according to the predominant flow pattern they produce, as well as to the range of viscosities over which they can be effectively used. 90% of all stirring operations can be carried out with these standard stirrer types.

Of the stirrer types which set the liquid in a radial motion or into a tangential flow in the case of high viscosities - only the turbine stirrer belongs to the high speed stirrers. It can be sensibly utilized only with low viscosity liquids and in baffled tanks. Its diameter ratio D/d is 3-5**.** Where d is the diameter impeller blade**.** The turbine stirrer causes high levels of shear and hence is well suited for dispersion processes.

The Pfaudler impeller stirrer was developed for use in enamel-coated vessels and thus has rounded stirring arms. It is installed with small bottom clearance at a *D/d* ratio of 1.5 and can be used both with and without baffles.

Cross-beam, grid and blade stirrers are slow-speed stirrers and are used at *D/d* = 1.5 to 2 both with and (in the case of viscous liquids) without baffles. They are particularly suitable for homogenization.

The slow-speed anchor stirrer is generally utilized with close wall clearance ($D/d \leq 1.05$) to intensify heat transfer in high viscosity liquids.

Pitched-blade turbines, and in particular propeller stirrers, belong to the group of high-speed stirrers, which accelerate the liquid in the axial direction. Both stirrer types are generally utilized with low viscosity liquids and baffled tanks. They are suitable for homogenization and suspension of solids. Multiple-stage pitched-blade stirrers are required to enhance the axial flow in vessels of $H/D > 1$ (e.g. in fermenters), especially in viscous media. Examples of such stirrers are cross-beam stirrers with pitched beams, the MIG and INTERMIG stirrers from EKATO, Schopfheim. They are operated at low speeds at *D/d* = 1.5 with baffles and at *D/d* = 1.1 without baffles and are used for homogenization, suspension of solids, and dispersion.

The very slow-speed helical ribbon stirrer is a close-clearance stirrer ($D/d \approx 1.05$) and is so operated that the liquid on the wall is transported downwards. Under these conditions this stirrer is the most suitable of all the stirrer types for homogenizing high viscosity liquids.

Apart from stirrer, different types of nozzles, spargers and baffles are used for mixing purposes. Single fluid nozzles are generally used as atomizer nozzles, in which the kinetic energy of the liquid propulsion jet is utilized for dispersion of its own. Spargers are utilized for distributing gas throughput in bubble columns and to a large extent in aerobical waste water treatment plants (so-called activated sludge ponds).

1.4 OBJECTIVES OF THE PRESENT WORK

As is evident from the diversity of application areas, the study of hydrodynamic behaviour of CSTR is very important for proper designing of the reactor even in presence of reaction. Often the behaviour of the reactor is found non-ideal and it has profound effect on the conversion of reactants to products. The non-ideal behaviour can be depicted well by RTD analysis. Following the experimental investigation of Burghardt and Lipowska (1972) and Lipowska (1974), this work studies the CFD simulation of CSTR. CSTR is also simulated with water exposed to air to understand the effect of air-water interface on the hydrodynamic behaviour of the CSTR.

The present work is undertaken to study the following aspects of

- Computational Fluid Dynamics modeling and simulation of CSTR to understand its non-ideal hydrodynamic behaviour in terms of residence time distribution (RTD).
- Validation of the CFD models by comparing the present simulated RTD results with the data available in the open literature.
- Study of hydrodynamic behaviour of CSTR with liquid water exposed to atmosphere

1.5 OUTLINE OF THE REPORT

Chapter 1 represents complete introduction of project work including definition of different types of reactors, concept of ideal and non-ideal reactors, concept of RTD, components of hardwires in CSTR etc. Also the objective of the project work is defined there.

Chapter 2 is devoted on the extensive literature survey on topic namely experimental and theoretical development of the RTD. In the theoretical survey, more emphasis is given on computational fluid dynamics (CFD) analyses of it.

Chapter 3 represents modelling equation of single phase and multiphase flow in CSTR. The model equation includes the equation of continuity and momentum equation for laminar as well as for turbulent flow.

Chapter 4 represents the computation study of CSTR to understand its mixing behaviour in terms of RTD. ANSYS Fluent software is used as the computational tool. The RTD is evaluated by finding impeller swept volume. The internal age distribution functions are compared with the experimental results available in the open literature. Further the effect of different operating parameters on the mixing efficiency also is studied.

Chapter 5 also has demonstrated the computational study of CSTR with the help of ANSYS Fluent. The RTD of the CSTR is studied by tracer injection method. The computed RTD functions are compared the available published experimental results. The effect of different operating parameters of the CSTR on the mixing behaviour also is studied in this chapter.

Chapter 6 mainly concentrates on the study of vortex formation of a CSTR operated in open atmosphere. The effect of types of impellers, rotation of impellers, presence of baffles and clearance of impellers on the vortex height is studied in this chapter. The computed values of the vortex height by ANSYS Fluent are compared with the theoretical value.

Chapter 7 deals with overall conclusion and future recommendations.

Chapter 2

LITERATURE REVIEW

The choice of the right chemical transformation, the right catalyst for it, and the right reactor type are the key for economically, environmentally friendly and energy efficient processes. The backbone of chemical reaction engineering is the ability to quantify kinetic transport interactions on a variety of scales and utilize them in assessing the effect of reactor performance on the whole process. The choice of the proper reactor type and operating conditions for a given process chemistry determine productivity and selectivity. While the reactor typically represents between 5% and 15% of capital and operating costs of the plant, it is well understood that the reactor choice determines the number and load on pre-reactor and post-reactor separation units and dictates the cost of the whole process. Therefore, the choice of the proper reactor type is essential and it should be based on a rational multi-scale approach (Dudukovic, 2010). This requires a reactor model which can capture the events on a multitude of scales at the right level as shown in Fig 2.1.

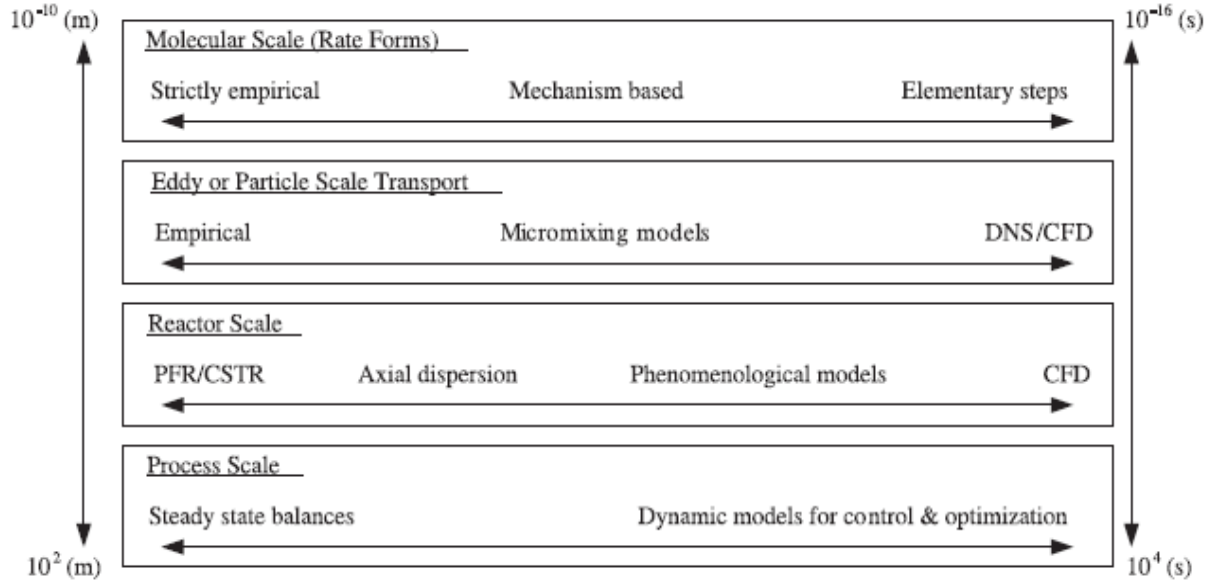

Figure 2.1: Schematic of the multi-scale reaction engineering methodology (Dudukovic, 2010).

The literature survey is carried out according to the work done in the present work. Here emphasis is directed on

- Background of ideal and non-ideal reactors
- RTD analysis of reactor
- Application of computational fluid dynamics (CFD) tools for designing reactors

2.1 BACKGROUND OF IDEAL AND NON-IDEAL REACTORS

Ideal reactors have three ideal flow or contacting patterns as shown in Fig. 2.2. Reactor designers often try to make real reactors approach these ideals as closely as possible.

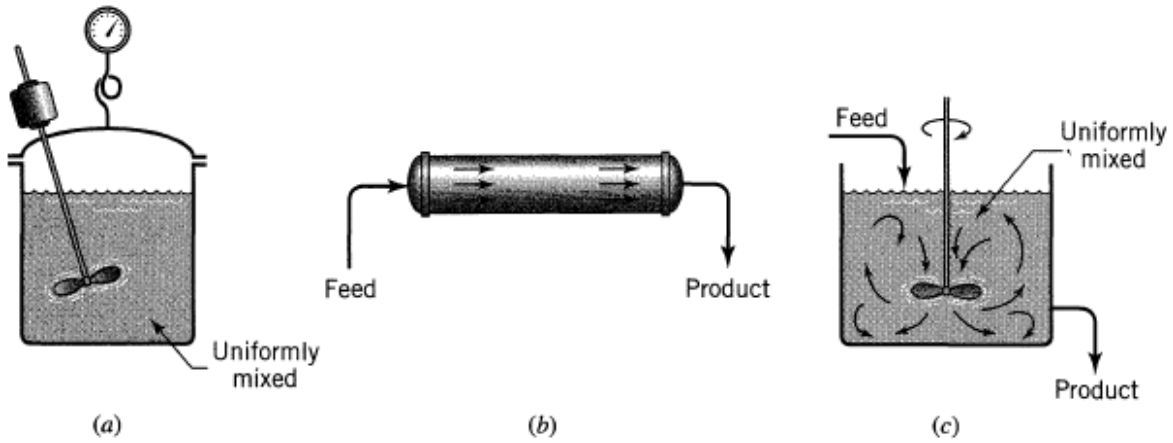

Figure 2.2: The three types of ideal reactors: (a) batch reactor, (b) plug flow reactor, and (c) mixed flow reactor (Levenspiel, 1999)

In the ideal batch reactor, of Fig. 2.2a the reactants are initially charged into a container, are well mixed, and are left to react for a certain period. The resultant mixture is then discharged. This is an unsteady-state operation where composition changes with time; however, at any instant the composition throughout the reactor is uniform.

The first of the two ideal steady-state flow reactors as shown in Fig. 2.2b is known as the plug flow, slug flow, piston flow, ideal tubular, and unmixed flow reactor Actually, there may be lateral mixing of fluid in a plug flow reactor; however, there must be no mixing or diffusion along the flow path. The necessary and sufficient condition for plug flow is for the residence time in the reactor to be the same for all elements of fluid.

The other ideal steady-state flow reactor shown in Fig. 2.2c is called the mixed reactor, the backmix reactor, the ideal continuous stirred tank reactor (CSTR), and, as its names suggest, it is a reactor in which the contents are well stirred and uniform throughout. Thus, the exit stream from this reactor has the same composition as the fluid within the reactor.

Most of the chemical reactors in the industries are non-ideal. The flow patterns in real reactors shown in Fig 2.3 do not conform exactly to those postulated for ideal plug flow and continuous stirred tank reactors. The figure clears that the deviation from the ideal flow

patterns can be caused by channeling of fluid, by recycling of fluid, or by creation of stagnant regions in the vessel. On the other hand, the conversions achieved in many real reactors so closely approximate those predicted on the basis of the idealized models that the design equations for these reactors can be used with negligible error. In other cases significant differences are noted between observed and predicted results. These differences may arise from a number of sources—from channeling of fluid as it moves through the reaction vessel, from longitudinal mixing caused by vortices and turbulence, from the presence of stagnant regions within the reactor, from bypassing or short-circuiting of portions of a packed reactor bed, from the failure of impellers or other mixing devices to provide perfect mixing, etc.

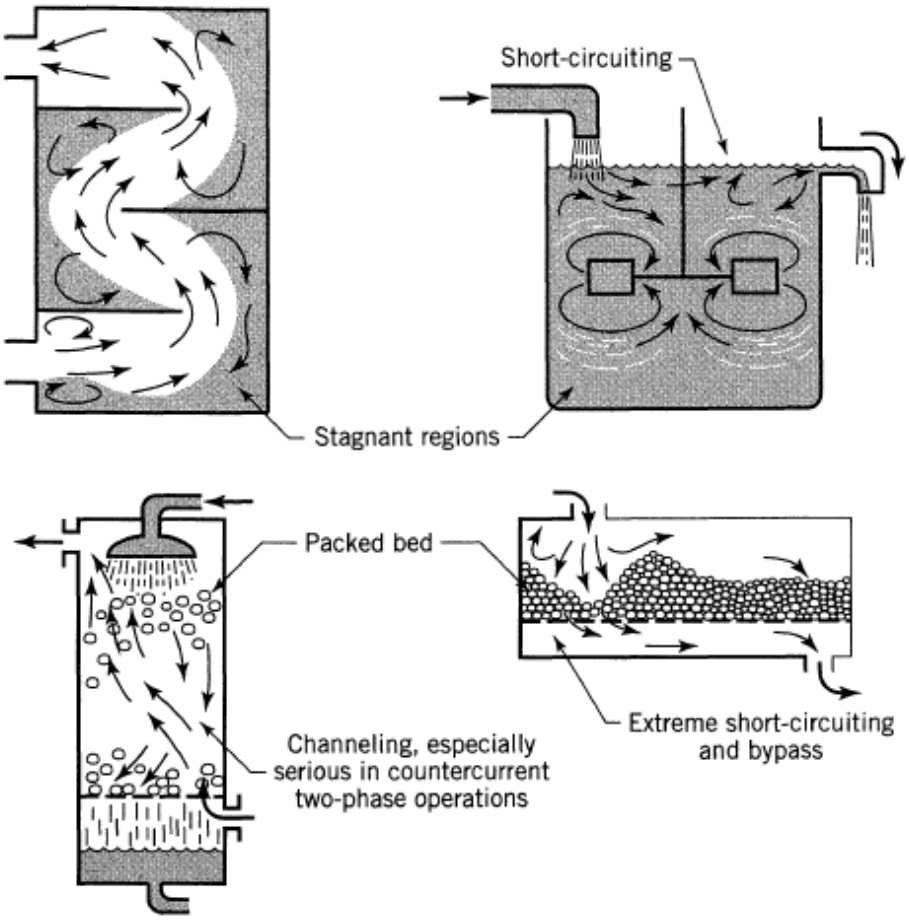

Figure 2.3: Nonideal flow patterns which may exist in process equipment (Levenspiel, 1999)

Overall the flow patterns inside the reactors are controlled by:

(i) the RTD or residence time distribution of material which is flowing through the vessel

(ii) the state of aggregation of the flowing material, its tendency to clump and for a group of molecules to move about together

(iii) the earliness and lateness of mixing of material in the vessel

Flowing material is in some particular state of aggregation, depending on its nature. In the extremes these states can be called *microfluids* and *macrofluids*, as sketched in Fig. 2.4.

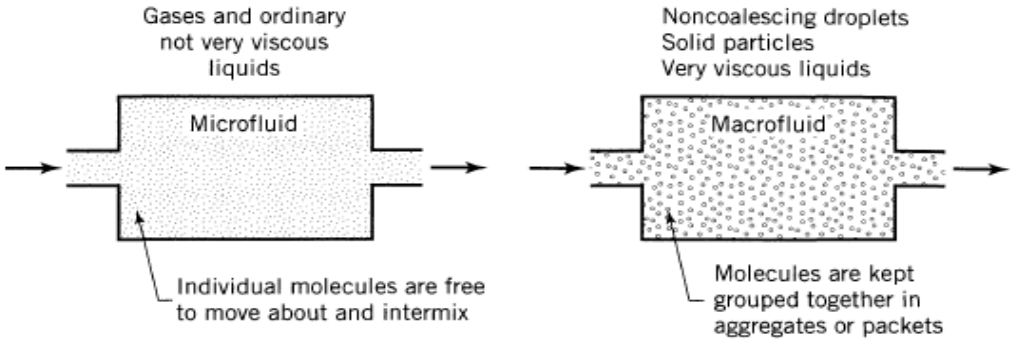

Figure 2.4: Two extremes of aggregation of fluid (Levenspiel, 1999)

The fluid elements of a single flowing stream can mix with each other either early or late in their flow through the vessel. Fig. 2.5 depicts it. Usually this factor has little effect on overall behavior for a single flowing fluid. However, for a system with two entering reactant streams it can be very important.

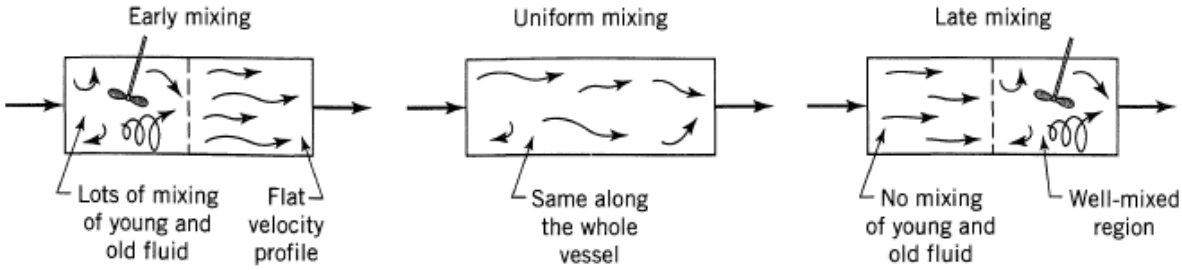

Figure 2.5: Examples of early and of late mixing of fluid (Levenspiel, 1999)

2.2 RTD ANALYSIS OF REACTOR

The residence time distribution (RTD) of a reactor is characteristics of the mixing that occurs in the chemical reactor. The RTD gives information on how long the various elements have been in the reactor, but it does not provide any information about the exchange of matter between the fluid elements. As it provides a quantitative measure of the degree of backmixing within a system, knowledge of the liquid RTD is important for a number of reasons (Fogler, 1999), allowing for accurate kinetic modeling of the system, and facilitating reactor design to achieve or preserve a desired flow pattern. Also, these reasons include the fact that RTD allows for a more thorough comparison between systems with different configurations or different zones of the reactor and represent a tool in successful process scale-up.

Danckwerts, 1953 in his much celebrated paper devised a generalized treatment of RTD and introduced the concept of "hold-back" and "segregation". The analysis of residence time distributions is a classical technique for predicting yields in isothermal, homogeneous reactors; and in some cases, the general concept of a reaction history distribution can be applied to heterogeneous or even non-isothermal reactors (Nauman and Collings, 1968). The yield of a first order reaction is uniquely determined by the residence time distribution. For reactions of order other than first, the yield depends on the state of micro-mixing; but it can often be closely bounded using the concepts of "complete segregation" and "maximum mixedness" (Zwettering, 1959 and Danckwerts, 1958). These studies stressed that an inlet-outlet tracer experiment supplies information about the macroscopic mixing patterns (macro mixing), but is of limited use in understanding the internal mixing process down to a molecular level of detail.

The RTD is determined experimentally by injecting an inert chemical, molecule, or atom, called a tracer, into the reactor at some time $t=0$ and then measuring the tracer concentration, C, in the effluent stream as a function of time. The chosen tracer should be nonreactive, easily detectable, should have same physical properties to reactor liquid, and should be completely soluble in the mixture (Fogler, 1999). The two used methods of injection are pulse input and step input. In a pulse input, a certain amount of tracer is injected into the reactor in very short time duration. For pulse injection the residence time distribution function is defined as

$$E(t)=\frac{C(t)}{\int_0^{\infty} C(t)dt} \qquad 2.1$$

Where $C(t)$ is the tracer concentration at the exit of the reactor, and the integral in the denominator is the area under the C curve.

In case step tracer experiment, the concentration of it changes from 0 to C_0 at time $t=0$, The stimulus response function, $F(t)$ for step input is

$$F(t)=\frac{C_{out}}{C_0} \qquad 2.2$$

The relation between the RTD function $E(t)$ and $F(t)$ is

$$E(t)=\frac{dF(t)}{dt}=\frac{d}{dt}\left[\frac{C(t)}{C_0}\right]_{step} \qquad 2.3$$

The significance of $F(t)$ and C - diagrams are well explained by Danckwerts, 1953 and these are shown in Fig. 2.6 and 2.7 respectively. v is the volumetric flow rate in the feed, V is the total liquid holdups in the reactor, and Q is the amount of tracer injected (not concentration) in the reactor within a very short duration.

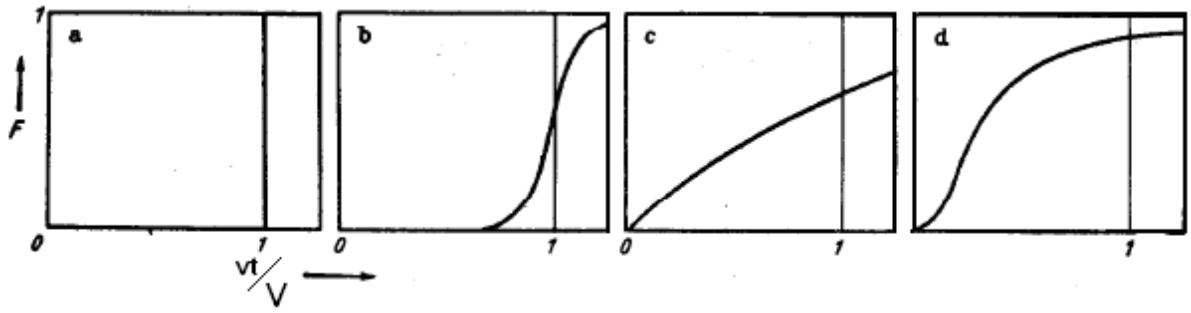

Figure 2.6: F-diagrams, (a) Piston Flow, (b) Piston flow with some longitudinal mixing, (c) Complete mixing, (d) Dead water (Danckwerts, 1953).

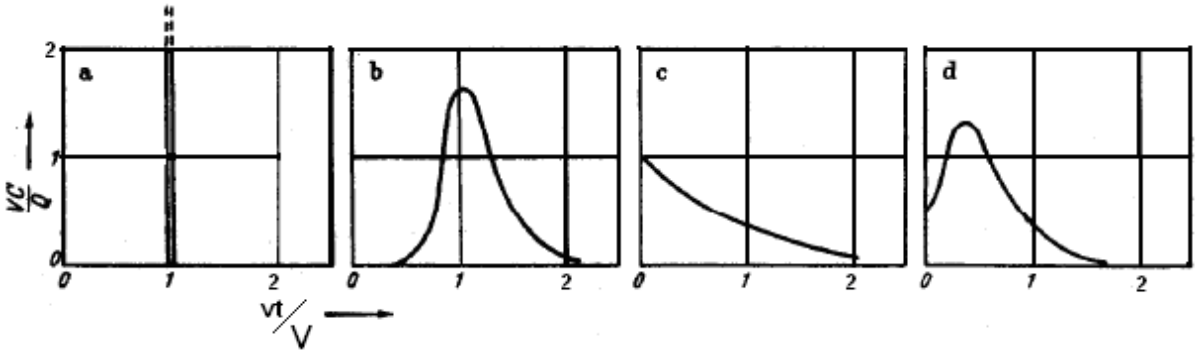

Figure 2.7: C-diagrams, (a) Piston Flow, (b) Piston flow with some longitudinal mixing, (c) Complete mixing, (d) Dead water Danckwerts, (1953).

In the above, the Perfect piston flow Fig. 2.6(a) will never occur with Newtonian fluids; there will always be some longitudinal mixing, due to viscous effects and molecular or eddy-diffusion. Fig. 2.6(b) illustrates the departure from piston flow caused by restricted longitudinal mixing. Fig. 2.6(c) is the diagram for perfect mixing; the equation of the curve is:

$$F(t)=1-e^{-V^{*}t/V} \qquad 2.4$$

Fig. 2.6(d) shows the presence of 'dead water' in the system; a considerable fraction of the fluid is trapped in eddies, and spends much more than the average length of time in the vessel, while most of the flow takes place through a restricted channel (Danckwerts, 1953).

The similar kind of phenomena occurs in case of pulse injection experiment, and it is shown in Fig. 2.7. Danckwerts had defined a term called holdback, which also discussed by Turner,

1982 in his review paper on RTD. It is defined as the average spending time of the fluid inside the reactor compared to the hydraulic residence time, $\tau = V/V^*$. Mathematically, it can be defined as

$$H = \frac{1}{\tau}\int_0^{\tau} F(t)dt \qquad 2.5$$

H varies from 0 for piston–flow to 1 when most of the space in the vessel is dead water. For completely mixed flow (Fig. 2.6 c), substituting Eq. 2.4 in Eq. 2.5 gives $H = 1/e$. The magnitude of H is a measure of the deviation from piston flow. A high hold-back means that much of the volume of the reactor is occupied by material which has already undergone reaction, while much reactant passes rapidly through the vessel by a "short-circuit" route.

The efficiency of mixing in a vessel can be given by a single quantity, S, called "segregation" (Danckwerts, 1953). The superimposition of $F-$diagram for a perfectly mixed system (Eq. 2.4) and for an imperfectly mixed system gives Fig. 2.8.

The size of shaded are ($(A_1 + A_2)$ measures the degree of departure from perfect mixing. But, $A_a = A_2$. Hence, only A_1 measures the degree of it , and mathematically segregation, S is

$$S = \int_0^{\tau} \left(F(t) - F_{impeffect}(t)\right)dt \qquad 2.6$$

When there is dead water in a system, the position of the curve may be inverted shown in Fig 2.9 with segregation, S as negative. S varies from $+1/e$ for piston flow to values approaching -1 when most of space in the system is dead water.

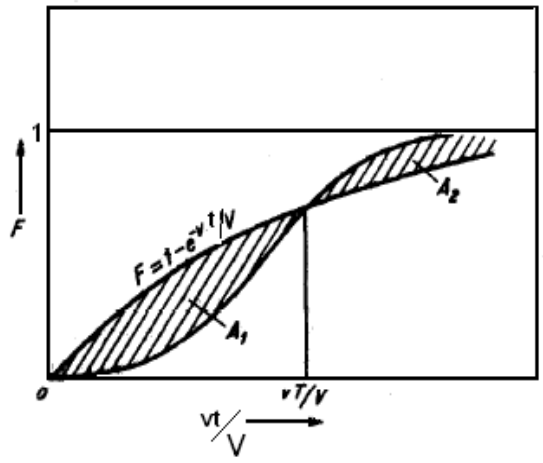

Figure 2.8: Superposition of perfect and imperfect mixing

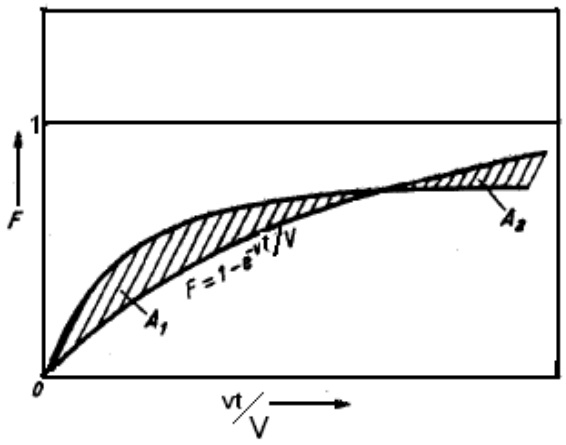

Figure 2.9: Superposition of perfect and imperfect mixing with dead volume

Levenspiel and Turner, 1970 have worked on the effect of the methods of injection and measurementof the tracer on the RTD when the fluid velocity is not uniform through the injection and measurement planes. They have taken laminar flow through a tube or parallel tubes, and non-uniform injecting velocities at the entrance. Two policies of tracer injection at the feed and two different policies of measurement at the exit were adopted.

A pulse of tracer was introduced in one of two ways, either proportional to the flow rate (method A), or evenly across the flowing stream (method B). The concentration of tracer was measured either by the mixing cup technique (method A'), or by a through-the-wall measurement (method B'). It was then shown that only one combination of pulse injection and of measurement, namely method A-A', gave the residence time distribution of fluid in the vessel. All other combinations, A-B', B-A', B-B', gave output tracer curves which do not represent the R.T.D. of fluid in the vessel. Levenspiel et al., 1970 have found the relation among C-curves for all possible four cases.

Longitudinal self-mixing is of interest in the study of fluids in flow. With respect to an analysis of fluid self-mixing the various physical situations may be placed in two broad categories depending on whether there is or whether there is not macroscopic variation in flow conditions at different locations along the flow path. No such variations occur in flow through long pipes and long packed beds which may be characterized as infinite in length. On the other hand significant variations may be expected to occur in flow through tanks, short pipes, fluidized beds, filter cakes as well as through and around obstructions. The work by Levenspiel and Smith, 1957 had discussed the evaluation method of D, "longitudinal dispersion coefficient" experimentally primarily for infinite pipe. They have developed the expression of D/uL (inverse Peclet number) as

$$\sigma^2 = 8\left(\frac{D}{uL}\right)^2 + 2\left(\frac{D}{uL}\right) \tag{2.7}$$

and it gives

$$\frac{D}{uL} = \frac{1}{8}\left(\sqrt{8\sigma^2 + 1} - 1\right) \tag{2.8}$$

If D/uL is small enough so that $(D/uL)^2$ can be neglected, and the D/uL becomes

$$\frac{D}{uL} = \frac{1}{2}\left(\frac{\sigma}{\tau_m}\right)^2 \tag{2.9}$$

Where u is the average velocity, $u = L/\tau$ and σ^2 is variance and expression of it is (Fogler, 1999)

$$\sigma^2 = \int_0^\infty (t - t_m) E(t) dt \qquad 2.10$$

and the mean residence time, τ_m is

$$\tau_m = \int_0^\infty t E(t) dt \qquad 2.11$$

The study has also shown that the maximum value of E or C - curve near to mean residence time, t_m increases with D/uL for very low magnitude of it, and reverse trend is observed for large value of it. It is found that if D/uL is of the order of 0.01 or greater the concentration curve flattens out rapidly, and this causes skewness. If varying flow conditions exist in different parts of the experimental section (like flow in CSTR) , an average D value will result (Levenspiel et al., 1970).

The experimental $C(t)$ curves give information about the mean fluid residence time, the variance of distributions, σ^2, and the RTD distribution functions at the reactor exit, inclusively in normalized form $E(t)$. The $E(t)$ curves show the presence of stagnant zones. When the maximum of $E(t)$ appears at $t < \tau_m$, it indicates the presence of short-circuits; while the maximum of $E(t)$ appears at $t > \tau_m$, it indicates the presence of the back mixing. The width of RTD curve is an appropriate measurement to determine the approach to plug flow (Xiao-chang, 2009).

The responses to a pulse input of tracer gives the RTD curve directly. Comparing the experimental RTD curve with a family of curves for the tanks-in-series model represents the simplest stage-wise model for non-ideal flow. The curve C for N_{cstr} tank-in-series can be expressed by (Fogler, 1999)

$$E(t) = \frac{t^{N_{cstr}-1}}{(N_{cstr}-1)!\,\tau_i^{N_{cstr}}} \exp(-t/\tau_i) \qquad 2.12$$

Because the total volume of the reactor is $N_{cstr} V_i$, then $\tau_i = \tau / N_{cstr}$, where τ represents the total reactor volume divided by the inlet volumetric flow rate. V_i is the volume of the ith reactor.

Levenspiel, 1999 suggested ways of finding the values of N from experimental RTD curves. The variance of curves expressed as

$$N_{cstr} = \frac{\tau_m^2}{\sigma^2} \qquad 2.13$$

The expression of $E(t)$which accounts the macro mixing effect gives the external age distribution. $E(t)$can not predict the molecular interaction happens inside the reactor. Buffham, 1983 has defined internal age distribution for measuring the extent of micro mixing within the reactor. It's expression is

$$I(t) = tE(t)/\tau \qquad 2.14$$

$I(t)dt =$the fraction of molecules inside the system which have an eventual residence time between $t$and $t + dt$(Robinson and Tester, 1986). They have defined cumulative internal RTD expression as

$$\Phi(t) = \int_o^t I(t)dt \qquad 2.15$$

It is used to characterize the nature of interior flow distribution. It accounts fraction of volume of the system used by total left stream ($F(t)$) through the exit at time t. In case of packed bed, it represents void fraction of the bed. They have developed the expression of $\Phi(t)$for fully developed laminar flow through a tube and compared it with the external cumulative RTD, $F(t)$(Danckwerts, 1953),

$$F(t) = \int_o^t E(t)dt \qquad 2.16$$

Robinson and Tester, 1986 also have worked on the performance of a reactor having reaction with diffusion using holdback as the parameter. Peclet number is used as the diffusional parameter. They also have analyzed the available experimental RTD data using cumulative internal RTD function.

Yablonskya 2009 has RTD analysis of PFR and CSTR in presence of reaction. For studying RTD, they have increased the concentration of one reactant at the inlet instead introducing tracer. The changed concentration at the outlet was observed. The reactive mixture index (REMI) was used for this study. The REMI is defined as

$$REMI(x) = \frac{1 - \frac{ET(X)}{ET(0)}}{X} \qquad 2.17$$

Where $ET(X)$ denotes the so-called escape time in terms of the conversion X, i.e., the average exit time of "surviving" molecules, the ones that do not react, when the total conversion is X. The value $ET(0)$ corresponds to the case where no reaction occurs. The value REMI(X) = 1 corresponds to a continuously stirred tank reactor (or CSTR, i.e. perfect

mixing) and REMI(X) = 0 to a plug flow reactor. For a non-ideal PFR (where diffusion can not be neglected), the REMI(X) value will lie between 0 and 1. They also have described the effect of Peclet number on REMI(X) of both types of reactors.

Van de Vusse, 1962 had developed a model CSTR taking the effect of loop flow rate and functions in term of RTD of it. The model assumes a circulating flow, created by the pumping action of the stirrer, and an isotropic homogeneous turbulence in the circulated fluid. Expressions for the conversion of a first-order reaction, the spread in residence times and the distribution function were derived. Correlations are proposed for the circulation rate parameter and the turbulent diffusivity parameter. The mixing process in a stirred batch reactor is evaluated and described as a function of time and location.

Kreft and Zuber, 1978 have done elaborate discussion on the physical meaning of dispersion equations and effect of initial and boundary conditions on its solution and RTD behaviour. They have considered separate concentration variables inside reactor's fluid and in fluid flux. They found solution for different injection and measurement methods are different at low Peclet numbers.

Trivedi and Vasudeva, 1974, have reported the results of an experimental investigation of the RTD in the low Reynolds number, low Dean number region for helical coils. They found that, under the conditions of negligible molecular diffusion and curvature ratio from 0.0036 to 0.0970 coiling results in an essentially unique RTD which is narrower than that for straight tubes. An empirical expression has been developed for taking into account the weak influence of curvature ratio on narrowing the RTD.

Turner, 1982, has pointed out that if molecular diffusion and chemical reaction are significant, the concept of residence-times itself becomes blurred. For different species in the "steady-flow**"** through a given system the observed residence time distribution may be found to depend upon the different diffusion coefficients-one tracer cannot give the answer for all species. Furthermore, if the molecules coming out are different from those going in, as a result of chemical reaction, it is difficult to define a residence time distribution. For example, if a compound has been synthesized, different parts of a given molecule may have spent different times in the system.

Saravanathamizhan et al. 2008 have studied on the residence time distribution of electrolyte in a continuous stirred tank electrochemical reactor covering wide range in the operating conditions. A three-parameter model was proposed to describe the electrolyte flow in the reactor consisting bypass, active and dead zones with exchange flow between active and dead zones. It was observed from the model simulations that the residence time distribution has

been increased with increase in the exchange flow ratio between active and dead zones and increase in the electrolyte flow rate. Further the experiments were carried out for the effluent color removal and the values are compared with theoretically calculated value and it is observed that the values are satisfactorily matching with experimental observations.

Martin, 2000 has presented an alternative method for interpreting RTD data, which is relatively easy to use and addresses some of the weaknesses of more conventional methods. An extension to the "tanks in series" concept is presented (ETIS) and united with the "reactor network" formulation. The suitability and appropriateness of the model is discussed and compared with the "closed" dispersion model. They had chosen a case study with a very large tank and simulated it by commercial CFD package. Using the transient concentration at the outlet they have developed an equivalent reactor network having number of plug flow and ideal CSTR combinations. The network predicts very well the RTD data.

The author Danckwerts, 1953 emphasizes generalized methods for predicting yields in unsteady reactors without specific assumptions concerning basic kinetics or the mixing phenomenon within the reactor. His aim was to present a unified view of reactor kinetics utilizing the theories of residence time distribution and micro-mixing. Nauman and Collinge, 1968 showed that the contact time distribution is the exact heterogeneous counterpart of the ordinary residence time distribution. Hocine, et al, 2008 proposed an intermediate way between the purely numerical approach and the experimental characterisation of the contamination transfers. The method lies on the determination of the experimental residence time distribution (RTD) curve generally obtained through the response of the system to a tracer release Zwettering, 1959 also proposed a model to determine residence time distribute on of continuous flow systems; and the concept of Danckwerts about the degree of mixing and segregation are extended to the case of continuous flow systems with an arbitrary but known residence time distribution.

The authors (Burghardt and Lipowska, 1972) have determined the residence time distribution for water and other liquids with higher viscosities by using inlet flow energy i.e., without mechanical stirrer and also with the use of mechanical stirrer. Peclet number has been correlated as a function of the remaining parameters describing the phenomenon of mixing. The RTD of the reactor is evaluated based on the exit concentration of potassium chloride with time. In the experiments the internal age distribution function $I(\theta)$was measured by using the method of step-wise change of concentration at inlet from C_0^- to C_0^+. The

concentration of the KCl in the outlet stream was measured by the conductometer. The non-dimensional RTD function F is

$$F(\theta) = \frac{C(t) - C_0^-}{C_0^+ - C_0^-} \qquad 2.18$$

Where, θ is the non-dimensional time, t/τ.

The internal age distribution function $I(\theta)$ were calculated from the formula

$$I(\theta) = 1 - F(\theta) \qquad 2.19$$

Or, $$I(\theta) = \frac{C_0^+ - C(t)}{C_0^+ - C_0^-} \qquad 2.20$$

Where $C(t)$ is concentration of KCl at any time, t.

They have found the condition for dispersed and ideal flow conditions.

Lipowska (1974) has done continuation of research in which criteria of ideal mixing has been determined for water and other viscous liquids. They have studied on the condition of mixing due to inlet flow energy in absence of stirrer and due to mechanical energy imparted by stirrer in case of CSTR with impeller. With rotating impeller the expression for $I(\theta)$ used is

$$I(\theta) = \exp\left[-\left(\frac{V^*}{Q} + 1\right)\theta\right] \qquad 2.21$$

where V^* is the inlet volumetric flow rate, Q is impeller pumping capacity given by $Q = 2.3nd_m^2 b\ \text{cm}^3/\text{sec}$, n is the rpm of the impeller, d_m is the impeller diameter, mm, and b is the height of the impeller blade, Cm. According to Eq. 2.15, mixing is ideal when $V^*/Q \to 0$. The volumetric flow rate is evaluated by $V^* = A_{in}u_{in}$, where A_{in} is the inlet normal cross sectional area and u_{in} inlet net velocity.

Raghuraman and Varma, 1973 had developed three parameters mathematical model for predicting RTD of multistage flow system, assuming backmix and dead regions in each stage, with a fraction of feed short-circuitingeach stage. In addition, a finite cross flow of material between dead and active regions was also considered. The models were developed using first principal mode followed by the development of RTD distribution equation by Laplace direct transformation and inverse transformation. They have found the number ideal stages required for predicting experimental RTD.

Plasari, 1977 had work on the mixing phenomena of CSTR with two inlet stream to avoid short circuiting. The purpose of the research is to study the jet induced flow behaviour of the

stirred CSTR. They have found that the nature of RTD is function of the size of the reactor, and it also depends on the direction of the rotation of the impeller.

Lintz and Weber, 1980 have worked on RTD characteristics multiple inlets CSTR in presence of an autocatalytic reaction. The working conditions are kept fixed (space velocity, reactant concentrations) in such a manner, that an ideal CSTR would work at the maximum of reaction rate. The conversion of the reactants at the outlets were measured with time and then compared with the maximum conversion for understanding the behaviour of real CSTR. They also have found the effect of geometry of the reactor on the mixing efficiency.

Many processes deal gas-liquid multiphase mixture. It is very much important to know the RTD of multiphase processes, Popovic et al., 1983 have contributed on it by finding out the RTD of gas in fermentation unit. Helium was used as the tracer and heat conductivity cell was used to measure the concentration of it at the exit. The experimental values of gas RTD was compared successfully with theoretical RTD. The gas phase mass transfer coefficient and power number were also found.

Thijert et al. 1992 had presented a measuring method and extensive experimental data on the gas phase RTD in a mechanically agitated gas-liquid reactor with standard dimensions over a wide range of superficial gas velocities, agitation rates and agitator sizes. An empirical relation for the mean residence time with superficial gas velocity was developed. They have shown the rate of absorption of tracer gas effects the RTD of the gas-liquid CSTR. They also have concluded that the RTD can be described by a single ideally mixed tank in series with a tube with plug flow.

Van der Lans, 1997 had done an excellent work on the gas phase RTD. They have found experimental RTDs for a scaled down version of a burner. RTD results have been used to derive a chemical reaction engineering model for the mixing process i.e. whole process burner can be represented as a combination of ideal CSTR and plug flow reactors. The RTDs of the chemical engineering models matches in excellent with the experimental data of the burner. The simplifications in flow pattern in the chemical engineering models allows implementation of more detailed chemistry, and make it possible to study chemistry in a well-defined mixing environment.

Sahle-Demessie, 2003 had also worked on gas phase RTD behaviour. They have studied experimentally the non-ideal behaviour of a photo catalytic reactor injecting acetone vapor as the tracer. The RTD curves show the effect of inlet flow rate and extent of mixing on the non-ideal behaviour of it. They have calculated equivalent number of ideal CSTR for a particular RTD.

Buffham and Nauman, 1984 have developed theoretical expression of RTD for recycle process with and without parallel elements. The effect of presence of dead time on the RTD was also found without flow limit state. Systems which lack dead, or stagnant or sluggish flow zones have exponential recycle flow limits; systems with stagnant or sluggish-flow zones have non-exponential limits; in the special case where dead zones appear at the limit, the limiting distribution is defective, being defective exponential if the flows are otherwise unbounded. They have defined a few terms. "Dead" zones are those which are completely outside the boundaries of the flow system, inaccessible to flow of fluid or any chemical species. "Stagnant" zones do not conduct fluid, but mass transfer can occur by molecular diffusion between them and the active flow region. "Sluggish-flow" zones conduct fluid, but at a rate much slower than the mean.

In most of the work on RTD, the RTD equations were derived based on the assumptions that inlet and outlet flow rates are constant, and also volume of the liquid in the system also time variant. But these variables usually vary with time in real life. Fernandez-sempere, et al. 1995 had developed a general expression of RTD while inlet, outlet flow rates and volume of liquid might vary with time. The steady state RTD expression can be derived from these transient RTD expressions. The transient RTDs have predicted well the experimental RTDs of sewage system where possibility of variation of flow rates and volume capacity of the sewage with time can not be neglected. Scargiali, 2004 had presented an experimental work on the retention time distribution of solid particles in a high-aspect-ratio vessel, stirred by three equally spaced Rushton turbines. The relevant data were obtained by a special technique named twin system approach (TSA). Using deconvolution of transient solid fraction data at the exit of the reactor with the help of z-transformation, the RTD data $E(t)$was generated. Particle tracing was performed by an effective particle-coating/optical-detection technique that allows particles recovery and reuse after each experimental run. The RTD data obtained has indicated that a cascade of ideally mixed tanks with backflow results into very good agreement with experiment.

Bruce et al. 2004 has characterized experimentally the mixing behavior of a liquid phase in a turbulent bed contactor (TBC). TBC is a gas–liquid–solid fluidized bed with liquid trickling down through an expanded bed of solids supported by the gas flowing counter-current to the liquid. In the work, an ideal mixed flow tank (MFT) is included in series with TBC. The RTD of the ideal MFT is deconvoluted from the RTD of the entire system to obtain the RTD of TBC alone. The experimental RTD curves are satisfactorily compared with axial dispersion

model. Correlations are developed for predicting the Peclet number and the axial dispersion coefficient. The Peclet number obtained through deconvolution decreases with increase in gas and liquid velocities, and particle diameter and increases with increase in static bed height and number of stages.

Cozewith and Squire, 2000 have studied on the composition distribution of functional groups in polymerization reactions. They have shown that the breadth of the composition distribution (CD) of functional groups is equal to the breadth of the RTD. They have developed the expressions for CD for one to three reactors in series for reactions which are first order in mer concentrations. It was found that when there are equal rate constants in each reactor, the CD expressions can be derived easily; but for unequal rate constants, a method involving integral delta function was employed. The results showed that distribution breadth is a very strong function of mer conversion. Relatively narrow distributions are only obtained in the limits of very high or very low conversion and the broadest distribution results at a conversion of about 60%. Narrowing the RTD by using tanks in series narrows the CD. For tanks in series, the breadth of the CD was found narrowest when the mer conversion is the same in each reactor in the train.

Arratia, et al.2004 have worked on finding the presence of segregated and chaotic regions inside a CSTR with acid/base reaction mechanism and fluorescent techniques. The effect of inlet/outlet stream position and Reynolds number on the dynamics of the mixing processes was examined. Numerical experiments in 3-D map were able to capture the main features of the CSTR flow by perturbing a batch system using an imposed axial flow. It was observed that under dynamic inlet flow conditions when the laminar steady flow is perturbed, giving rise to an asymmetric flow pattern that is able to destroy toroidal segregated regions. The presence of inlet and outlet flow creates an asymmetry on the mixing flow mechanism leading to a more efficient mixing process than with a batch reactor. Moreover, it was observed that once the flow is stopped, both distorted toroidal regions return to their unperturbed state. This led to use periodic pumping system which destroys completely the toridal. The most interesting result is that at a given and constant inlet/outlet flow rate, the mixing efficiency decreases at a higher agitation speed (Re).

The RTD of the horizontal stirred bed reactor for polypropylene production was investigated experimentally by Dittrich and Mutsers, 2007 in a cold-flow horizontal mixing apparatus. For the pulse–response experiments, a small amount of colored tracer powder was quickly added to the powder inlet stream. At the reactor outlet, powder samples were taken every few minutes, and the fraction of the colored particles in the white bulk material was determined

by a computerized digital imaging method. The experimental data are compared with the RTD of a cascade of continuous stirred tank reactors (CSTRs) with equal volumes. The number of CSTRs in a series necessary for simulating the experimental pulse–response curves increases with rising throughput and decreasing residence time. The catalyst RTD is determined by the degree of axial backmixing in the reactor while the polymer RTD mainly depends on the axial net flow profile and therefore on the catalyst activity profile.

Residence time distribution in extrusion were modeled by Kumar et al. 2008 assuming plug flow in series with a finite number of continuously stirred tank reactors with some dead volume fractions. A full factorial design $(4\times3\times3\times2)$ of four starch moisture contents, three screw speeds, three nozzle diameters and two barrel temperatures was used. Each experiment was replicated twice with a total of 144 experiments. The parameter-values of RTD were averages of the replications. The complete model with 2 or 3 CSTRs was best-fit and represented the experimental residence time distribution well.

Madhuranthakam et al. 2009 had conducted the RTD and liquid hold up experiments in a static mixer (SM) reactor with hydrogen and hydrogenated nitrile butadiene rubber solution systems. The intricate net shaped internal structure splits a single flow into several partial flows and these partial flows in turn mix together after one complete rotation which is obtained after every four elements in this type of reactor. The experimental results from the RTD experiments were conveniently modeled using a plug flow with axial dispersion model. The RTD curves were found symmetric around the mean residence time, which emphasizes the fact that all fluid elements have uniform time history. The observed absence of no long tails or double peaks in RTD shows that there are no stagnant zones or channeling in SM. It was also found that with the introduction of gas into the reactor, the gas caused more dispersion and eventually made the SM reactor to behave almost like CSTR.

The constructed soil filter (CSF), also known as soil biotechnology (SBT) is used for wastewater treatment. CSF is a bioconversion process for removal of oxidizable organics, inorganics and pathogens, for applications in wastewater treatment and solid waste management. The flow pattern is unpredictable, since these are triggered by small scale heterogeneity, difficult to capture by conventional sampling methods in the unsaturated zone. Nemade, 2009 has worked on the RTD of CSF. They have used the plug flow model with dispersion, and Peclet number was used as the dispersion parameter. The model assumes that there exist two parallel channels consisting of a bulk flow path (inter-particle channel) and a capillary path (intra-particle channel) through which liquid passes and dispersion occurs in

both channels. The model was found efficient to predict the experimental RTD. In addition mass transfer coefficient of oxygen was calculated while oxygen is absorbed by the liquid enters the CSF.

Residence time distributions (RTD) for aqueous maltodextrin solutions were determined in two kinds of spouted bed dryers: (i) conventional spouted bed, (ii) spout-fluid bed with draft tube submerged in a bed (Osorio-Revilla, 2011). In drying operations, it is essential to have a detailed knowledge of the RTD of the product particles, since the quality of the product is strongly dependent on the time spent inside the drying chamber. A known dry solids sample from the collected product powder was redissolved to its original concentration, filtered to eliminate any turbidity and the dye concentration determined. The RTD curves were well represented by the response of an ideal stirred tank with a superimposed bypass which varied with the type of dryer. The mean residence time of RTD was found unaffected by the variations of the spouting air flow rate.

The hydrodynamic properties of a catalyst packing are very important for its catalytic performance. The influence of the structural properties of the carbon nanofiber/graphite felt composite and the physical properties of a liquid on the permeability and the flow behavior were studied by Cao, 2011. Ethanol mixtures with different concentrations were used as a working fluid to determine the influence of the liquid surface tension on the permeability of the composite by pressure drop measurement. Cyclohexane and water are used as a working fluid respectively to investigate the effect of the liquid wettability on the flow behavior in the composite by residence time distribution (RTD) experiments and piston dispersion exchange model.

2.3 APPLICATION OF COMPUTATIONAL FLUID DYNAMICS (CFD) TOOLS FOR DESIGNING REACTORS

The performance of stirred tank reactor depends on appropriate adjustment of the reactor hardware and operating parameters. Parameters like reactor and impeller shapes, aspect ratio of the reactor vessel, and number, type, location and size of impellers, degree of baffling, etc., provide effective means to control the performance of stirred reactors (Rushton et al. 1950a and b).

The flow generated by rotating impeller (Wolf and Manning, 1966) interacts with stationary baffles and produce complex, three dimensional and recirculating turbulent flow. The mean flow generated by impeller causes bulk motion which is responsible for convective transport of momentum, heat and mass. The generated turbulence determines the eddy diffusion of momentum, heat and mass. Therefore, the overall performance of stirred reactor depends on

the flow field and corresponding turbulence characteristics generated by impeller. The flow near the impeller is unsteady in nature due to cyclic passage of the blade and as go away from the impeller the fluid motion is stationary.

On the basis of the direction of generated flow, impellers are classified into two broad categories

(i) radial flow impellers (ii) axial flow impellers. The energy input which results in the movement of impeller is mainly used for producing turbulence in case of radial flow impellers while for convection in case of axial flow impellers. Radial flow impellers are more suited for applications such as gas-liquid, liquid-liquid and other multiphase dispersions. Axial flow impellers are used for blending, heat transfer and solid suspension.

The axial impeller discharges fluid mainly axially, parallel to the impeller shaft. The fluid is pumped through the impeller, normally towards the bottom of the tank. The flow makes a turn at bottom, then flow moves along the bottom and rises near the tank wall. In a tank reactor with radial impellers, the discharge of fluid is radially out from the blade towards the tank wall. The flow splits at the tank wall, and approximately 50% of the fluid circulates towards the surface while the rest to the bottom. This creates two region of low mean velocity.

The baffles are installed in the tank to avoid the circulatory motion of fluid i.e. to modify flow and destroy surface vortices. The use of it provides turbulent mixing in the reactor. Baffles mounted on the tank wall are common but bottom baffles, floating surface baffles and disk baffles at the impeller shaft are also possible. The baffles mounted at certain distance from the tank wall helps to avoid the dead zones. In a tank with radial impeller, suitable baffles produce strong top to bottom currents from the radial discharge. The installation of baffles increases the power consumption. For axial flow impeller, the need for baffling is not as great as for radial flow impellers.

Harvey and Greaves, 1982 have simulated the flow in turbulence using standard $\kappa-\varepsilon$ turbulence model for the first time. They have treated baffles as a source of a pressure induced drag on swirling component of the flow. They have found the qualitative agreement of the radial and axial velocity profiles. Deviations between the computed results with experimental values as much as 25% in radial velocity and 100% in tangential velocity were observed. Comparison for radial, axial, tangential velocities, and the turbulent kinetic energy was presented mainly in the impeller discharge stream.

Middleton et al. 1986 have carried out CFD simulation of the turbulent flow using standard $\kappa-\varepsilon$ turbulence model. No quantitative comparison of the mean flow and turbulent characteristics was presented there. The predicted flow field was used to study the effect of mixing on the yield of a typical consecutive reaction.

Ranade and Joshi 1990 have simulated the flow produced by the radial flow impeller using black box approach in conjunction with $\kappa-\varepsilon$ turbulence model. They have systematically investigated the sensitivity of the internal boundary conditions and the turbulence parameters of $\kappa-\varepsilon$ model on the predictions. Axial velocity predictions were found to be in good agreement with their measurements. Good comparison of radial, tangential velocities, and the turbulent kinetic energy in the impeller centre plane was observed. While poor prediction was observed in rest of the region.

Luo et al. 1993 have solved the time-dependent equations in two domains that were fixed with respect to their moving reference frame (MRF) using the standard $\kappa-\varepsilon$ turbulence model. Finite volume mesh at the interface was allowed to slide. The tangential velocity was under predicted by as much as 500% for most of the radial region while maximum deviation in axial velocity was found to be around 20%. No comparison for the turbulent characteristics was presented.

Dong et al. 1994 have simulated stirred tank flow using MRF and $\kappa-\varepsilon$ model. Flow away from the impeller region was well predicted while the magnitudes of axial and radial velocities were overestimated in the near impeller region. The turbulent kinetic energy was found to be over predicted in the impeller stream.

Lee et al. 1996 have used sliding mesh (SM) technique to simulate the impeller rotation. Severe under predictions (maximum deviation 200%) were observed in case of the turbulent kinetic energy predictions. Instantaneous radial velocity was overpredicted in most of the region with maximum departure of 35% from experimental data.

Rigby et al. 1997 have also employed SM technique to simulate the action of rotating impeller. Reasonable agreement with the experimental data for the location of impeller was observed. Comparison of all the three velocity components showed slight underpredictions in the impeller centre plane and slightly above the impeller.

Kuncewicz et al. 1997 have proposed the two-dimensional model for the prediction of flow pattern in stirred vessel. Tangential velocity prediction was found very poor (maximum deviation 100%) while axial velocity agreed reasonably well.

Venneker and van den Akker, 1997 have attempted the simulation of the flow using the black box approach along with the $\kappa-\varepsilon$ turbulence model. The computed radial velocities agreed

well throughout the tank while axial velocity predictions were satisfactory in most of the region (under predicted by as much as 50% below the impeller). The turbulent kinetic energy predictions were good except near the shaft and the bottom of the impeller where they were severely under predicted.

Brucato et al. 1994 have carried out CFD simulations of the flow in stirred tanks using various impeller models, namely black box approach, inner–outer technique and sliding grid approach along with the standard $\kappa-\varepsilon$ turbulence model. They also have presented a comparison with alternative modelling approaches.

Tabor et al. 1998 have made use MRF approach and the sliding mesh (SM) approach. The standard $\kappa-\varepsilon$ turbulence model was used to model the turbulence. They have recommended MRF for low diameter to height ratio of the tank, and suggested its inapplicability for the small blade-baffle gap and the cases where the time dependent features are of importance.

Ranade et al. 2001 have carried out the simulation of the flow pattern produced by the Rushton turbine by using a snap shot approach. They have used the standard $\kappa-\varepsilon$ model. Closer quantitative agreement was obtained for the radial velocity. The axial and tangential velocity predictions were found to be far away from the experimental data while the turbulent kinetic energy was severely under predicted with the experimental data in the impeller region.

Montante et al. 1999 have carried out simulations to study the effect of impeller clearance on the prediction of flow patterns. They varied the clearance ratio from 0.12 to 0.33. They have used three different turbulence models (i) standard $\kappa-\varepsilon$ model, (ii) RNG $\kappa-\varepsilon$ model, and (iii) RSM. Impeller–baffle interaction was modelled using SM and inner–outer approach. They have reported the velocity vector plots to show the clearance effect on number of circulation loops.

Alcamo et al. 2005 have simulated the turbulent flow field using Large Eddy simulation in an un-baffled stirred tank, stirred by Rushton turbine. The Smagorinsky model was used to model sub-grid scales. The simulated results were compared with experimental data and they found an excellent agreement especially for mean tangential velocities.

Javed et al. 2006 carried out mixing studies using CFD as well as experiments. They considered eight different locations in bulk and impeller region as concentration measurement locations. The comparison of mean axial, tangential, and radial velocities was reported and simulation results were in very good agreement with the experimental data.

Ochieng et al. 2008 carried out mixing studies in stirred tank at low clearance. They have shown that at a low impeller clearance, the Rushton turbine generates a flow field that

evolves from the typical two loops to a single loop flow pattern similar to that of an axial impeller. This single loop flow pattern resulted in an increase in axial flow and a decrease in mixing time at a constant power number. They have also carried out experiments and simulation by adding a draft tube in the tank to improve axial velocity and were able to achieve significant improvement in mixing performance.

Sahle-Demessie, 2003 also have simulated the annular cylindrical photo catalytic reactor using Fluent 6.2 software. They have used laminar incompressible fluid flow model along with partials tracking mechanism for developing RTD. For this, they have injected enough number small sized solid particles at the inlet and measured number of particles at the outlet with time. The effect of RPM and type of fan on RTD also found. The simulated data are found in good agreement with the experimental data. Axial or mixed flow fans are observed better for reducing backmixing which is obtained in case of radial fans.

Mixing in microchannels is one of the most important technical issues that are critical to the development and application of microchemical systems. Adeosun and Lawal, et al. 2010 had worked on it in terms RTD of the microchannel. The work involved the use of CFD simulations as a vital design, optimization and characterization tool; fabrication of the mixing units using silicon-MEMS technology; and performing experiments to validate the numerical predictions of the mixing characterization. Results of the comparison between the normalized experimental RTDs and those from CFD simulation show good agreement at low Reynolds flow regime (Re<29).

Ciofalo et al., 2004 has done both the experimental and theoretical study on RTD of a CSTR. The experimental results for the baffled tank are compared to computational fluid dynamics (CFD) predictions of the RTD using the $\kappa - \varepsilon$ model in Fluent software for transitional flow regime in the tank, i.e., impeller Reynolds number between 10 and 10,000. All the qualitative aspects of the predicted RTDs were found similar to those measured experimentally. The mean residence times as well as the variances of the residence time were accurately predicted by CFD in the transition flow regime. They have examined the effect of impeller speed on the mean residence time and variance. It was observed that mean residence increases with increase impeller speed until reaches to a constant value to approximately the space time or holdup time of the reactor. For an ideal reactor the value of σ/τ_m should be 1.0, which was observed, within experimental error, at higher impeller rpms.

Xiao-chang et al. 2009 have done RTD study on a new tubular shaped continuous stirred reactor using number of tee type impeller supported on a coaxial shaft. They have performed

both the experimental work and theoretical analysis by Fluent 6.3. The tracer is injected as a pulse input. The characteristics of experimental RTDs were predicted well by Fluent at different speeds of the impeller and at different inlet flow rates. It was observed that the tubular reactor with a stirrer can improve the flow profile by narrowing the RTD curve, decreasing mean residence time and avoiding back mixing, but a high stirring speed broadens the RTD curve drastically. As the flow rate increases, the mean residence time as well as the variance of RTD was found to decrease proportionally. As the rotation speed increases, no evident effect on the mean residence time was observed, whereas the variance got enlarged greatly.

Venneker et al. 2010 has done an excellent experimental work on the hydrodynamics of CSTR of shear thinning liquids such as aqueous solution of carboxy methyl cellulose and Xanthan gum. Thy have found the all the time average velocity components at different locations of the CSTR, and noted the condition for Reynolds similarity when velocities at different locations becomes independent of viscosity i.e. in turn on Reynolds numbers. They also have shown the effect of Reynolds number on Flow number, Fl defined as

$$Fl = \frac{Q}{ND^3} \tag{2.22}$$

Where D is the diameter of the impeller, N is the rpm of it, and Q stands for flow rate of fluid pumped by impeller. In general Q (Mishra et al., 1998) is

$$Q = 2\pi \int_0^{D/2} \left(r v_z\right)\Big|_{z_1} dr + \pi D \int_{z_1}^{z_2} v_r \Big|_{D/2} dz \tag{2.23}$$

Where D, v_r and v_z are respectively impeller diameter, radial velocity, and axial velocity; z_1 and z_2 are the boundaries of the impeller-swept volume in the axial direction. The second term in Eq. 2.22 is negligible for the axial flow impellers (Patwardhan and Joshi, 1999; Kumaresan and Joshi, 2006).

Kolhapure et al. 2004 has simulated a single phase multijet tubular reactor to investigate the performance of it using Fluent software. Finite-rate/eddy-dissipation formulation in the Fluent software was used to model the turbulence–chemistry interactions. The work found visualization of flow, concentration and temperature distributions in the reactor and quantification of the impact of fluid dynamics and chemistry on performance. The mixing efficiency at the reactor outlet was described typically by the coefficient of variation of a nonreacting species. The reacting CFD tool were used for designing reactor internals that increase performance and operating flexibility of mixing-sensitive chemical processes.

For continuous stirred tank reactors, aubin et al., 2006 have used ANSYS CFX5 to create mesh sizes for the flow in the vessel. The numerical simulation of the flow in the vessel has been performed using ANSYS CFX5 which is a general purpose commercial CFD package that solves the Navier–Stokes equations using a finite volume method and a coupled solver.
The commercial mesh generator CFX-Build (aubin et al., 2006) was used to create a mesh composed of tetrahedral, prismatic and pyramidal elements, the latter types being generated during the mesh inflation process to increase the boundary layer resolution on walls, e.g., around the blades and on the tank walls. In this application, the mesh on the impeller blades was constructed from an IGES CAD file, allowing the full details, including the thickness of the blade, to be modelled. The baffles, however, are modelled as walls with zero-thickness. A preliminary grid convergence study was carried out in order to verify that the flow solution is grid independent. For this, velocities and turbulent quantities were monitored at different positions in the vessel and the results of three different grid sizes were compared.

For multiphase modelled stirred reactors, FLUENT 6.2 CFD has been used by many researchers (Murthy et al., 2007) to simulate three phase stirred suspension. The Eulerian multi-fluid model along with the standard $\kappa-\varepsilon$ turbulence model has been adopted to describe the flow behaviour of each phase, where the gas, liquid and solid phases all are treated as different continua, interpenetrating and interacting with each other everywhere in the computational domain. In FLUENT, the derivation of the conservation equations for mass and momentum for each of the three phases is done by phase weighted Favre-averaging (Viollet and Simonin, 1994) the local instantaneous balances for each of the phases, and then no additional turbulent dispersion term is introduced into the continuity equation.
The simulation of partially baffled stirred vessels with free surface has been carried out using CFD models (Torrea et al., 2007). Their simulations showed that the free surface could be captured well using the standard VOF method available in ANSYS CFX but their cases resulted in smooth, parabolic shaped interfaces and no entrainment of gas into the impeller swept region.
A three-dimensional flow field in the oxidation ditch (one of the waste water treatment reactor) aerated with surface aerators is simulated by Fan, et al., 2006 CFD models. The two-fluid model and the standard *k*–ε model were used for the turbulent solid–liquid two-phase flow.

Zheng, et al., 1997 have employed CFD to study polymerization system and showed the mixing affects, monomer conversion, initiator consumption and the molecular weight distribution.

Thermal polymerization of styrene in a CSTR was simulated by Patel et al. 2010 at 140^0C to explore the effect of mixing on polymerization. Although polymerization reactions are exothermic, isothermal operation was considered in this study. Several simulations were conducted to investigate the impact of the impeller speed, the effect of residence time and input–output stream locations on styrene conversion and the mixture homogeneity. The conversions predicted using Fluent was compared with those obtained from CSTR model and experimental data. The effect of impeller speed and variable residence time on the conversion of monomer was determined.

Chapter 3

COMPUTATIONAL FLUID DYNAMICS MODEL EQUATIONS

Computational fluid dynamics (CFD) is the science of determining a numerical solution to governing equations of fluid flow whilst advancing the solution through space or time to obtain a numerical description of the complete flow field of interest. The important aspect in CFD is to understand the linkage between the flow and the design objective. The chemical engineers are interested in mixing, pressure drop, residence time distribution (RTD), heat transfer and mass transfer across fluid-fluid and fluid-solid interface. CFD methods are based on the first principles of mass, momentum and energy conservation, as described by the Navier-Stokes equations. These methods involve the solution of conservation equations of mass, momentum, energy and species at thousands of locations within the flow domain. The computed solution provides flow variables such as velocity, pressure, temperature, density, concentration, etc. CFD emerges as one of the foremost important subject for designing various types of chemical, mechanical, pharmaceutical and bio-processes. The availability and advancements in commercial CFD software make the area more attractive and comfortable to the engineers, scientists etc for understanding and designing the processes. All codes of the commercial CFD contain three main elements: (i) a pre-processor (ii) a solver and (iii) a post-processor. In pre-processor, the preparation of geometry and generation the sub-division of the domain into a number of smaller, non overlapping sub-domains: a grid (or mesh) of cells (or control volumes or elements) are carried out. Using the specified boundary conditions, the governing partial differential equations are solved by suitable numerical method and algorithm in the solver step. In the post processing step, the CFD results are analyzed by vector and contour plots, and also by distribution of different scalars, vectors and different flux terms.

There are different ways of solving the non-linear Navier Stokes equation. The most useful methods are: finite difference, finite volume, finite element and spectra method. The commercial software ANSYS Fluent 13.0 uses finite volume method for integrating the

equations. The conservation of a general flow variable Φ within a finite control volume can be expressed as a balance between the various processes tending to increase or decrease it. In words we have:

$$\begin{bmatrix}\text{Rate of change of}\\ \Phi \text{ with time in}\\ \text{the control volume}\end{bmatrix} = \begin{bmatrix}\text{Net flux of } \Phi \text{ due}\\ \text{to convection into}\\ \text{the control volume}\end{bmatrix} + \begin{bmatrix}\text{Net flux of } \Phi \text{ due}\\ \text{to diffusion into}\\ \text{the control volume}\end{bmatrix} \pm \begin{bmatrix}\text{Net rate of creation or}\\ \text{dissipation of } \Phi \text{ inside}\\ \text{the control volume}\end{bmatrix}$$

In general Φ can be density of fluid, ρ, velocity components, (υ_x, υ_y, and υ_z in rectangular coordinate system).

For all flows, ANSYS FLUENT solves conservation equations for mass and momentum. For flows involving heat transfer or compressibility, an additional equation for energy conservation is solved. For flows involving species mixing or reactions, a species conservation equation is solved or, if the non-premixed combustion model is used, conservation equations for the mixture fraction and its variance are solved. Additional transport equations are also solved when the flow is turbulent. In the present work isothermal systems are chosen, and hence, only hydrodynamic equations are solved. Depending upon the flow regimes, there are two kinds of flow regimes, (i) laminar flow and (ii) turbulent flow. The theoretical CFD model equations are available in a number of literatures (Ranade, 2002; Date, 2005, Tannehill, 1997; Anderson, 1995; ANSYS, 2009; Wilcox, 1993). The present work has used ANSYS Fluent for the simulation study of the mixing characteristics of continuous stirred tank reactors. Therefore, the theoretical background and the required CFD model equations are picked up selectively from ANSYS, 2009.

3.1 LAMINAR FLOW EQUATIONS

The general conservation of mass or continuity equation can be written as follows:

$$\frac{\partial \rho}{\partial t} + \nabla.(\rho \vec{\upsilon}) = S_m \qquad 3.1$$

Where, $\vec{\upsilon}$ is the velocity vectors.

Eq. 3.1 is valid for incompressible as well as compressible flows. The source S_m is the mass added to the continuous phase from the dispersed second phase (e.g., due to vaporization of liquid droplets).

The conservation of momentum equation in an inertial (non-accelerating) reference frame is given by

$$\frac{\partial}{\partial t}(\rho\vec{\upsilon})+\nabla.(\rho\vec{\upsilon}\vec{\upsilon})=-\nabla p+\nabla.(\bar{\bar{\tau}})+\rho\vec{g}+\vec{F} \qquad 3.2$$

Where, p is the static pressure and $\bar{\bar{\tau}}$ is the stress tensor (Eq. 3.3); $\vec{g}$ and $\vec{F}$ are the gravitational body force and external body forces respectively. It also contains other model-dependent source terms such as porous-media. The stress tensor $\bar{\bar{\tau}}$ is given by

$$\bar{\bar{\tau}}=\mu\left[\left(\nabla\vec{\upsilon}+\nabla\vec{\upsilon}^{T}\right)-\frac{2}{3}\nabla.\vec{\upsilon}I\right] \qquad 3.3$$

Where μ is the molecular viscosity, I is the unit tensor, and the second term on the right hand side is the effect of volume dilation.

The equation of mass transfer for species k is

$$\frac{\partial}{\partial t}(\rho\omega_k)+\frac{\partial}{\partial x_j}(\rho u_j\omega_k)=\frac{\partial}{\partial x_j}\left(\rho D_{eff}\frac{\partial\omega_k}{\partial x_j}\right)+R_k \qquad 3.4$$

Where ω_k is the mass fraction of kth species, D_{eff} is the effective diffusivity of the species in the mixture and R_k is rate of reaction.

The above equations can be rearranged in view of application finite volume discretization method, and it is shown separately for single phase and multiphase flow cases.

3.1.1 Single Phase Flow

For an arbitrary scalar Φ_k, ANSYS FLUENT solves the equation

$$\frac{\partial(\rho\Phi_k)}{\partial t}+\frac{\partial}{\partial x_i}\left(\rho u_i\Phi_k-\Gamma_k\frac{\partial\Phi_k}{\partial x_i}\right)=S_{\Phi_k} \qquad k=1,\ldots,N \qquad 3.5$$

Where Γ_k and S_{Φ_k} are the diffusion coefficient and source term for each of the N scalar equations. For isotropic diffusivity, Γ_k could be written as $\Gamma_k I$ where I is the identity matrix. The meanings of Γ_k, S_{Φ_k} for each Φ_k are listed in Table 3.1.

Table 3.1: Generalized representation of transport equations

Equation	Φ_k	Γ_k	S_{Φ_k}
3.1	1	0	0
3.3	u_i	μ	$-\frac{\partial p}{\partial x_i}+\rho\vec{g}+\vec{F}$
3.4	ω_k	D_{rff}	R_k

For steady state case, with negligible convective contribution, Eq. 3.5 becomes

$$-\frac{\partial}{\partial x_i}\left(\Gamma_k\frac{\partial\Phi_k}{\partial x_i}\right)=S_{\Phi_k} \qquad k=1,...,N \qquad 3.6$$

and for convective-diffusive steady flow case, the equation becomes

$$\frac{\partial}{\partial x_i}\left(\rho u_i\Phi_k-\Gamma_k\frac{\partial\Phi_k}{\partial x_i}\right)=S_{\Phi_k} \qquad k=1,...,N \qquad 3.7$$

3.1.2 Multiphase Flow

For multiphase flow there are two ways to solve the transport equations, (i) per phase and (ii) for the mixture.

In per phase method, an arbitrary k scalar in phase-l is denoted by Φ_l^k; the transport equation inside the volume of phase-l is

$$\frac{\partial\left(\alpha_l\rho_l\Phi_l^k\right)}{\partial t}+\nabla.\left(\alpha_l\rho_l\vec{u}_l\Phi_l^k-\alpha_l\Gamma_l^k\nabla\Phi_l^k\right)=S_l^k \qquad k=1,...,N \qquad 3.8$$

Where α_l, ρ_l and u_l are the volume fraction, physical density, and velocity of phase-l, respectively. Γ_l^k and S_l^k are the diffusion coefficient and source term, respectively in phase-l. In this case, scalar Φ_l^k is associated only with one phase (phase-l) and is considered an individual field variable of phase-l.

If Φ_l^k is shared between phases or considered uniform in all coexisting phases, then scalar is considered associated with mixture of phases and represented by Φ^k. The transport equation for the scalar in the mixture becomes

$$\frac{\partial\left(\rho_m \Phi^k\right)}{\partial t} + \nabla . \left(\rho_m \vec{u}_m \Phi^k - \Gamma_m^k \nabla \Phi^k\right) = S_m^k \qquad k = 1,...,N \tag{3.9}$$

Where mixture density ρ_m, mixture velocity u_m, and mixture diffusivity for the scalar k Γ_m^k are calculated by

$$\rho_m = \sum_k \alpha_l \rho_l \tag{3.10}$$

$$\rho_m \vec{u}_m = \sum_l \alpha_l \rho_l \vec{u}_l \tag{3.11}$$

$$\Gamma_m^k = \sum_l \alpha_l \Gamma_l^k \tag{3.12}$$

$$S_m^k = \sum_l S_l^k \tag{3.13}$$

To calculate mixture diffusivity, individual diffusivities for each material associated with individual phases must be specified.

3.2 FLOWS WITH ROTATING REFERENCE FRAMES

In ANSYS FLUENT, the default method of solution of the equations is in a stationary (or inertial) reference frame. The equations in a stationary reference frame are discussed above. However, some problems can be solved advantageously in a moving (or non-inertial) reference frame. Examples are problems with moving parts like rotating blades, impellers, etc. In moving reference frame, the equations of motion are modified to incorporate the additional acceleration terms which occur due to the transformation from the stationary to the moving reference frame. For some problems, the whole computational domain moves and it becomes part of the single moving reference frame, and it is called single reference frame approach. But for more complex problem, it is necessary to multiple reference frame with the combination stationary and moving reference frame. Here, the computational domain is divided into multiple cell zones with well defined interfaces between the zones. The treatment of interfaces results in two approximate steady state methods: (i) multiple reference frame (MRF) approach and (ii) the mixing plane approach. If unsteady interaction between stationary and moving parts becomes important, sliding mesh approach is used.

3.2.1 Equations for a Rotating Reference Frame

The transformed fluid velocities from the stationary frame to the rotating frame is

$$\vec{\upsilon}_r = \vec{\upsilon} - \vec{u}_r \tag{3.14}$$

Where, $\vec{\upsilon}_r$ is the relative velocity i.e. the velocity viewed from rotating frame, $\vec{\upsilon}$ is the absolute velocity. The whirl velocity i.e. the velocity due to moving frame $\vec{u}_r$ is given by

$$\vec{u}_r = \vec{\omega} \times \vec{r} \tag{3.15}$$

Here $\vec{\omega}$ is the angular velocity of the rotating reference frame relative to the stationary (inertial) reference frame and $\vec{r}$ is the distance of the stationary control volume from the rotating reference frame.

The momentum equations in rotating reference frame are formulated in two different ways

- Using relative velocity, $\vec{\upsilon}_r$ as the dependent variable, and it is known as the relative velocity formulations.
- Using absolute velocity, $\vec{\upsilon}$ as the dependent variable, and it is known as the absolute velocity formulation.

Both formulations are used in pressure based solver by ANSYS FLUENT, whereas the absolute velocity formulation is used in density based solver.

3.2.1.1 Relative Velocity Formulation

For the relative velocity formulation, the governing equations of fluid flow for a steadily rotating frame can be written as follows:

Conservation of mass:

$$\frac{\partial \rho}{\partial t} + \nabla . \rho \vec{\upsilon}_r = 0 \tag{3.16}$$

Conservation of momentum:

$$\frac{\partial}{\partial t}(\rho \vec{\upsilon}_r) + \nabla . (\rho \vec{\upsilon}_r \vec{\upsilon}_r) + \rho(2\vec{\omega} \times \vec{\upsilon}_r + \vec{\omega} \times \vec{\omega} \times \vec{r}) = -\nabla p + \nabla . \bar{\bar{\tau}}_r + \vec{F} \tag{3.17}$$

The momentum equation contains two additional acceleration terms: the Coriolis acceleration $(2\vec{\omega}\times\vec{\upsilon}_r)$, and the centripetal acceleration $(\vec{\omega}\times\vec{\omega}\times\vec{r})$. The viscous stress, $\bar{\bar{\tau}}_r$ is

$$\bar{\bar{\tau}}_r = \mu\left[\left(\nabla\vec{\upsilon}_r + \nabla\vec{\upsilon}_r^T\right) - \frac{2}{3}\nabla.\vec{\upsilon}_r I\right] \quad 3.18$$

3.2.1.2 Absolute Velocity Formulation

The governing equations of fluid flow for steadily rotating frame in terms if absolute velocity formulations are

Conservation of mass:

$$\frac{\partial\rho}{\partial t} + \nabla.\rho\vec{\upsilon}_r = 0 \quad 3.19$$

Conservation of momentum:

$$\frac{\partial}{\partial t}(\rho\vec{\upsilon}) + \nabla.(\rho\vec{\upsilon}_r\vec{\upsilon}) + \rho(\vec{\omega}\times\vec{\upsilon}) = -\nabla p + \nabla.\bar{\bar{\tau}} + \vec{F} \quad 3.20$$

3.2.2 Single Rotating Reference Frame (SRF) Modeling

In SRF whole computational domain is taken up under the rotating reference frame. In such cases, the equations Eq. 3.16 to 3.18 or Eq. 3.19 to 3.20 are used in the simulation. Walls with any shape which are moving with the reference frame are the boundary of the system and the relative velocity on the moving walls must be zero. When walls are non-moving, still SRF modeling approach can be used but with slip condition on the wall so that absolute velocity becomes zero on the wall. Flow boundary conditions like at the inlet and outlet can be prescribed either in stationary or rotating reference frame. For example, for inlet velocity, it can be specified either as relative velocity or absolute velocity.

3.2.3 Flow in Multiple Rotating Reference Frames

In many cases the physical domain of the problem may contain multiple rotating zones or combination of rotating and stationary zones. In these cases, the model is divided into multiple fluid/solid cell zones, with interface boundaries separating the zones. Zones with moving components should be solved using the moving reference frame equations (Eq. 3.16 to 3.18 or Eq. 3.19 to 3.20), whereas stationary zones is solved with the stationary frame

equations (Eq. 3.1 and 3.2). At the interface of moving and stationary zones, the treatment of the equations is different, and based on the method of treatment there are three methods:

- Multiple Reference Frame (MRF) model
- Mixing Plane Model (MPM)
- Sliding Mesh Model (SMM)

3.2.3.1 Multiple Reference Frame (MRF) Model

In MRF, the rotating zones which includes rotor and flow surrounding it do not move physically i.e. mesh remains fixed in the computation. If the interaction between rotor and stator is small, MRF model is a good choice e.g. in continuous stirred tank reactor, the interaction between impeller and baffles is weak, hence MRF model can be used. At the interfaces between rotating and stationary cell zones, a local reference frame transformation is performed to enable flow variables in one zone to be used to calculate fluxes at the boundary of the adjacent zone. At the interface between moving/stationary flow is nearly uniform (mixed out) and hence, continuation of velocity at the interface i.e. equality of it in both the reference frame is assumed.

The interface treatment applies both for the velocity and velocity gradients, since these vector quantities change with a change in reference frame. Scalar quantities, such as temperature, pressure, density, turbulent kinetic energy, etc., do not require any special treatment, and thus are passed locally without any change. At the interface the discretized diffusional terms in one domain require the values for velocities in other domain.

When relative velocity formulation is used, velocity in each subdomain is calculated relative to motion of subdomain. The conversion equation from relative velocity to absolute velocity is given below:

$$\vec{\upsilon} = \vec{\upsilon}_r + (\vec{\omega} \times \vec{r}) + \vec{\upsilon}_t \qquad 3.21$$

Where, $\vec{\upsilon}_t$ is the translation velocity. The gradient of absolute velocity vector is

$$\nabla \vec{\upsilon} = \nabla \vec{\upsilon}_r + \nabla(\vec{\omega} \times \vec{r}) \qquad 3.22$$

When absolute velocity formulation is used, the velocities are stored in absolute frame I in both the zones, and hence, at the interface no transformations are required for the velocity vectors.

3.2.3.2 The Mixing Plane Model

If the flow at this interface is not uniform, the MRF model may not provide a physically meaningful solution. The sliding mesh model and mixing plane model can be used then. But, when sliding mesh model is not feasible, mixing plane model can be cost effective alternative.

In the mixing plane approach, each fluid zone is treated as a steady-state problem. Flow-field data from adjacent zones are passed as boundary conditions that are spatially averaged or "mixed" at the mixing plane interface. Three profile averaging methods are available in the mixing plane model, (i) area averaging, (ii) mass averaging and (iii) mixed out averaging. The mixed-out averaging method is derived from the conservation of mass, momentum and energy. If reverse flow occurs, it better to start with area averaging method and then move to mixed-out method of averaging. This mixing removes any unsteadiness that would arise due to circumferential variations in the passage-to-passage flow field (e.g., wakes, shock waves, separated flow), thus yielding a steady-state result.

The mixing plane model involves with certain limitations:

- The mixing plane model requires the use of the absolute velocity formulation, but not the relative velocity formulations.
- The large eddy simulations (LES) turbulence model cannot be used with the mixing plane model.
- The models for species transport and combustion cannot be used with the mixing plane model.
- The general multiphase models (VOF, mixture, and Eulerian) cannot be used with the mixing plane model.
- The mixing plane model is a reasonable approximation so long as there is not significant reverse flow in the vicinity of the mixing plane.

3.2.3.3 Sliding Mesh Model

In sliding meshes, the relative motion of stationary and rotating volume segments in a rotating machine gives rise to unsteady interactions. These interactions include: (i) potential interaction which results in flow unsteadiness due to pressure waves which propagate both upstream and downstream, (ii) wake interactions that results in flow unsteadiness due to wakes from upstream rotor to downstream stator, and (iii) shock interactions happens at transonic/supersonic state flow. When a time-accurate solution for rotor-stator interaction (rather than a time-averaged solution) is desired, the sliding mesh model must be used to compute the unsteady flow field and the sliding mesh model is the most accurate method for simulating flows in multiple moving reference frames, but also the most computationally demanding. Most often, the unsteady solution is time periodic i.e. the unsteady solution repeats with a period related to the speed of the moving domains. The shape of the interface changes with time and hence, dynamic mesh model is used to capture the unsteady movement of the meshes of the moving zones. With respect to dynamic meshes, the conservation equation for a general scalar, Φ on an arbitrary control volume, V, whose boundary is moving, can be written as

$$\frac{\partial(\rho\Phi)}{\partial t}+\nabla.\rho\Phi(\vec{\upsilon}-\vec{\upsilon}_g)=\nabla.(\Gamma\nabla\Phi)+S_\Phi \qquad 3.23$$

Where υ_g is moving mesh velocity. The integral form of Eq. 3.23 is

$$\frac{\partial}{\partial t}\int_V \rho\Phi dV+\int_{\delta V}\rho\Phi(\vec{\upsilon}-\vec{\upsilon}_g)d\vec{A}=\int_{\delta V}\Gamma\nabla\Phi.d\vec{A}+\int_V S_\Phi dV \qquad 3.24$$

Here δV is used to represent the boundary of the control volume V. Applying first order backward difference formulae, the time derivative term can be written as

$$\frac{\partial}{\partial t}\int_V \rho\Phi dV=\frac{(\rho\Phi V)^{n+1}-(\rho\Phi V)^n}{\Delta t} \qquad 3.25$$

Where n and $n+1$represent the old and present time. At (n+1)th time V^{n+1} is computed from

$$V^{n+1}=V^n+\frac{dV}{dt}\Delta t \qquad 3.26$$

The volume time derivative, dV/dt is computed from

$$\frac{dV}{dt} = \int_{\delta V} \vec{\upsilon}_g . d\vec{A} = \sum_j^{n_f} \vec{\upsilon}_{g,j} . \vec{A}_j \qquad 3.27$$

Where n_f is the number of faces on the control volume and $\vec{A}_j$ is the j face area vector. The dot product $\vec{\upsilon}_{g,j} . \vec{A}_j$ on each control volume face is calculated by

$$\upsilon_{g,j} . \vec{A}_j = \frac{\delta V_j}{\Delta t} \qquad 3.28$$

In the sliding mesh formulation, the control volume remains constant, therefore $dV/dt = 0$ and $V^{n+1} = V^n$. Thus the time derivative terms can be represented as

$$\frac{\partial}{\partial t} \int_V \rho \Phi dV = \frac{\left((\rho \Phi)^{n+1} - (\rho \Phi)^n\right) V}{\Delta t} \qquad 3.29$$

Two or more cell zones are used in the sliding mesh technique. Each cell zone is bounded by at least one "interface zone" where it meets the opposing cell zone. The interface zones of adjacent cell zones are associated with one another to form a "mesh interface." The two cell zones will move relative to each other along the mesh interface. The cell zones slide (i.e., rotate or translate) relative to one another along the mesh interface in discrete steps. Since the flow is inherently unsteady, a time-dependent solution procedure is required.

3.3 TURBULENT FLOW

Turbulence is a natural phenomenon in fluids that occurs when velocity gradients are high, resulting in disturbances in the flow domain as a function of space and time. Examples include smoke in the air, condensation of air on a wall, flow in a combustion chamber, ocean waves, stormy weather, atmospheres of planets, and interaction of the solar wind with magnetosphere, among others. The effects produced by turbulence may or may not be desirable. Intense mixing may be useful when chemical mixing or heat transfer is needed. On the other hand, increased mixing of momentum results in increased frictional forces, so the power required pumping the fluid or the drag force on a vehicle is increased. The engineer needs to be able to understand and predict these effects in order to achieve a good design. In some cases, it is possible to control the turbulence, at least in part.

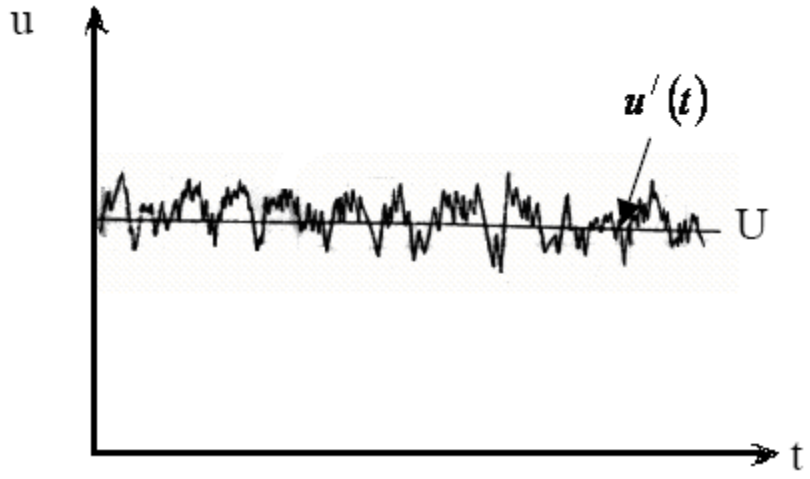

Figure 3.1: Turbulent Velocity

In turbulent flow, the velocity shown in Fig 3.1 can be decomposed into a steady mean value U with a fluctuating component $u'(t)$ gives actual velocity, $u(t)=U+u'(t)$. In general, it is most attractive to characterize a turbulent flow by the mean values of velocity components and pressure $(U,V,W,P$ etc.$)$ and the statistical properties of te respective fluctuations $(u',\upsilon',w',p'$ etc.$)$. Turbulence is an eddying motion, which has a wide spectrum of eddy sizes and eddy velocities. Thus, it is also characterized by the size of eddies form inside the system and the flow falls either in large eddy or small eddy class.

Substitution of actual velocity in terms of mean and fluctuating velocity components gives Reynolds-averaged Navier-Stokes (RANS) equation. The continuity and momentum equations here is

$$\frac{\partial \rho}{\partial t}+\frac{\partial}{\partial x_i}\left(\rho U_i\right)=0 \qquad 3.30$$

$$\frac{\partial}{\partial t}\left(\rho U_i\right)+\frac{\partial}{\partial x_j}\left(\rho U_i U_j\right)=-\frac{\partial P}{\partial x_i}+\frac{\partial}{\partial x_j}\left[\mu\left(\frac{\partial U_i}{\partial x_j}+\frac{\partial U_j}{\partial x_i}-\frac{2}{3}\delta_{ij}\nabla.U\right)\right]+\frac{\partial}{\partial x_j}\left(-\rho\overline{u_i' u_j'}\right) \qquad 3.31$$

Additional terms now appear that represent the effects of turbulence. These Reynolds stresses, $-\rho\overline{u_i' u_j'}$, must be modeled in order to close Eq. 3.31.

A turbulence model should be useful in a general purpose CFD code and hence, it must have wide applicability, be accurate, simple and economic to run. The most common turbulence models are classified below:

Classical models	Based on (time averaged) Reynolds equations
1	Zero equation model – mixing length model
2	Two-equation model - $\kappa - \varepsilon$ model
3	Reynolds stress model (RSM)
4	Algebraic stress model (ASM)
Large eddy simulation (LES)	Based on space-filtered equations
Direct numerical simulation (DNS)	

In the present work $\kappa - \varepsilon$ turbulent model is used and it is only discussed here. There are three types of $\kappa - \varepsilon$ model used in ANSYS FLUENT and these are

- Standard $\kappa - \varepsilon$ model
- Renormalization-group (RNG) $\kappa - \varepsilon$ model
- Realizable $\kappa - \varepsilon$ model

3.3.1 Standard $\kappa - \varepsilon$ Model

The standard $\kappa - \varepsilon$ model is a robust and economic model which provides reasonable accuracy of the practical problems. It is a semi-empirical model based on the transport model of turbulent kinetic energy (κ) and its dissipation rate (ε). The derivation of $\kappa - \varepsilon$ model assumes fully turbulent state of the fluid i.e. the effect of molecular viscosity on the flow is negligible.

The transport equation for κ is

$$\frac{\partial}{\partial t}(\rho\kappa) + \frac{\partial}{\partial x_i}(\rho\kappa\upsilon_i) = \frac{\partial}{\partial x_i}\left[\left(\mu + \frac{\mu_t}{\sigma_k}\right)\frac{\partial\kappa}{\partial x_i}\right] + G_\kappa + G_b - \rho\varepsilon - Y_M + S_\kappa \qquad 3.32$$

and the transport equation for ε is

$$\frac{\partial}{\partial t}(\rho\varepsilon)+\frac{\partial}{\partial x_i}(\rho\varepsilon\upsilon_i)=\frac{\partial}{\partial x_i}\left[\left(\mu+\frac{\mu_t}{\sigma_\varepsilon}\right)\frac{\partial\varepsilon}{\partial x_i}\right]+C_{1\varepsilon}\frac{\varepsilon}{\kappa}(G_k+C_{3\varepsilon}G_b)-C_{2\varepsilon}\rho\frac{\varepsilon^2}{\kappa}+S_\varepsilon \qquad 3.33$$

Where μ_t is the turbulent viscosity, G_κ is the generation of turbulence kinetic energy due to the mean velocity gradients, G_b is the generation of turbulence kinetic energy due to buoyancy, Y_M represents the contribution of the fluctuating dilatation in compressible turbulence to the overall dissipation rate, $C_{1\varepsilon}, C_{2\varepsilon}$, and $C_{3\varepsilon}$ are constants, σ_κ and σ_ε are the turbulent Prandtl numbers for κ and ε respectively, S_κ and S_ε are user-defined source terms.

The turbulent or eddy viscosity μ_t is calculated from

$$\mu_t=\rho C_\mu\frac{\kappa^2}{\varepsilon} \qquad 3.34$$

Where C_μ is a constant.

The model constants $C_{1\varepsilon}, C_{2\varepsilon}, C_\mu, \sigma_\kappa$ and σ_ε have the following default values

$$C_{1\varepsilon}=1.44, C_{2\varepsilon}=1.92, C_\mu=0.09, \sigma_\kappa=1.0 \text{ and } \sigma_\varepsilon=1.3 \qquad 3.35$$

These default values have determined experimentally for air and water system and found good enough for wide range of systems. But if necessary the constant can be changed.

From the exact equation for the transport of κ, the production of turbulence kinetic energy, G_κ is defined as

$$G_k=-\rho\overline{u_i'u_j'}\frac{\partial u_j}{\partial x_i}=\frac{1}{2}\mu_t\left[\nabla\overline{U}_i+\left(\nabla\overline{U}_i\right)^T\right]^2 \qquad 3.36$$

If nonzero gravitational field and temperature gradient are present together, the model considers the generation of κ due to buoyancy force. The generation of turbulence due to buoyancy force is given by

$$G_b=\beta g_i\frac{\mu_t}{\mathrm{Pr}_t}\frac{\partial T}{\partial x} \qquad 3.37$$

Where Pr_t is the Prandtl number for thermal energy and g_i is the component of velocity vector in the i[th] direction, For standard and realizable $\kappa-\varepsilon$ model the default values of Pr_t is 0.85. In case of RNG $\kappa-\varepsilon$ model, $\mathrm{Pr}_t = 1/\alpha$, where α is calculated from

$$\left|\frac{\alpha-1.3929}{\alpha_0-1.3929}\right|^{0.6321}\left|\frac{\alpha+2.3929}{\alpha_0+2.3929}\right|^{0.3679}=\frac{\mu}{\mu_t} \qquad 3.38$$

Where $\alpha_0 = 1/\mathrm{Pr} = k/\mu C_P$

The coefficient of thermal expansion, β, is defined as

$$\beta = -\frac{1}{\rho}\left(\frac{\partial\rho}{\partial T}\right)_P \qquad 3.39$$

The effect of buoyancy on the ε is not well understood. The effect is determined by the value of $C_{3\varepsilon}$, which is calculated by

$$C_{3\varepsilon} = \tanh\left|\frac{\upsilon}{u}\right| \qquad 3.40$$

Where υ, the component velocity is parallel to the gravitational direction and u is the component of flow velocity perpendicular to its direction. $C_{3\varepsilon}$ becomes 1.0 if main flow direction is aligned with the direction of gravity, and it becomes zero if the flow direction is perpendicular to the direction of gravity.

In case of high Mach-numbers compressible flow, the turbulence gets effected by "dilatation dissipation", Y_M. It is expressed as

$$Y_M = 2\rho\varepsilon M_t^2 \qquad 3.41$$

Where M_t is the turbulent Mach-number, defined as

$$M_t = \sqrt{\frac{\kappa}{a^2}} \qquad 3.42$$

Where a is the speed of sound. In case of incompressible fluid Y_M is zero.

3.3.2 RNG $\kappa-\varepsilon$ Model

The RNG-based $\kappa-\varepsilon$ turbulence model is derived from the instantaneous Navier-Stokes equations, using a mathematical technique called "renormalization group" (RNG) methods. The RNG is better than standard $\kappa-\varepsilon$ model with wide range of application and better performance especially for more strained fluid flow problems and swirling flow. The standard $\kappa-\varepsilon$ model is good at high Reynolds number, while RNG model is very efficient for low to high range of Reynolds number.

The transport equation for κ is

$$\frac{\partial}{\partial t}(\rho\kappa)+\frac{\partial}{\partial x_i}(\rho\kappa\upsilon_i)=\frac{\partial}{\partial x_i}\left[\alpha_k\mu_t\frac{\partial\kappa}{\partial x_i}\right]+G_\kappa+G_b-\rho\varepsilon-Y_M+S_\kappa \tag{3.43}$$

The transport equation for ε is

$$\frac{\partial}{\partial t}(\rho\varepsilon)+\frac{\partial}{\partial x_i}(\rho\varepsilon\upsilon_i)=\frac{\partial}{\partial x_i}\left[\alpha_\varepsilon\mu_t\frac{\partial\varepsilon}{\partial x_i}\right]+C_{1\varepsilon}\frac{\varepsilon}{\kappa}(G_k+C_{3\varepsilon}G_b)-C_{2\varepsilon}\rho\frac{\varepsilon^2}{\kappa}-R_\varepsilon+S_\varepsilon \tag{3.44}$$

The calculation methods and values common terms in RNG transport equations are same to standard $\kappa-\varepsilon$ model with $C_\mu=0.0845$at high Reynolds number. At low Reynolds number, the following equation is integrated to obtain μ_t.

$$d\left(\frac{\rho^2\kappa}{\sqrt{\varepsilon\mu}}\right)=1.72\frac{\hat{\nu}}{\sqrt{\hat{\nu}^3-1+C_\nu}}d\hat{\nu} \tag{3.45}$$

Where $C_\nu\approx100$and the μ_t is calculated from

$$\mu_t=\hat{\nu}\mu \tag{3.46}$$

The $\alpha_\kappa=\alpha_\varepsilon=\alpha$ terms can be calculated using Eq. 3.41. R_ε is found solving Eq. 3.52.

$$R_\varepsilon=\frac{C_\mu\rho\eta^3(1-\eta/\eta_0)\varepsilon^2}{1+\beta\eta^3}\frac{\varepsilon^2}{\kappa} \tag{3.47}$$

Where $\eta\equiv S\kappa/\varepsilon$, $\eta\approx3.0$, $\eta_0=4.38$, and $\beta=0.012$.

The derived values of $C_{1\varepsilon}=1.42$ and $C_{2\varepsilon}=1.68$ are used in RNG model.

3.3.3 Realizable $\kappa-\varepsilon$ model

The term "realizable" means that the model satisfies certain mathematical constraints on the Reynolds stresses, consistent with the physics of turbulent flows. Neither the standard $\kappa-\varepsilon$ model nor the RNG $\kappa-\varepsilon$ model is realizable. In many cases it predicts more accurately the spreading rate of both planar and round jets. The flows involving rotation, boundary layers formations under strong adverse pressure gradients, separation, and recirculation can be predicted better by realizable $\kappa-\varepsilon$ model.

The transport equation for κ in the realizable $\kappa-\varepsilon$ model is same to standard model. The modified realizable ε model is

$$\frac{\partial}{\partial t}(\rho\varepsilon)+\frac{\partial}{\partial x_i}(\rho\varepsilon\upsilon_i)=\frac{\partial}{\partial x_i}\left[\left(\mu+\frac{\mu_t}{\sigma_\varepsilon}\right)\frac{\partial\varepsilon}{\partial x_i}\right]+\rho C_1 S_\varepsilon-\rho C_2\frac{\varepsilon^2}{\kappa+\sqrt{\nu\varepsilon}}+C_{1\varepsilon}\frac{\varepsilon}{\kappa}C_{3\varepsilon}G_b+S_\varepsilon \qquad 3.48$$

Where

$$C_1=\max\left[0.43,\frac{\eta}{\eta+5}\right],\ \eta=S\frac{\kappa}{\varepsilon},\ S=2S_{i,j}S_{i,j} \qquad 3.49$$

Eq. 3.34 is used to calculate turbulent viscosity, μ_t with C_μ as

$$C_\mu=\frac{1}{A_0+A_s\dfrac{kU^*}{\varepsilon}} \qquad 3.50$$

Where

$$U^*\equiv\sqrt{S_{ij}S_{ij}+\tilde{\Omega}_{ij}\tilde{\Omega}_{ij}} \qquad 3.51$$

and

$$\tilde{\Omega}_{ij}=\Omega_{ij}-2\varepsilon_{ijk}\omega_k \qquad 3.52$$

$$\Omega_{ij}=\overline{\Omega}_{ij}-\varepsilon_{ijk}\omega_k \qquad 3.53$$

$\overline{\Omega}_{ij}$ is the mean rate of rotation tensor viewed in a rotating reference frame with the angular velocity ω_k. The constants A_0 and A_s are

$$A_0 = 4.04,\ A_s = \sqrt{6}\cos\phi \tag{3.54}$$

Where

$$\phi = \frac{1}{3}\cos^{-1}\left(\sqrt{6}W\right) \tag{3.55}$$

$$W = \frac{S_{ij}S_{jk}S_{kj}}{\bar{S}^3} \tag{3.56}$$

$$\bar{S} = \sqrt{S_{ij}S_{ij}} \tag{3.57}$$

$$S_{ij} = \frac{1}{2}\left(\frac{\partial u_j}{\partial x_i} + \frac{\partial u_i}{\partial x_j}\right) \tag{3.58}$$

The other constants terms are

$C_{1\varepsilon} = 1.44, C_2 = 1.9$, $\sigma_\kappa = 1.0$ and $\sigma_\varepsilon = 1.2$

In this study the both the single phase models and multiphase models are used for solving the respective category problems. This model will calculate one transport equation for the momentum and one for continuity for each phase, and then energy equations are solved to study the thermal behaviour of the system. The theory for this model is taken from the ANSYS Fluent 12.0.

3.4 MULTIPHASE MODELING EQUATIONS

A large number of flows encountered in nature and technology are a mixture of phases. Physical phases of matter are gas, liquid, and solid, but the concept of phase in a multiphase flow system is applied in a broader sense. In multiphase flow, a phase can be defined as an identifiable class of material that has a particular inertial response to and interaction with the flow and the potential field in which it is immersed. Currently there are two approaches for the numerical calculation of multiphase flows: the Euler-Lagrange approach and the Euler-Euler approach.

3.4.1 Euler-Lagrange approach

The Lagrangian discrete phase model in ANSYS FLUENT follows the Euler-Lagrange approach. The fluid phase is treated as a continuum by solving the Navier-Stokes equations, while the dispersed phase is solved by tracking a large number of particles, bubbles, or

droplets through the calculated flow field. The dispersed phase can exchange momentum, mass, and energy with the fluid phase.

3.4.2 Euler-Euler approach

In the Euler-Euler approach, the different phases are treated mathematically as interpenetrating continua. Since the volume of a phase cannot be occupied by the other phases, the concept of phase volume fraction is introduced. These volume fractions are assumed to be continuous functions of space and time and their sum is equal to one.

In ANSYS FLUENT, three different Euler-Euler multiphase models are available: the volume of fluid (VOF) model, the mixture model, and the Eulerian model.

In the present work VOF model is used and hence discussed here. The VOF model is a surface-tracking technique applied to a fixed Eulerian mesh. It is used for two or more immiscible fluids where the position of the interface between the fluids is of interest. In the VOF model, a single set of momentum equations is shared by the fluids, and the volume fraction of each of the fluids in each computational cell is tracked throughout the domain.

3.4.2.1 Volume of Fluid (VOF) Model

The VOF formulation in ANSYS FLUENT is generally used to compute a time-dependent solution, but for problems in which concerned are only with a steady-state solution; it is possible to perform a steady-state calculation provided solution is independent of initial guess. In case of vortex formed system with liquid-gas interface, the solution depends on the initial liquid height and hence transient solution method should be chosen.

3.4.2.1.1 Volume Fraction Equation

The tracking of the interface(s) between the phases is accomplished by the solution of a continuity equation for the volume fraction of one (or more) of the phases. For the q^{th} (fluid's volume fraction) phase, this equation has the following form:

$$\frac{1}{\rho_q}\left[\frac{\partial}{\partial t}\left(\alpha_q \rho_q\right)+\nabla.\left(\alpha_q \rho_q \vec{\upsilon}_q\right)=S_{\alpha_q}+\sum_{p=1}^{n}\left(\dot{m}_{pq}-\dot{m}_{qp}\right)\right] \qquad 3.59$$

Where $\dot{m}_{qp}$ is the mass transfer from phase q to phase p and $\dot{m}_{pq}$ is the rate of mass transfer from phase p to phase q. By default, the source term on the right-hand side of Eq. 3.8, S_{α_q} is zero, but we can specify a constant or user-defined mass source for each phase. The volume fraction equation will not be solved for the primary phase; the primary-phase volume fraction will be computed based on the following constraint:

$$\sum_{p=1}^{n} \alpha_q = 1 \qquad 3.60$$

3.4.2.1.2 Material Properties

The properties appearing in the transport equations are determined by the presence of the component phases in each control volume. In a two-phase system, for example, if the phases are represented by the subscripts 1 and 2, and the mixture density in each cell is given by

$$\rho = \alpha_2 \rho_2 + (1 - \alpha_2)\rho_1 \qquad 3.61$$

In general, for n phase system, the volume-fraction-averaged density takes on the following form:

$$\rho = \sum \alpha_q \rho_q \qquad 3.62$$

All other properties (e.g., viscosity) are also computed in this manner.

3.4.2.1.3 Momentum Equation

A single momentum equation is solved throughout the domain, and the resulting velocity field is shared among the phases. The momentum equation, shown below, is dependent on the volume fractions of all phases through the properties ρ and μ.

$$\frac{\partial}{\partial t}(\rho \vec{\upsilon}) + \nabla.(\rho \vec{\upsilon}\vec{\upsilon}) = -\nabla p + \nabla.\left[\mu\left(\nabla \vec{\upsilon} + \nabla \vec{\upsilon}^T\right)\right] + \rho \vec{g} + \vec{F} \qquad 3.63$$

One limitation of the shared-fields approximation is that in cases where large velocity differences exist between the phases, the accuracy of the velocities computed near the interface can be adversely affected.

Chapter 4

STUDY OF RTD OF CSTR USING SWEPT VOLUME METHOD

Mixing is an important feature for continuous reactors. Good mixing improves the efficiency of heat and mass transfer. If the reactants are fed into the reactor premixed, the reaction can start from the entry of reactor itself. On the other hand, under non premixed conditions, reactants must first come in contact for reaction to occur. The mixing time depends on contact time**.** In general mixing can occur due to diffusion, pumping fluid in the reactor and also due to presence of mechanical agitator.

Diffusional mixing relies on concentration or temperature gradients within the fluid inside the reactor. This approach is common with micro reactors where the channel thicknesses are very small and heat can be transmitted to and from the heat transfer surface by conduction. In larger channels and for some types of reaction mixture (especially immiscible fluids), mixing by diffusion is not practically acceptable because of low rate of mixing.

In a continuous reactor, the product is continuously pumped through the reactor. This pump can also be used to promote mixing. If the fluid velocity is sufficiently high, turbulent flow conditions exist (which promotes mixing). The disadvantage with this approach is that it leads to long reactors with high pressure drops and high minimum flow rates. This is particularly true where the reaction is slow or the product has high viscosity. This problem can be reduced with the use of static mixers. Static mixers are baffles in the flow channel which are used to promote mixing. They are able to work with or without turbulent conditions. Static mixers can be effective but still require relatively long flow channels and generate relatively high pressure drops. The oscillatory baffled reactor is specialized form of static mixer where the direction of process flow is cycled. This permits static mixing with low net flow through the reactor. This has the benefit of allowing the reactor to be kept comparatively short.

In most cases, the continuous reactors use mechanical agitation for mixing (rather than the product transfer pump). Whilst this adds complexity to the reactor design, it offers significant

advantages in terms of versatility and performance. With independent agitation, efficient mixing can be maintained irrespective of product throughput or viscosity. It also eliminates the need for long flow channels and high pressure drops.

The mixing performance of a continuous stirred tank reactor (CSTR) can be characterized by residence time distribution analysis. Many experimental and theoretical works on RTD of CSTR have been carried out by a number of researchers (Zwettering, 1959; Danckwerts, 1953; Danckwerts, 1958; Levenspiel and Turner, 1970; Trivedi and Vasudeva, 1974; Lipowska, 1974; Levenspiel et al., 1970; Turner, 1982; Buffham, 1983; Robinson and Tester, 1986; Martin, 2000; Arratia, et al.2004; Hocine, et al, 2008; Yablonskya 2009; Xiao-chang, 2009 etc.). Lipowska, 1974 has done experimental work on the RTD of CSTR for water-glycerin solution. The experimental RTD profiles for a CSTR was developed using potassium chloride as the tracer. The work was carried in their paper covers the effect of viscosity, dimensions of tank, stirrer and feed tube diameter on the RTD behaviour. The present work includes the simulation and prediction of Lipowska, 1974 experimental data at the specified conditions given in the paper. The simulation work was done by the commercial CFD software, ANSYS FLUENT.

4.1 SPECIFICATION OF PROBLEM

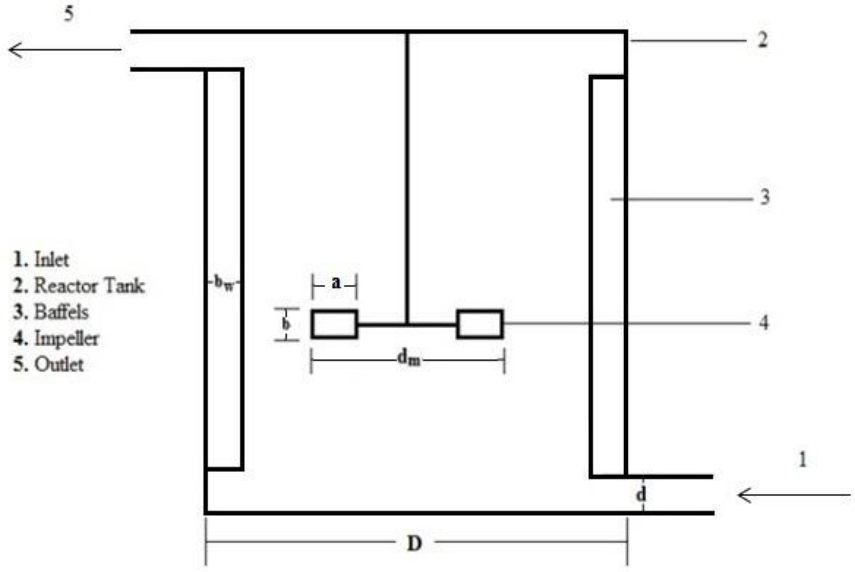

Figure 4.1: Schematic diagram of CSTR (Lipowska, 1974).

A schematic representation of a CSTR with a single inlet and outlet streams is shown in Fig. 4.1 (Lipowska, 1974). Three different tanks used in the present work have diameters of 99, 172 and

250 mm, and the inlet tube diameters are 2, 7.2 and 8.8 mm. Combinations of the above dimensions gives nine tank-inlet tube systems for which the value of *d/D* ratio varied within the limits of 0.008 to 0.0889. The dimension of the reactor and its accessories are given in Table 4.1.

Lipowska, 1974 have found the RTD of the reactor without and with baffles and moving stirrer. The purpose of their work was to find out the tank Reynolds number, which accounts the inlet energy, sufficient for ideal mixing condition. They also have found the minimum number of impeller rotation sufficient to reach ideal mixing in moving stirrer case. For ideal mixing of the liquid solely by the inlet energy, the following relations must be fulfilled (Burghardt and Lipowska, 1972)

$$\mathrm{Re} = \frac{4V^{*}\rho}{\pi D\mu} \geq 13.5 \qquad 4.1$$

Where Re is the tank Reynolds number based on the tank diameter, and ρ and μ are the liquid density and viscosities respectively, V^{*} is the inlet volumetric flow rate. Eq. 4.1 was developed for a fixed inlet (6.6 mm) and tank diameter (170 mm). Therefore in terms of inlet diameter, *d*, the inlet Reynolds number, Re_{in} can be written form Eq. 4.1 as

$$\mathrm{Re}_{in} = \frac{\mathrm{Re}}{d/D} = \frac{4V^{*}\rho}{\pi\, d\mu} \geq 347 \qquad 4.2$$

Table 4.1: Dimensions of the reactor

S.No		
1	Tank diameter, *D*	99,172,250mm
2	Inlet diameter, *d*	2,7.2,8.8mm
3	No of baffles	4
4	Baffles width (b_w)	*D*/12
5	Type of stirrer	Turbine disc impeller
6	Number of blades in the impeller	6
7	Ratio of impeller to the tank diameter	(d_m/*D*)=1/3
8	Length of the impeller blade, *a*	(d_m/4)
9	Height of the impeller blade, *b*	d_m/5
10	Clearance, *C*	d_m
11	Height of liquid, *H*	*D*

Lipowska, 1974 have extended the work of Burghardt and Lipowska, 1972 to determine the dependency of Re_t and Re_{in} on the d/D ratio. The equations are

$$\mathrm{Re} \geq 569.1\left(\frac{d}{D}\right)^{1.09} \tag{4.3}$$

$$\mathrm{Re}_{in} \geq 569.1\left(\frac{d}{D}\right)^{0.09} \tag{4.4}$$

The above equation shows a little effect of *d/D* ratio on Re_{in}. The equations allow us to calculate the minimum inlet volumetric flow necessary for the ideal mixing of liquid without stirrer.

In case of mixing with mechanical stirrer, the number of revolutions needed for ideal mixing can be evaluated from (Lipowska, 1974)

$$n = 2428.2\ \mathrm{Re}^{-1.215}\left(\frac{d}{D}\right)^{0.088} \tag{4.5}$$

and the correlations for impeller Reynolds number, Re_m for ideal mixing is

$$\mathrm{Re}_m = \frac{n d_m^2 \rho}{\mu} = 269.8\ \mathrm{Re}^{-0.215}\left(\frac{d}{D}\right)^{0.088} \tag{4.6}$$

Lipowska, 1974, in his experimental findings of RTD, has used step change of potassium chloride (KCl) concentration in the feed. But they have not mentioned the exact concentration of KCl in the feed stream. Thus it becomes difficult to guess the exact input data of KCl in the feed. Fortunately the expression for RTD function, $I(\theta)$ (internal age distribution function) for the moving impeller case is given in the paper and the equation for it is

$$I(\theta) = \exp\left[-\left(\frac{V^*}{Q}+1\right)\theta\right] \tag{4.7}$$

where $\theta = t/\tau$, τ is the holdup time of liquid in the tank, V^* is the inlet volumetric flow rate, Q is impeller pumping capacity given by

$$Q = 2.3 n d_m^2 b\ \mathrm{cm}^3/\mathrm{sec} \tag{4.8}$$

Where n is the rpm of the impeller. According to Eq. 4.7, mixing is ideal when $V^*/Q \to 0$. The inlet volumetric flow rate is evaluated by $V^* = A_{in} u_{in}$, where A_{in} is the inlet normal cross sectional area and u_{in} net inlet velocity. The work in this chapter finds the value of Q using ANSYS FLUENT followed by calculation of $I(\theta)$ for moving stirrer CSTR. The computed values of $I(\theta)$ are

compared with the experimental $I(\theta)$ values found by Lipowska, 1974 using tracer injection method. In CSTR with out stirrer and baffles, the definition of Q is not valid. Hence, different KCl concentrations in the feed are taken in the simulation for finding $I(\theta)$ using the following expression.

$$I(\theta) = \frac{C_0^+ - C(t)}{C_0^+ - C_0^-} \qquad 4.9$$

Where KCl concentration in the inlet changes from C_0^- to C_0^+, and $C(t)$ is the concentration of KCl in the outlet at any time, t.

In this chapter, the computed values of $I(\theta)$ either using Eq. 4.7 or Eq. 4.9 are compared with the experimentally found data using tracer injection method (Lipowska, 1974). The effects of number of rotation of the impeller and the viscosity of water-glycerin solution on the nature of mixing also are studied theoretically here.

4.2 MATERIAL AND FLOW PROPERTIES

The liquid used in the present work is water – glycerin solution same to Lipowska, 1974. The properties of the solution are given in Table 4.2 and 4.3.

Table 4.2: Parameters used for non moving case [Lipowska, 1974]

No of experiments	*D* (mm)	*d* (mm)	μ (cP)	ρ (kg/m^3)	*V** (l/hr)	τ (min)	Type of Flow
1	99	2	1	1000	0.621	72.6	Dispersion
2	99	2	1	1000	1.028	44.86	-do-
3	99	2	1	1000	1.563	29.33	Dispersion
4	99	2	1	1000	1.922	24.84	Ideal
5	250	2	7.75	1141	12.82	57.44	Dispersion
6	250	2	7.75	1141	12.30	61.07	-do-
7	250	2	7.75	1141	17.42	42.27	Ideal

Where τ is the time constant or holdup time of the reactor and is defined as

$$\tau = \frac{V}{V^*} \qquad 4.10$$

Eq. 4.10 is used to find out the liquid volume, V inside the reactor for a given τ . In without stirrer case, the concentration of KCl in feed in terms of mass fraction ranges from 10^{-4} to 10^{-6}. The diffusivity of KCl in the solution is taken as 1.95 X 10^{-9} m^2/s (Harned and Nuttal, 1949).

Table 4.3: Parameters used for moving impeller case [Lipowska, 1974].

No of experiments	D(mm)	d (mm)	μ (cP)	μ (kg/m^3)	V* (l/hr)	τ (min)	N rpm	Type of Flow
1	99	7.2	9.2	1150	2.653	20.46	50	Dispersion
2	99	7.2	9.2	1150	2.653	20.46	70	-do-
3	99	7.2	9.2	1150	2.524	18.11	80	Ideal
4	99	7.2	9.2	1150	2.524	18.11	90	Ideal
5	172	2	9.8	1183	12.24	19.58	20	Dispersion
6	172	2	9.8	1183	12.56	19.04	30	Dispersion
7	172	2	9.8	1183	12.56	19.04	35	Ideal
8	250	8.8	19.7	1179	16.42	44.83	12	Dispersion
9	250	8.8	19.7	1179	16.50	44.60	20	Dispersion
10	250	8.8	19.7	1179	16.50	44.60	25	Ideal
11	250	8.8	19.7	1179	16.50	44.60	40	Ideal

4.3 GEOMETRY AND MESHING OF THE REACTOR

The geometry of the CSTR with four baffles and a single stirrer as shown in Fig. 4.2a is designed using Ansys 12.0 workbench. The inlet and outlet tubes are also shown in the figure. The CSTR is divided into two parts: stationary and moving zones. The moving zone includes stirrer and cylindrical disk volume around the impeller, which is clearly visible in Fig. 4.2a. Both the zones are connected by interface. The meshing based on the physics and size of the problem is carried out in the workbench

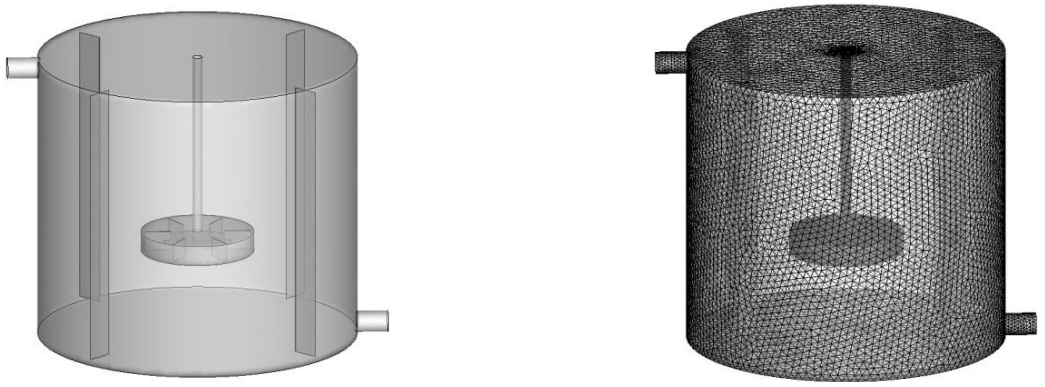

(a) (b)

Figure 4.2: Geometry of the stirred tank reactor prepared in ANSYS Workbench.

The type of mesh chosen is unstructured tetrahedral. The meshed CSTR is shown in Fig. 4.2b. The number elements depend on the size of the CSTR. Hence it is equal to 7, 35,231, 8, 14,782 and 8, 74,273 for the tank with diameters of 99mm, 172mm. and 250mm respectively.

4.4 MODEL EQUATIONS AND SOLUTION ALGORITHM

In the simulation work by ANSYS Fluent 12.0, laminar flow model is used. The CSTR without stirrer and baffles are solved only with laminar models. The MRF (multiple reference frames) model is used for solving moving stirrer case. The respective CFD model equations are discussed in Chapter 3. The hydrodynamics equations of CSTR with water-glycerin solution are solved first by steady state solver. Under convergence of these equations, KCl is introduced in the tank by a step change. The mass equation for KCl along with the hydrodynamics equations are then solved by unsteady state method. The well-known SIMPLE algorithm is used to solve the CFD equations. Pressure gradients are discretized using standard central difference scheme. The convective terms in the momentum equations are discretized by first order upwind scheme for the sake of stability. The discretized partial differential equations are solved by Gauss-Seidel iterative method. After each iteration, the dependent variables are modified by relaxation method and used in the next iteration until the solutions are converged. The equation used for relaxation method is as follows:

$$u_{i,j}^{l+1} = \alpha u_{i,j}^{l+1} + (1-\alpha) u_{i,j}^{l} \qquad 4.11$$

Where, $u_{i,j}$ is the velocity at the nodal point, and α is the under-relaxation factor. The values of under-relaxation factors for pressure, momentum, density, body forces and KCl mass equations are 0.3, 0.7, 1.0, 1.0 and 1.0 respectively. A stringent value all the residual of the transport equations is used in the simulation and it is of the order of 10^{-3}. In each system, with constant liquid viscosity, the inlet flow rates/rotation of the impeller have been changed from lower to higher values, until the residence function $I(\theta)$ fitted the ideal mixing line i.e. the curve for $\exp(-\theta)$ function.

Power number depends on the tip speed and on the projected area of the blades.The Power number is calculated by the following equation,

$$N_P = \frac{P}{\rho N^2 d_m^5} \qquad 4.12$$

Where P is the power input, which is calculated from the torque, Γ applied on the impeller shaft, where *N* should be used in rotation per second.

The torque is estimated from the pressure differential on the blades and the shear stress, τ, on the disc which is given as

$$\Gamma = \sum_i (p_1 - p_2)_i . r_i . \delta A_i + \sum_j \tau_j . r_j . \delta A_j \qquad 4.13$$

Where the summation is done over the control cells i corresponding to each blade, and j corresponds to the disc.

The power is then calculated from the measurements of the torque and the shaft speed

$$P = 2\pi N \Gamma \qquad 4.14$$

Flow number is calculated by the following equations

$$N_q = \frac{Q}{N d_m^3} \qquad 4.15$$

The impeller Reynolds number is defined as

$$\mathrm{Re}_m = \frac{\rho N d_m^2}{\mu} \qquad 4.16$$

Where *Q* is the flow discharge through the impeller or the swept volume of the impeller. The discharge flow was estimated by calculating a summation of differential discharge flow over a cylindrical area spanning the width of the impeller blades.

4.5 BOUNDARY CONDITIONS

The cell zone consists of state of the material (either fluid or solid) in the respective zone. The mixture of water-glycerin solution is considered as a single phase. 273K temperature and 101 325 Pa pressure is used as the operating condition. Water enters the reactor through the inlet pipe, and the velocity of water at the inlet is used as specified value. At the exit boundary of the outlet pipe, the gauge pressure is taken as zero. The rotation of the impeller is specified. On the wall including impeller and shaft, and baffles no slip condition is used.

4.6 RESULTS AND DISCUSSIONS

4.6.1 Study on Mixing without Stirrer and Baffles

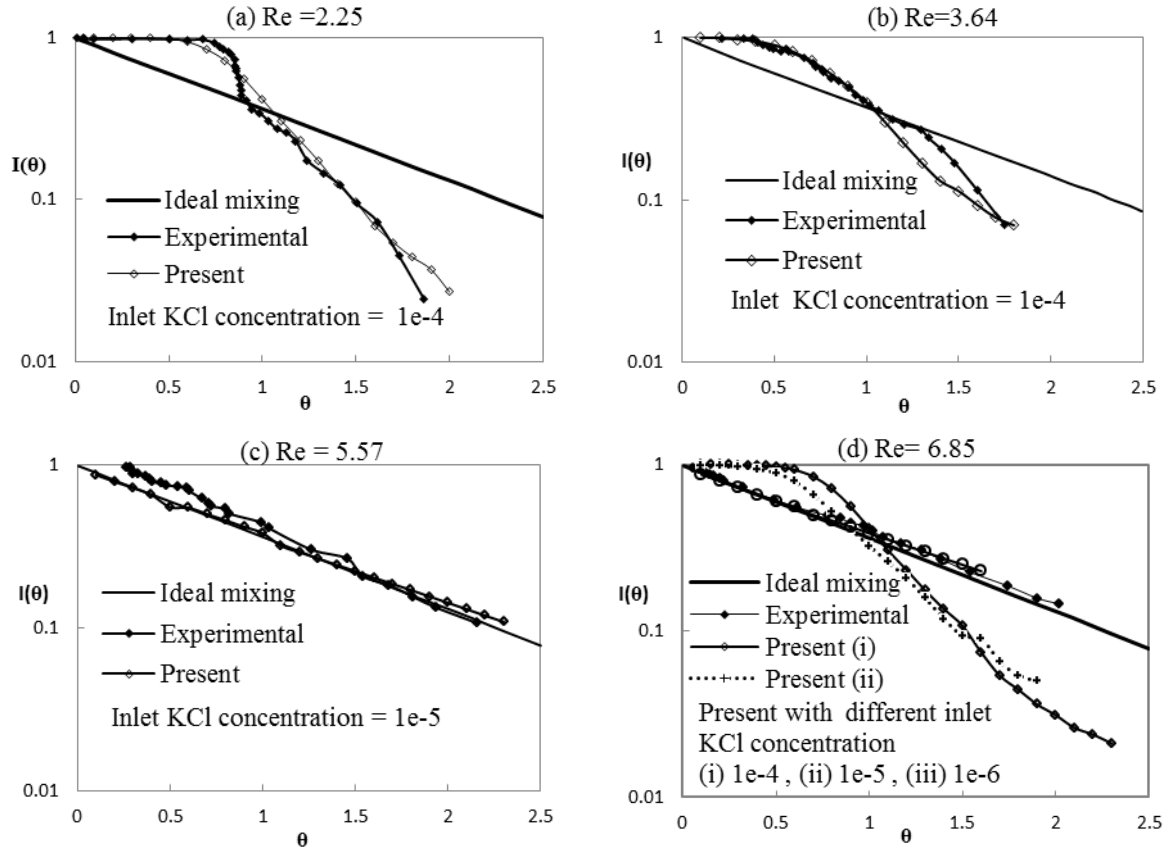

Figure 4.3: Plot of $I(\theta)$ vs. θ for a CSTR without stirrer and baffles and with *D* = 99 mm, *d* = 2mm, $\mu = 1$ cp and ρ = 1000Kg/m^3

Potassium chloride is injected in the tank as tracer and the concentration of it is noted with time at the outlet. $I(\theta)$ is calculated using Eq. 4.9. The mixing line represents ideal mixing condition with $I(\theta) = \exp(-\theta)$. Using the parameters given in Table 4.2, the computations are carried with very low concentration of KCl in the rage of 10^{-4} to 10^{-6} mass fraction at the inlet. The computed values of $I(\theta)$ are compared with experimental data (Lipowska, 1974) and also with mixing line in Fig. 4.3 for *D* = 99mm and in Fig. 4.4 for *D* = 250mm. The figures depict that $I(\theta)$ depends on the inlet KCl concentration and at high Re value, a match with experimental data is observed at relatively lower KCl concentration. The results show an excellent agreement with the experimental results with proper feed KCl concentration. Both the figures depict that the hydrodynamics of CSTR approaches dispersion flow to ideal mixing with increasing tank Reynolds number (Re) as given along the respective figures. The present computed values are in

well agreement with the fluid mixing state as given in Table 4.2. When KCl enters the tank through larger diameter inlet, it spreads more in liquid inside the tank compared to the lower diameter inlet. Therefore, the system approaches ideal mixing state at much lower value of Reynolds number as inlet tube diameter increases from 2 mm to 8.8 mm.

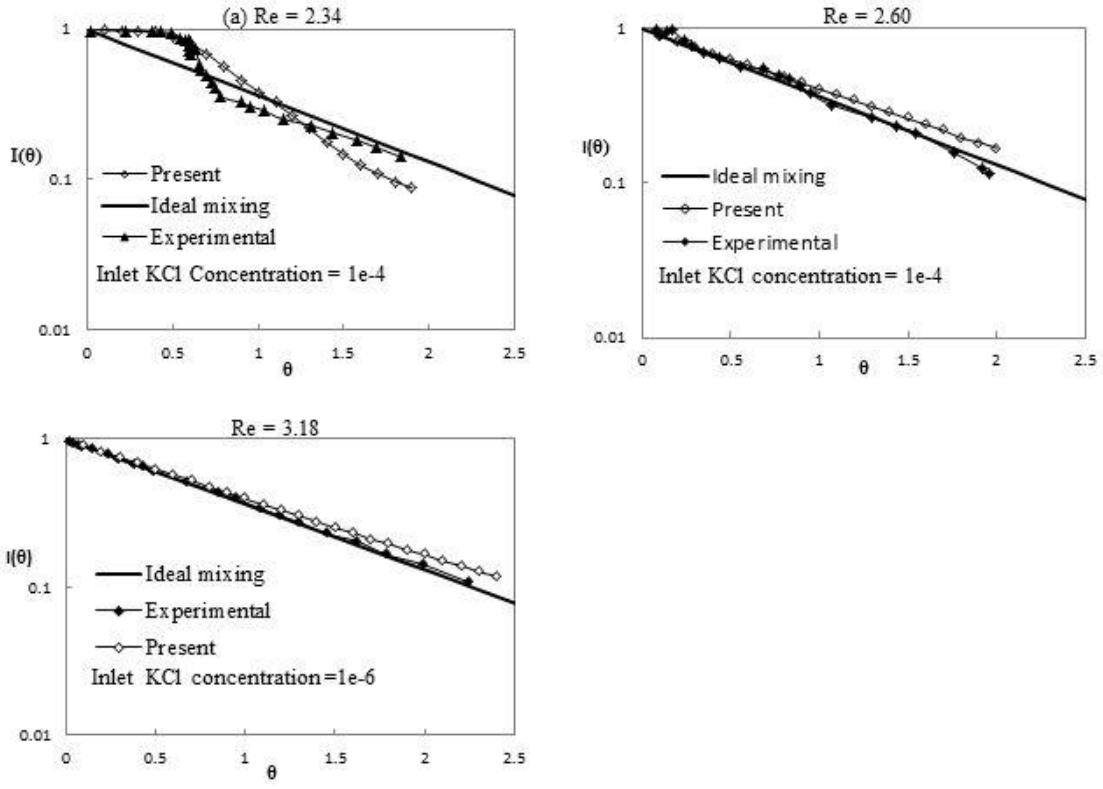

Figure 4.4: Plot of $I(\theta)$ vs. θ for a CSTR without stirrer and baffles and with D = 250 mm, d = 8.8 mm and $\mu = 7.75$ cp, ρ = 1000Kg/m3

4.6.2 Study on Mixing with Stirrer and Baffles

Lipowska, 1974 had conducted experiments for moving stirrer for different tank diameters (99,170 and 250mm), inlet diameter (2, 8.8mm) and with different liquid viscosities given in Table 4.3. For given values of D, d and μ, the liquid flow rates and the number of impeller revolutions are varied.

The internal age distribution, *I(θ)* using Eq. 4.7 is evaluated for finding the fluid mixing state in moving impeller case. The swept volume or impeller pumping capacity, *Q* in each case was

evaluated by Eq. 2.23 and taking the iso-surface as the cylindrical disk volume around the impeller as shown in Fig. 4.2. The comparative study between experimental results (Lipowska, 1974) and the present computed values for moving stirrer case are presented in Fig. 4.5, 4.6 and 4.7. The conditions are mentioned along each graph.

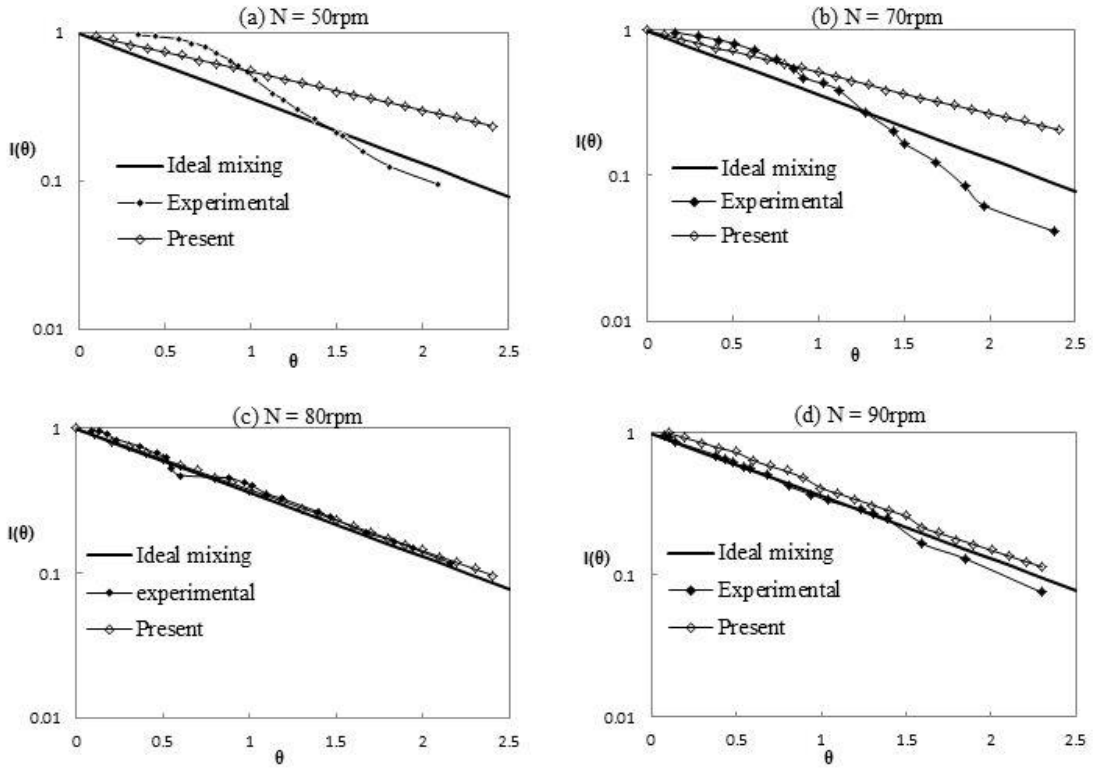

Figure 4.5: Plot of $I(\theta)$ vs. θ for a CSTR with stirrer and baffles and with D = 99mm, d = 7.2 mm, μ = 9.2cp and ρ = 1145 Kg/m^3

In all the figures (Fig. 4.5 to 4.7), the experimental $I(\theta)$ values are obtained from tracer, KCl injection method. Eq. 4.8 shows that the value Q is constant for a particular impeller with fixed angular motion. Thus, the value of V^*/Q is also constant for a particular run. Therefore, the variation of $I(\theta)$ with θ is linear. The linear variation is also observed in the present computed values as shown in Fig. 4.5 to 4.7. The mismatch between the values of experimental and the present values is obvious. But a careful observation finds that the computed values can predict the fluid mixing sate perfectly as mentioned in Table 4.3. The computed $I(\theta)$ approaches the ideal mixing line with increase in impeller rotation, N and the graphs depict that at higher values

of N the CFD results are in excellent agreement with the experimental data. The figures also depict that at initial moment there is a transient Q up to certain θ, and hence a relatively better agreement of computed $I(\theta)$ with the experimental data was observed. It is observed in the figures that the required RPM of the impeller decreases to reach ideal mixing state with increase in the diameter of the vessel.

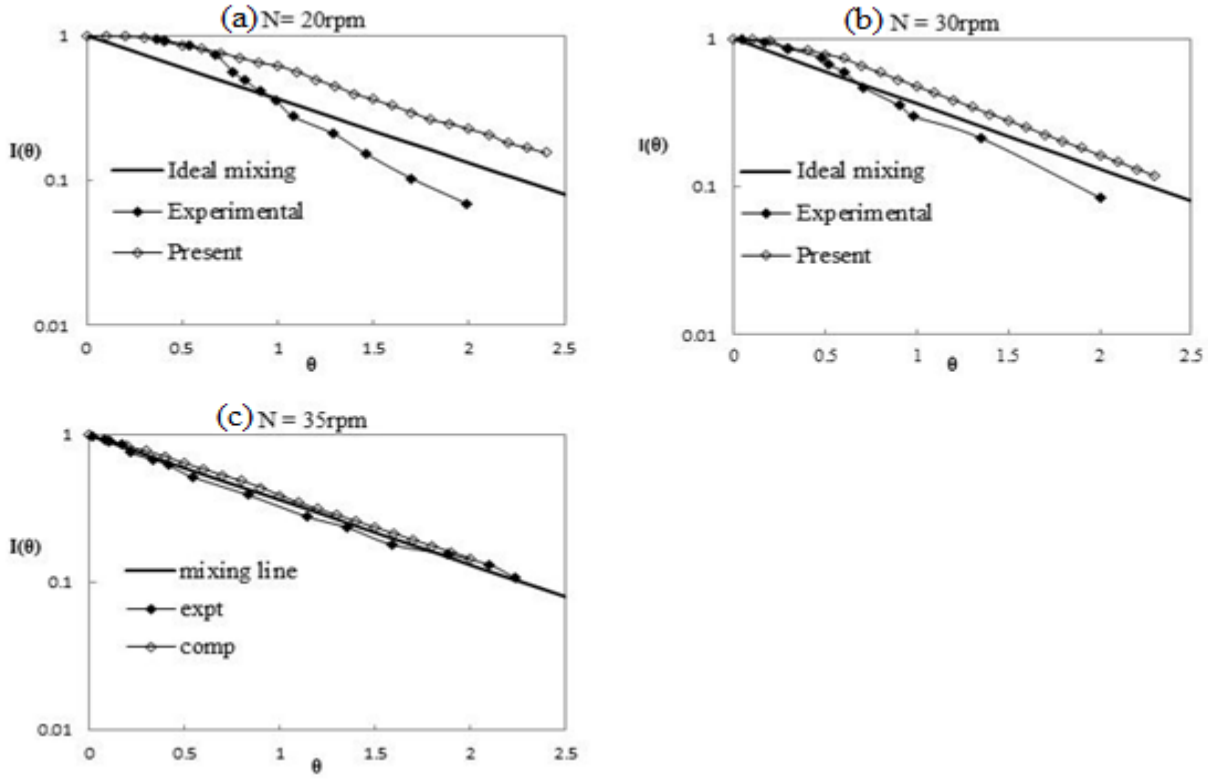

Figure 4.6: Plot of $I(\theta)$ vs. θ for a CSTR with stirrer and baffles and with D = 172mm, d = 2mm, μ = 9.8cp and ρ = 1163Kg/m^3

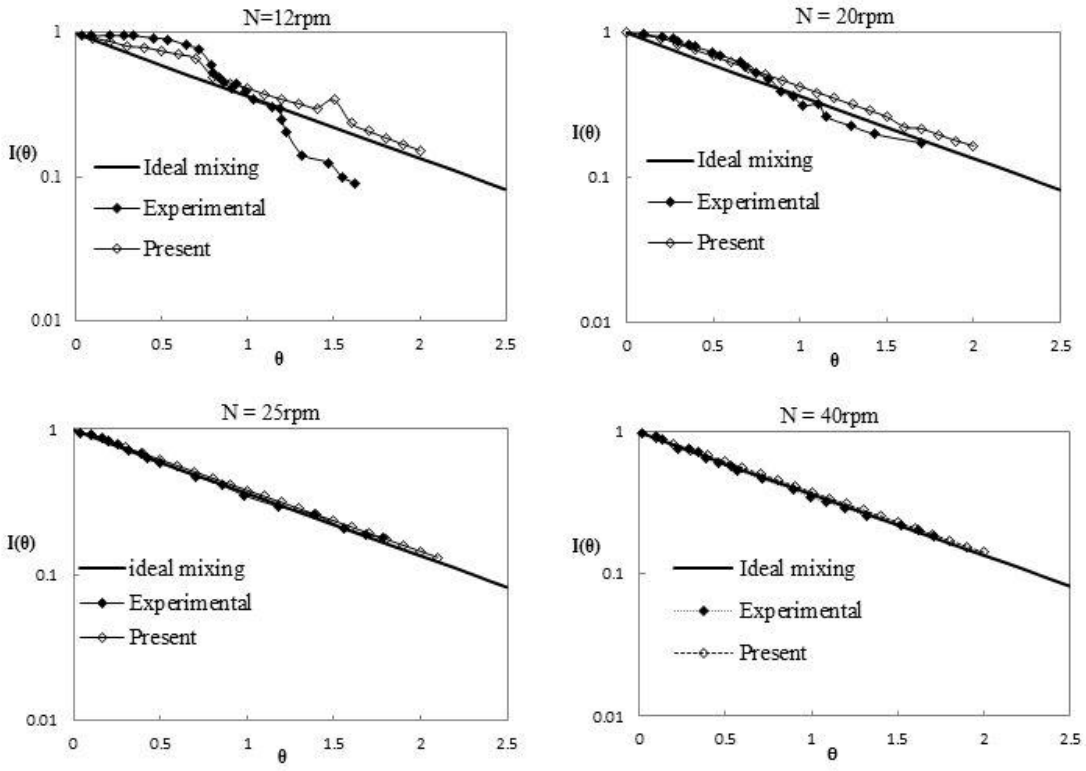

Figure 4.7: Plot of $I(\theta)$ vs. θ for a CSTR with stirrer and baffles and with D = 250mm, d = 8.8mm, μ =19.7cp and ρ = 1179Kg/m^3

4.6.3 Effect of Tank Reynolds Number, RPM of the Impeller, Position of the Outlet, Viscosity and Density of Liquid on the Mixing

The effect of Re, N, position of the outlet, and fluid viscosity and density on the mixing behaviour of liquid in CSTR is studied. Fig. 4.8 represents the effect of Re on $I(\theta)$. At Re 0.98, dispersion flow occurs, at Re 1.03 the mixing line goes relatively closer to ideal mixing line , and further increase in Re to 1.5 and then to 2.03 results in the mixing line to follow ideal mixing line. The energy with the inlet flow increases with increase in V^*, which increases proportionately with Re. This inlet energy helps to mix-up the liquid mixture. Therefore, $I(\theta)$ approaches ideal mixing line with increase in Re as observed in Fig. 4.8.

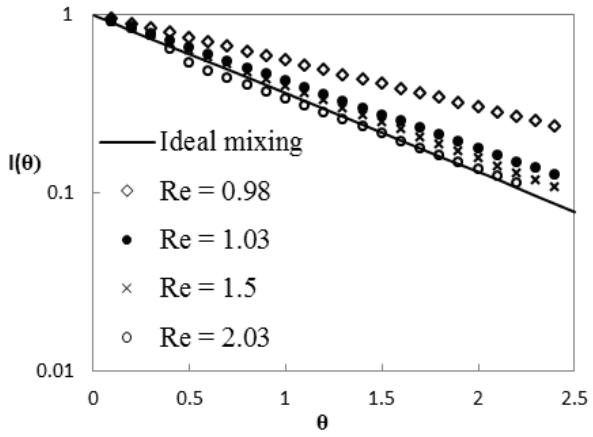

Figure 4.8: Effect of tank Reynolds number, Re on $I(\theta)$ for a CSTR with stirrer and baffles and with D = 99mm, d = 6.6mm, N= 50rpm, $\mu = 9.2$ cP

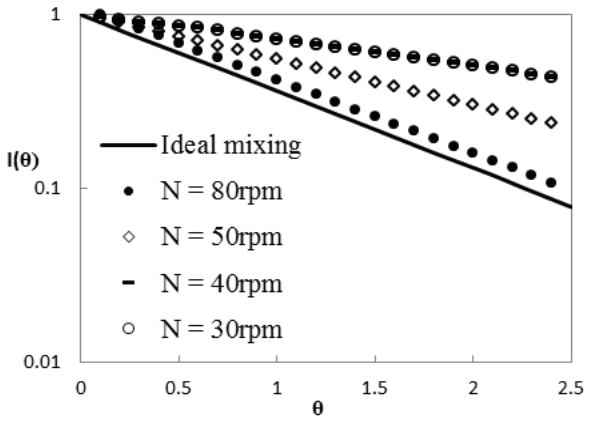

Figure 4.9: Effect of N on $I(\theta)$ for a CSTR with stirrer and baffles and with D = 250mm, d = 6.6mm, μ =9.2cp and ρ = 1145kg/m^3, Re = 1.03

The effect of impeller rpm on the mixing efficiency is demonstrated in Fig. 4.9. It can be observed in the figure that the nature of the flow changes from dispersion to ideal mixing state with increase in *N*. A distinct dispersion flow happens at N equal to 30 and 40 (these two curves are superimposed), and also at 50, whereas at N, 80 the mixing is very near to ideal mixing condition. This is happening naturally as it is well known that the amount of mechanical energy imparted on fluid increase with increase in *N*, and hence more mixing.

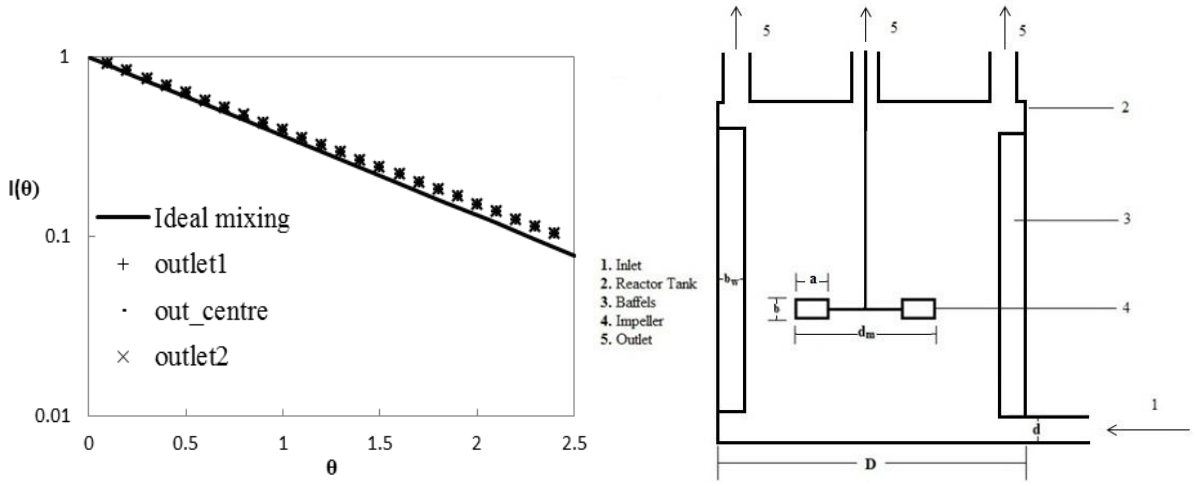

(a) (b)

Figure 4.10: Effect of outlet position on $I(\theta)$ for a CSTR with stirrer and baffles and with D = 99mm, d = 6.6mm, Re = 1.03, $\mu = 9.2$ cP, N = 50 rpm

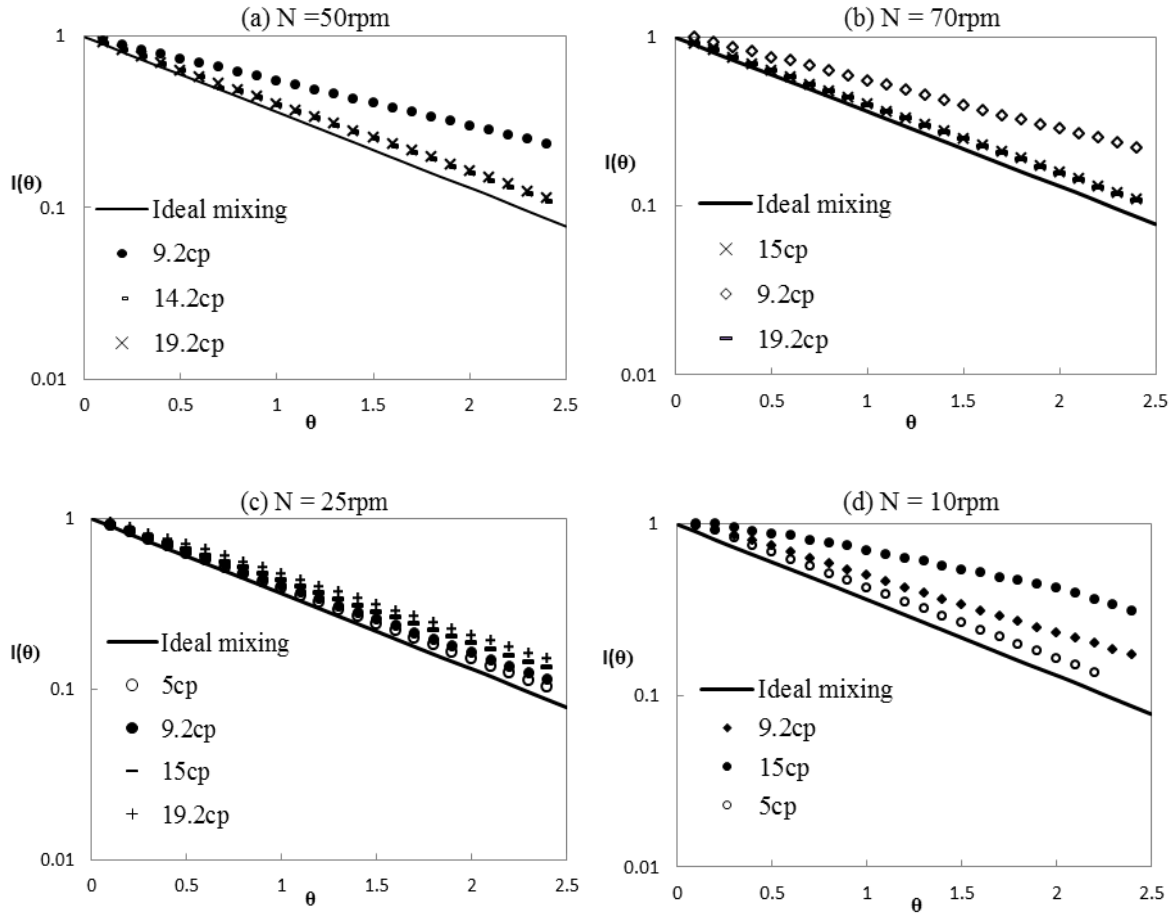

Figure 4.11: Effect of viscosity of liquid on $I(\theta)$ for a CSTR with stirrer and baffles with D = 99mm, d = 6.6mm, Re = 1.03.

The outline can be kept at different location on the top surface of the cylinder which is shown in Fig. 4.10b. Expecting a possible effect on the mixing behaviour, the system is simulated with different outlet position at 50 rpm impeller speed. But it shows no effect on the mixing behaviour and all the mixing line observed in Fig. 4.10 are following mixing line. The absence of the effect of outlet position might have happened due to use of high impeller speed.

Viscosity of fluid has certain effect on the hydrodynamic behaviour of it and in turn on the mixing behaviour. The effect of viscosity of liquid on $I(\theta)$ at different impeller speeds is shown in Fig. 4.11. The effect of viscosity on $I(\theta)$ at high *N* is just reverse of lower values of it. Fig. 4.11 shows that the mixing of liquid moves towards ideal mixing state with increase in viscosity at Re 50 and 70, whereas it moves away from ideal mixing line for *N*, 25 and 10. For a particular Re, V^* increases with increase in viscosity. The viscous force also increases with viscosity. The impeller does more mechanical work at higher values of *N*, and it makes viscous force negligible. Thus the increase of V^* with increase in viscosity results in more mixing, and mixing of liquid moves towards ideal mixing condition at higher impeller rotation. But at lower values of *N*, the amount of energy given by the impeller to the liquid is smaller relatively, and it becomes insufficient for overcoming the viscous force. At low impeller speeds, the curve shows an dispersed flow with partial cirulation of liquid. Due to domination of viscous force at lower *N*, the mixing line moves away from the ideal mixing line.

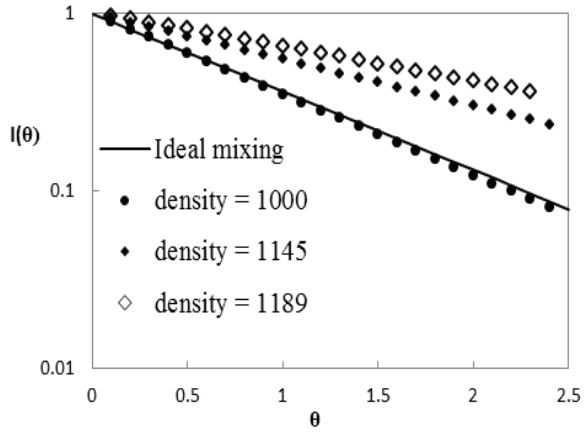

Figure 4.12: Effect of density of liquid on $I(\theta)$ for a CSTR with stirrer and baffles and with D = 99mm, d = 6.6mm, Re = 1.03, $\mu = 9.2$ cP, N = 50 rpm

The effect of density on the mixing behaviour is depicted in Fig. 4.12. According to Eq. 4.1, V^* decreases with increase the density, and it means that contribution of inlet flow energy decreases with increase in density. The mixing line therefore moves away from the ideal mixing line with incease of density of fluid.

4.6.4 Contours of KCl Mass Fraction without Stirrer and Baffles

The contours of mass fraction of KCl for CSTR without impeller and baffles are shown in Fig. 4.13 to 4.16. The graphs are shown in the increasing order of tank Reynolds number, Re at different time θ. The comparison shows that at θ, 0.4, KCl reaches closer to the outlet with increase in Re. It happens due to movement of KCl with inlet fluid like jet towards the opposite wall, and then movement of it up along the wall surface. Due to increase in inlet energy with Re, the homogeneity of the liquid in CSTR increase with increase in Re. The figure also reveals that at lower Re, KCl disperses in the solution at early time compare to higher Re flow. It is also observed that at any Re, KCl fills more space of the cylinder as θ increases.

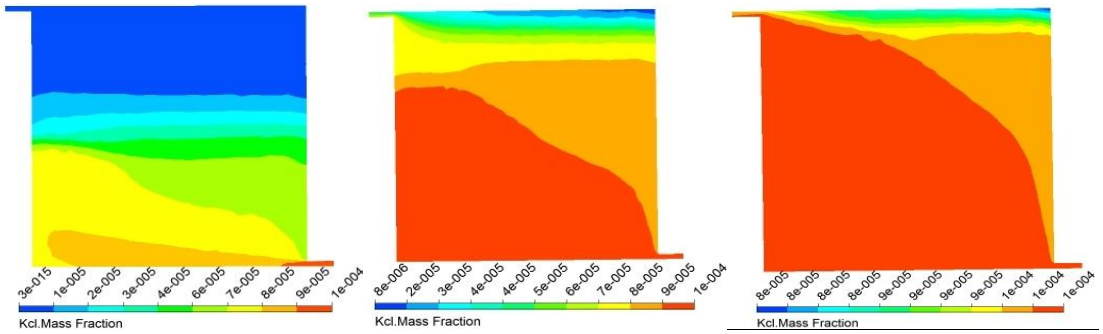

(a) θ = 0.4 (b) θ = 1.0 (c) θ = 2.0

Figure 4.13: The contours of tracer mass fraction for Re = 2.25, D = 99mm, d =2mm, μ = 1cP for the CSTR without moving stirrer

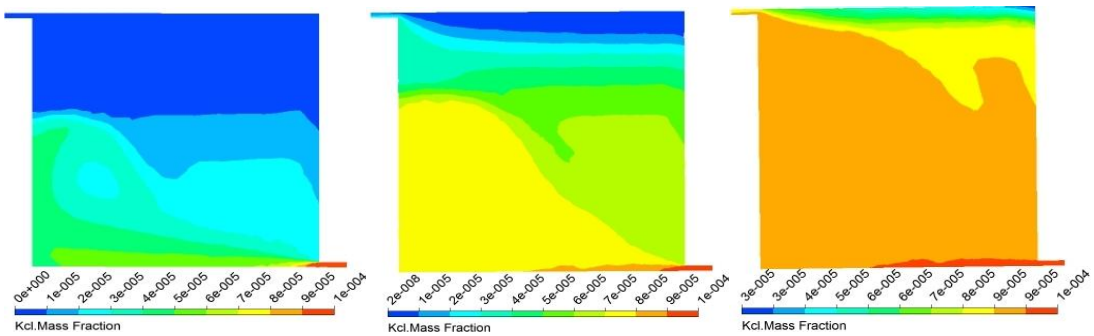

(a) θ = 0.4 (b) θ = 1.0 (c) θ = 2.0

Figure 4.14: The contours of tracer mass fraction at Re = 3.64, D = 99mm, d = 2mm μ = 1cp and ρ = 1000Kg/ for the CSTR without moving stirrer

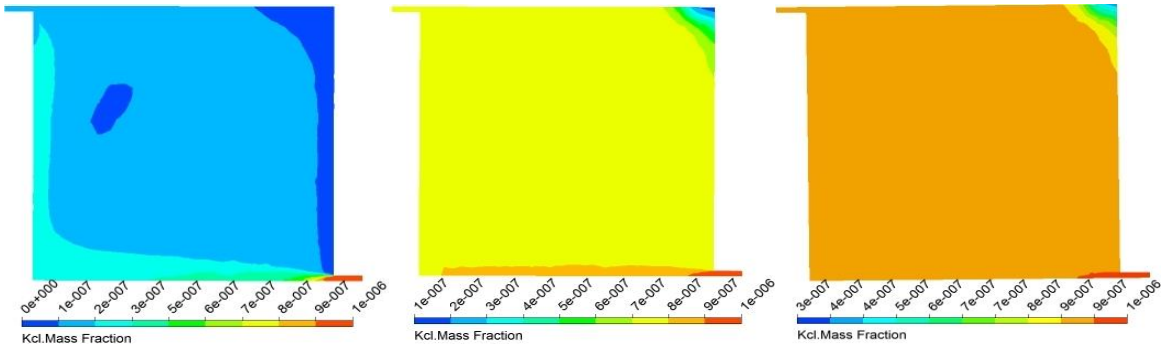

(a) θ = 0.4 (b) θ = 1.0 (c) θ = 2.0

Figure 4.15: The contours of tracer mass fraction atRe = 5.57, D = 99mm, d = 2mm μ = 1cp and ρ = 1000Kg/m^3 for the CSTR without moving stirrer.

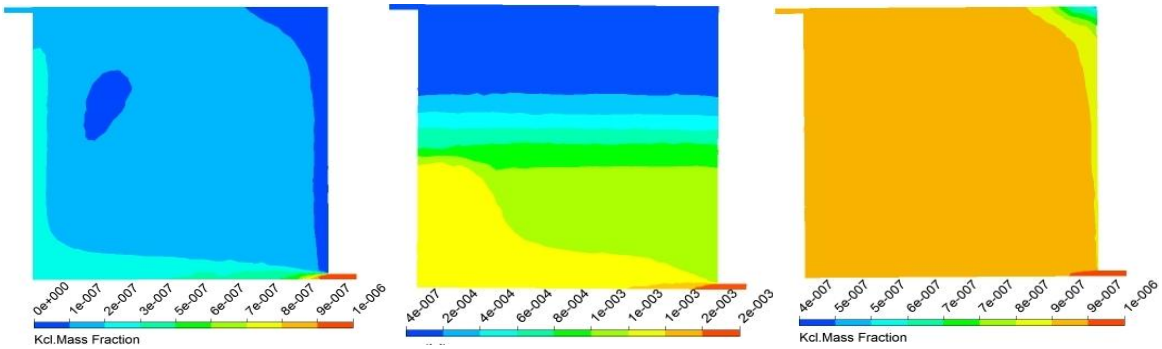

(a) θ = 0.4 (b) θ = 1.0 (c) θ = 2.0

Figure 4.16: The contours of tracer mass fraction at Re = 6.85, D = 99mm, d = 2mm μ = 1cp and ρ = 1000Kg/m^3 for the CSTR without moving stirrer.

4.6.5 Contours of Pressure

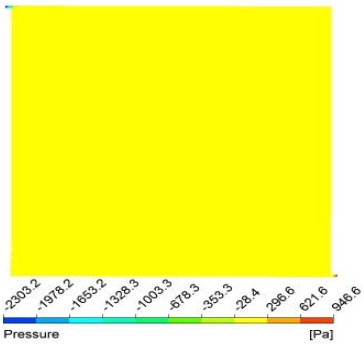

(a) Without stirrer and baffles

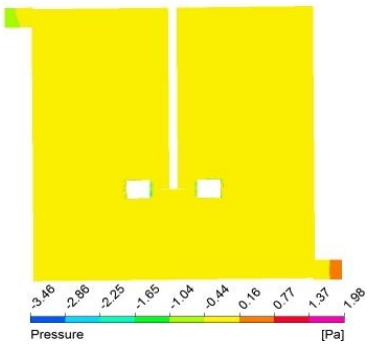

(b) N = 50rpm

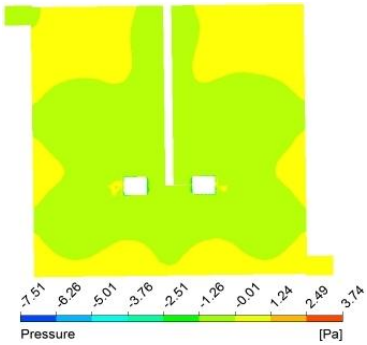

(c) N = 70rpm

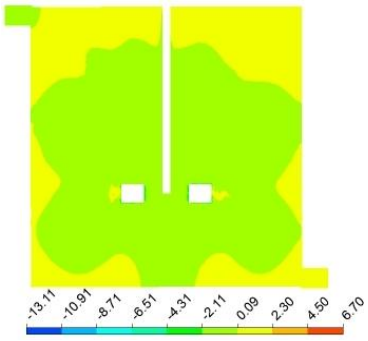

(d) N = 90rpm

Figure 4.17: The contours of pressure for D = 99 mm, (a) d = 2mm, μ = 1cp Re = 2.25, (b-d) d = 6.6mm, μ = 9.2cp, Re = 0.98.

The pressure contours shown in Fig. 4.17 represents that there is an increase in pressure only very near the impeller blades, the impeller is getting enveloped by low pressure area, which itself again surrounded by higher pressure area. The low pressure area increases with increase in RPM of the impeller. It happens because impeller results in higher velocity of the fluid around it, and in turn, it decreases the pressure. The increase of pressure nearer to impeller in radial direction is proportional to impeller speed and overall study shows that it does not depend on the tank diameter. The pressure distribution is found uniform for static impeller case, and the figure also shows that the magnitude of pressure is high in case of without impeller and baffles CSTR.

4.6.6 Velocity Vectors

Fig 4.18 to 4.21 show velocity vector plots in presence and in absence of impeller. By using vectors, the position and motion of a particle can be identified. The flow patterns are shown by

creating plane through the centerline of the CSTR in ANSYS Fluent at different impeller revolutions.

(a) (b)

Figure 4.18: Velocity vectors of CSTR without impeller and baffles with (a) *D* = 99 mm, d = 2mm, Re = 2.25, $\mu = 1cP$; (b) *D* = 250 mm, d = 2 mm, Re = 2.34, $\mu = 7.75cP$.

Fig 4.18 shows that there is no uniformity in flow for CSTRs with two different diameters. The velcoity vector depicts the unsymmetrical flow patterns around the diagonal line connecting the inlet and outlet tubes. It is also observed that with increase in size of the CSTR from 99mm to 250mm diameter the vortex loops decreases. In case of 250mm diameter channel, at the top right side of the reactor ciculation loop is found absent.

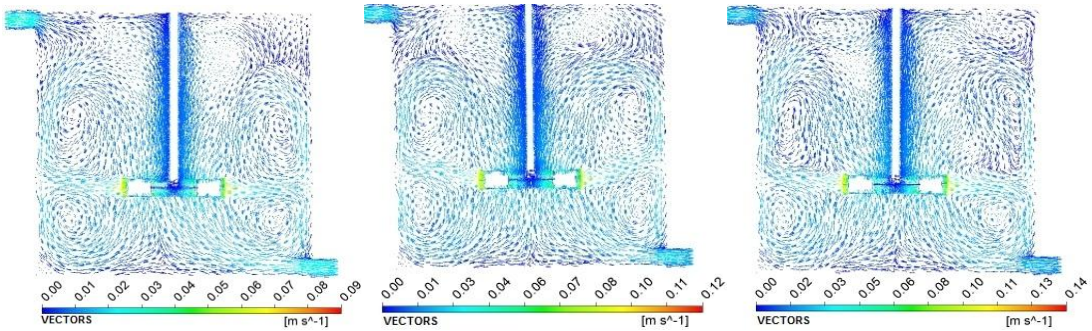

(a) N = 50rpm (b) N = 70rpm (c) N = 80rpm

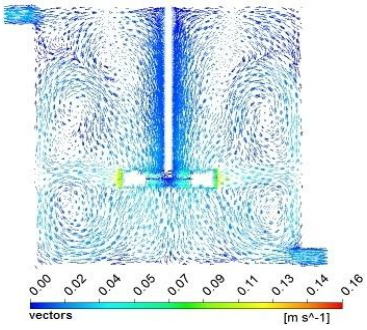

(d) N = 90rpm

Figure 4.19: Velocity vectors with moving impeller having D = 99mm, d = 6.6mm, Re = 0.98 and $\mu = 9.2$ cP.

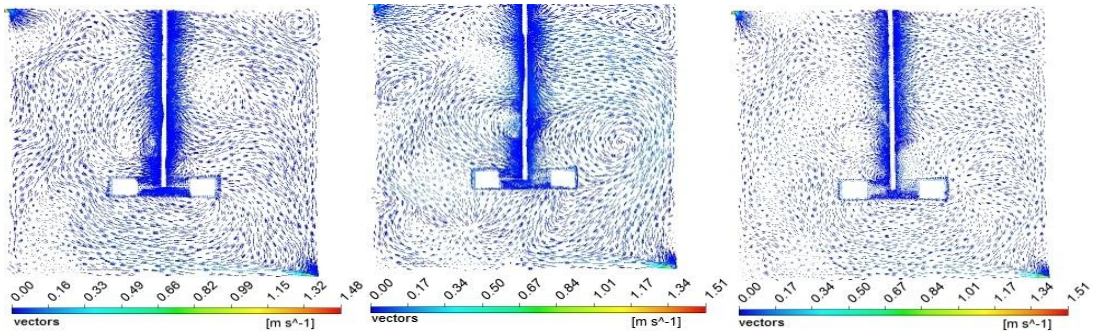

(a) 20rpm (b) 30rpm (c) 35rpm

Figure 4.20: Velocity vectors with moving impeller having D =172mm, d = 2mm, Re = 3.04, $\mu = 9.8cP$.

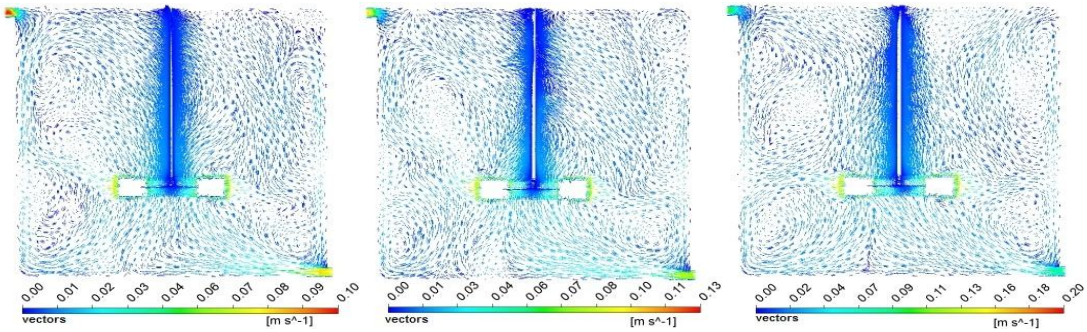

(a) N = 20rpm (b) N = 25rpm (c) N = 40rpm

Figure 4.21: Velocity vectors with moving impeller having D =250mm, d = 8.8mm, Re = 1.37 and $\mu = 19.7cP$.

The velocity vectors for different sized CSTR are shown in Fig. 4.19 to 4.21. The figures show that the flow stream is discharged from the impeller in the radial direction, with part of the flow recirculating along the vessel wall moves towards the bottom and rest part moves towards top surface, and it results in four circulation loops around the impeller specially at high impeller speeds. In Fig 4.19, the flow direction is found unstable, varying from radial to axial. It is also observed in Fig. 4.19 that the size of the loops increases with increase in impeller speed and also the loop moves more towards the baffels as rpm inmcreases. Fig. 4.20 and 4.21 confirms that formation of loops occur only at higher rpm and the velocty ditribution at lower impeller speed is almost similar to the without moving case as shown in Fig. 4.18.

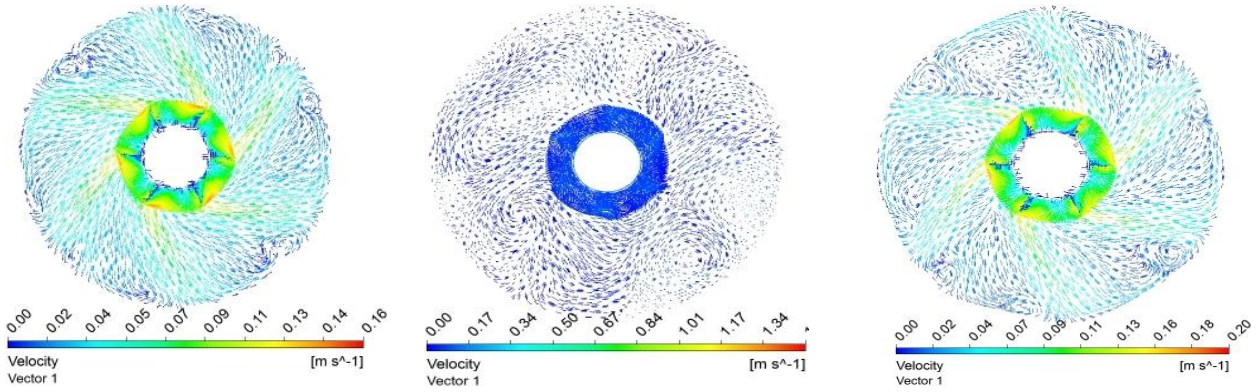

(a) (b) (c)

Figure 4.22 Velocity vectors for a CSTR with (a) D = 99mm, d = 7.2mm, μ = 9.2cp, ρ = 1145kg/m^3, N = 90rpm, Re = 0.98; (b) D = 172mm, d = 2mm, μ = 9.8cP, ρ = 1151kg/m^3, N = 35rpm, Re =3.04; (c) D = 250mm, d = 8.8 mm, μ = 19.7cp, ρ = 1179kg/m^3, N = 40rpm, Re = 1.37.

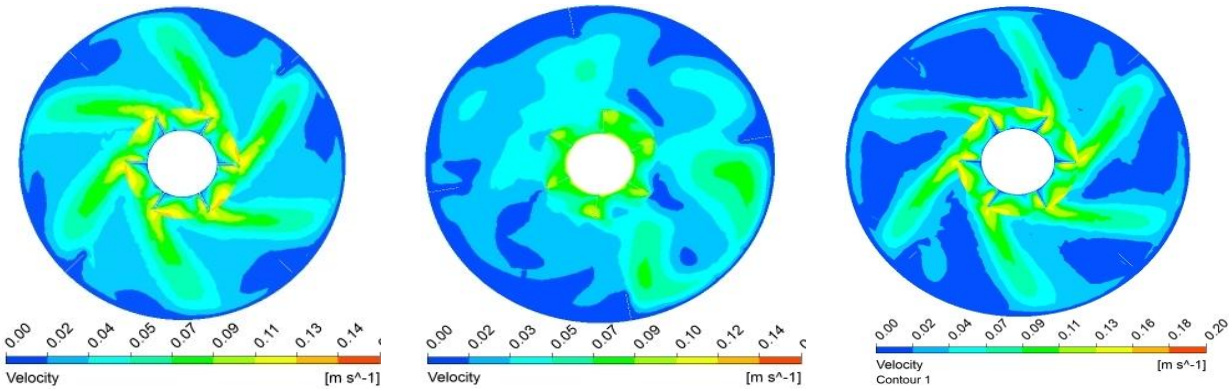

(a) (b) (c)

Figure 4.23 Velocity contours for a CSTR with (a) D = 99mm, d = 7.2mm, μ = 9.2cp, ρ = 1145kg/m^3, N = 90rpm, Re= 0.98; (b) D = 172mm, d = 2mm, μ = 9.8cP, ρ = 1151kg/m^3, N = 35rpm, Re = 3.04 ; (c)) D = 250mm, d = 8.8 mm, μ = 19.7cp, ρ = 1179kg/m^3, N = 40rpm, Re = 1.37.

The vectors and contours of velocity around the impeller are shown in Fig. 4.22 and Fig. 4.23 respectively. Both the figures shows the presence of six vortex loops. The vector plots represent that fluid flows in outward direction from impeller to the wall of the CSTR.

4.6.7 Contors of Vorticity

Vorticity is a precise physical quantity defined by curl of velocity and mathematically, it is defined as

$$\varpi = \nabla \times V \qquad 4.17$$

Vorticity is a vector field. Vorticity has the interesting property that it evolves in a perfect fluid in such a manner that the flow carries the vortex lines along with it. Furthermore, when viscous stresses are important, vortex lines diffuse through the moving fluid with a diffusion coefficient that is equal to the kinematic viscosity. The contours of voticities for moving and non-moving stirrer case are discussed in Fig. 4.24 to 4.28.

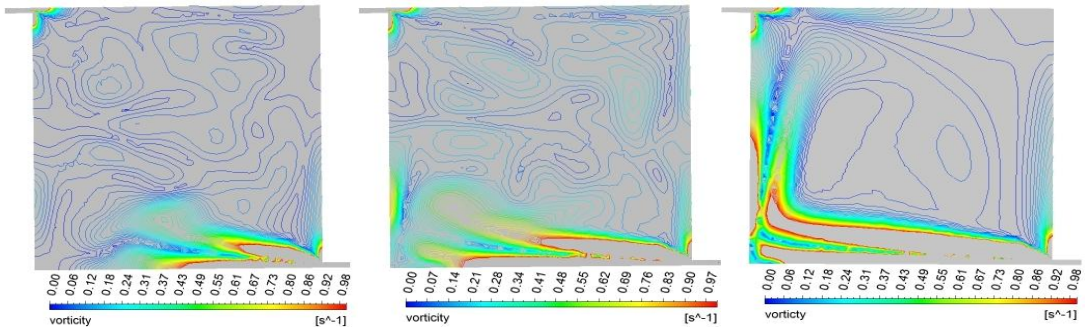

(a) Re = 2.25 (b) Re = 3.64 (c) Re = 5.57

(d) Re = 6.85

Figure 4.24: Vorticity contours without stirrer and baffles for D = 99mm, d = 2mm, μ = 1cp and ρ = 1000kg/m^3 .

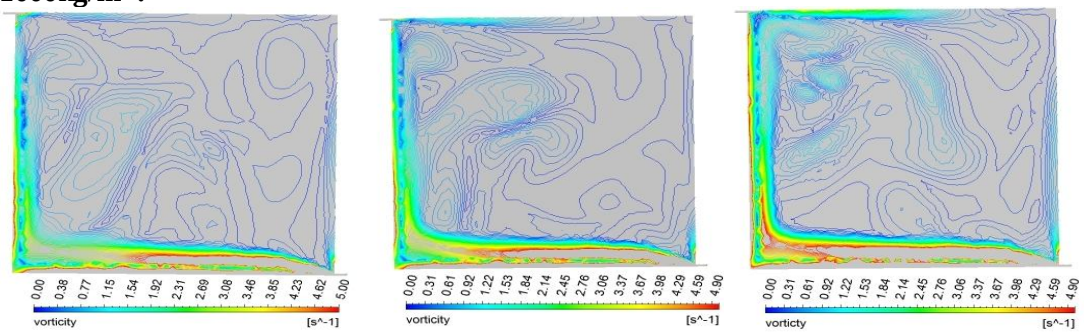

Re = 2.34 (b) Re = 2.60 (c) Re = 3.18

Figure 4.25: Vorticity contours without stirrer and baffles for D = 250mm, d = 2mm, μ = 7.75cp and ρ = 1141 kg/m^3.

Fig. 4.21 to 4.22 shows that the vorticity is high near the inlet. It is found extended more to the downstream with increase in tank Reynolds number, Re i.e. with decreasing the effect of viscous force on the flow and it results in higher rate of mixing of KCl. In the central zone of the reactor more uncertainty in the flow direction is observed. The vortex formation is observed less near the walls and almost absent in certain regions. As Reynolds number increases, the vortices are found less distributed throughout the reactor. In absence of impeller; the vortex moves like a jet horizontally to the opposite wall and then moves vertically parallel to the walls. The length of the jet increases with increase in Re due to decrease in viscous loss of vorticity.

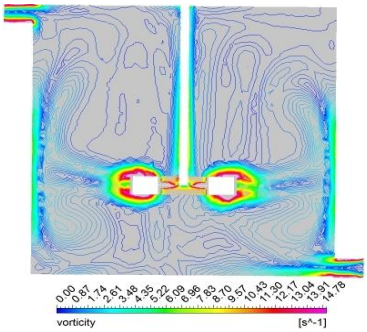

(a) N = 50rpm

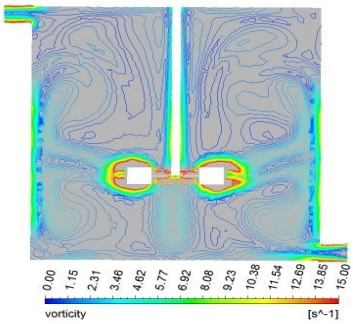

(b) N = 70rpm

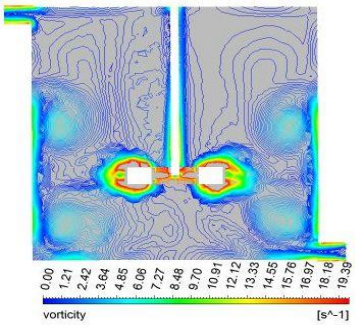

(c) N = 80rpm

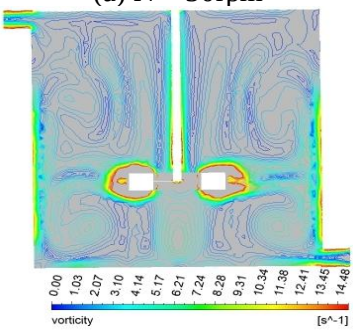

(d) N = 90rpm

Figure 4.26: Contours of vorticity for moving impellers with baffles and with *D* = 99mm, *d* = 7.2mm, μ = 9.2cp and ρ = 1145kg/m^3, Re = 0.98.

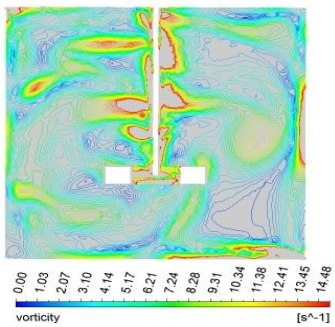

(a) N = 20rpm

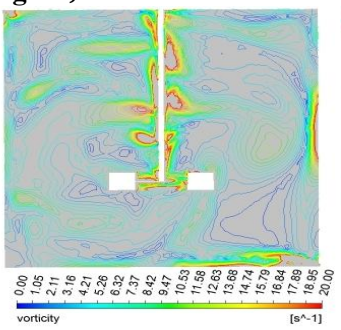

(b) N = 30rpm

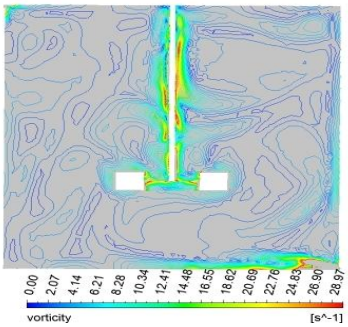

(c) N = 35rpm

Figure 4.27: Contours of vorticity for moving impellers with baffles and with D = 250mm, d = 2mm, μ = 9.8cp and ρ = 1145kg/m^3, Re = 1.37.

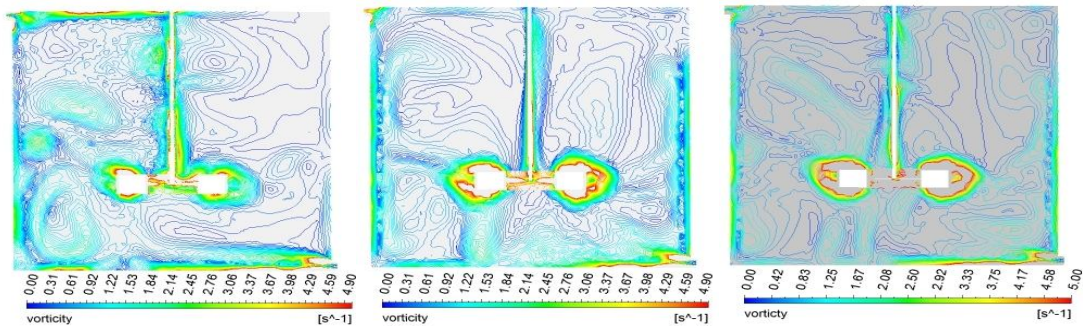

(a) N = 20rpm (b) N = 25rpm (c) N = 40rpm

Figure 4.28: Contours of vorticity for moving impellers with baffles and with D = 172mm, d = 8.8mm, μ = 19.7cp and ρ = 1179kg/m^3, Re = 3.04

To understand the hydrodynamics behaviour of CSTR in presence of moving impellers and baffles, the vorticity contours are presented in Fig. 4.26 to 4.28. All the figures show that the effect of inlet flow on CSTR vorticity is suppressed by rotating impeller. Fig. 4.26 shows that as 99mm diameter CSTR is operated at high Re, the vorticity contours clearly represents the occurrence of four loops in CSTR. It also shows that the size and position of the loops depends on the impeller speeds. As diameter of the CSTR increases the distribution of vorticity becomes non-uniform as depicted in Fig. 4.27 and 4.28. These two figures also represent that at lower rpm of the impeller the vorticity distribution is also equally get effected by the inlet flow.

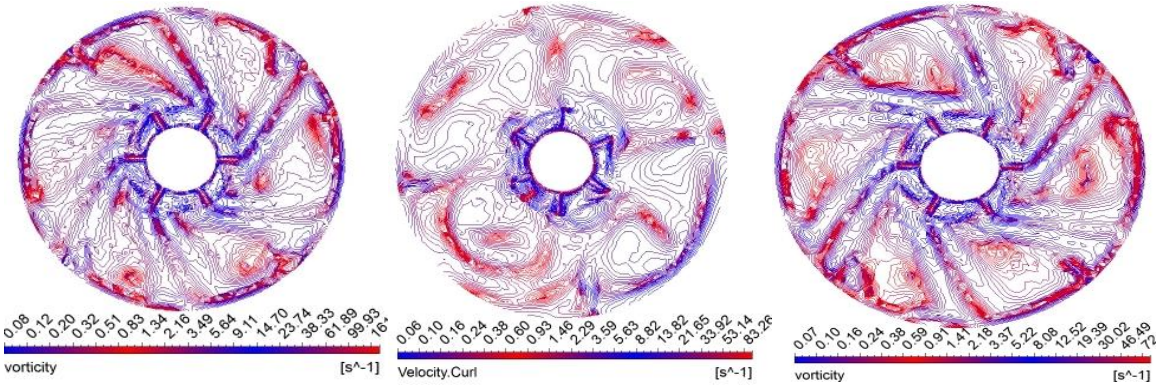

(a) (b) (c)

Figure 4.29: Vorticity contours for a CSTR with moving impellers and baffles with (a) D = 99mm, d = 7.2mm, μ = 9.2cp, ρ = 1145kg/m^3, N = 90rpm, Re = 0.98; (b) D = 172mm, d = 2mm, μ = 9.8cP, ρ = 1151kg/m^3, N = 35rpm, Re = 3.04; (c)) D = 250mm, d = 8.8 mm, μ = 19.7cp, ρ = 1179kg/m^3, N = 40rpm, Re = 1.37.

The contours of vorticity around the impeller are shown in Fig. 4.29. It shows the presence of six individual vortex loops each generated by individual impeller blade. The loops are also moving in angular direction.

4.6.8 Velocity Profiles

All fluid particles do not travel at the same velocity within reactor. The velocity distributions of fluid with radial position at different axial positions are presentenced in the following figures.

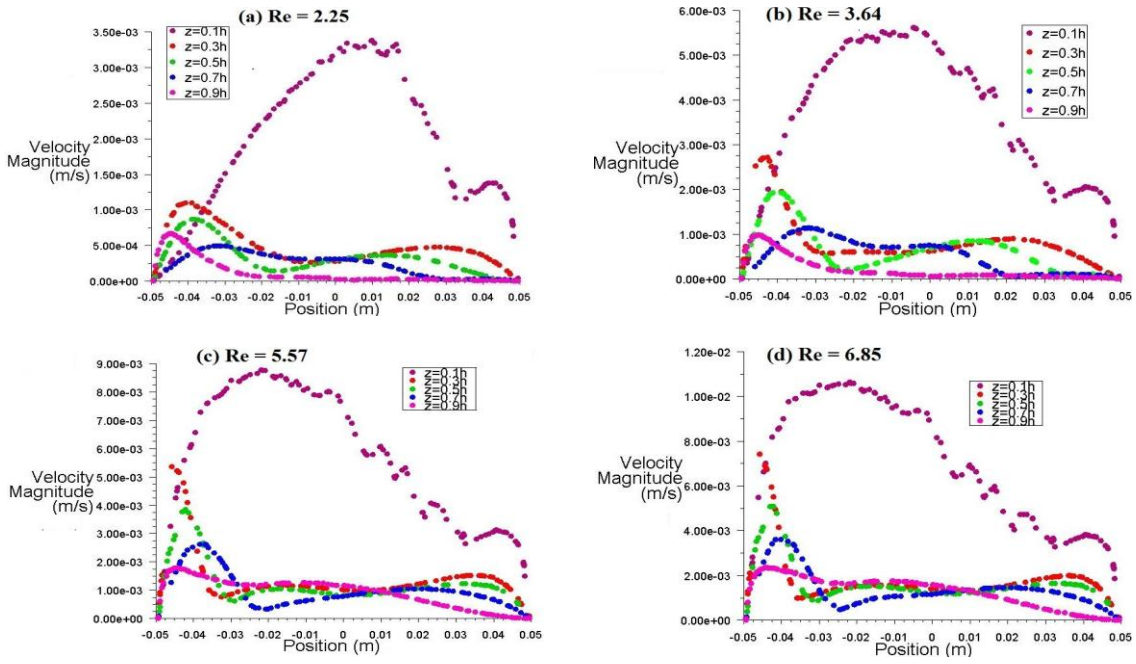

Figure 4.30: Variation of velocity with radial positionn at different axial positons without impeller and baffles for D = 99mm, d = 2mm, μ = 1cp and ρ = 1000kg/m^3.

Fig. 4.30 and Fig. 4.31 show the velocity distributions for non-moving impeller case. The bottom surface of the cylinder is represented by $z = 0$. Both the figure show that among all the profiles velocity passes through the maximum at $z = 0.1H$ and it occurs very close central axis. It happens due to pass of inlet fluid along the horizontal plane at $z = 0.1H$. The maximum velocity here moves from positive radial position to negative radial side as tank Reynolds number increases. This is due to penetration of inlet fluid jet more to the left wall. In the upward axial direction, the variation of velocity shows it passes through maximum nearer to wall opposite of inlet port. This happens due to upward movement of fluid along left wall surface, which was also depicted in vorticity distribution diagram.

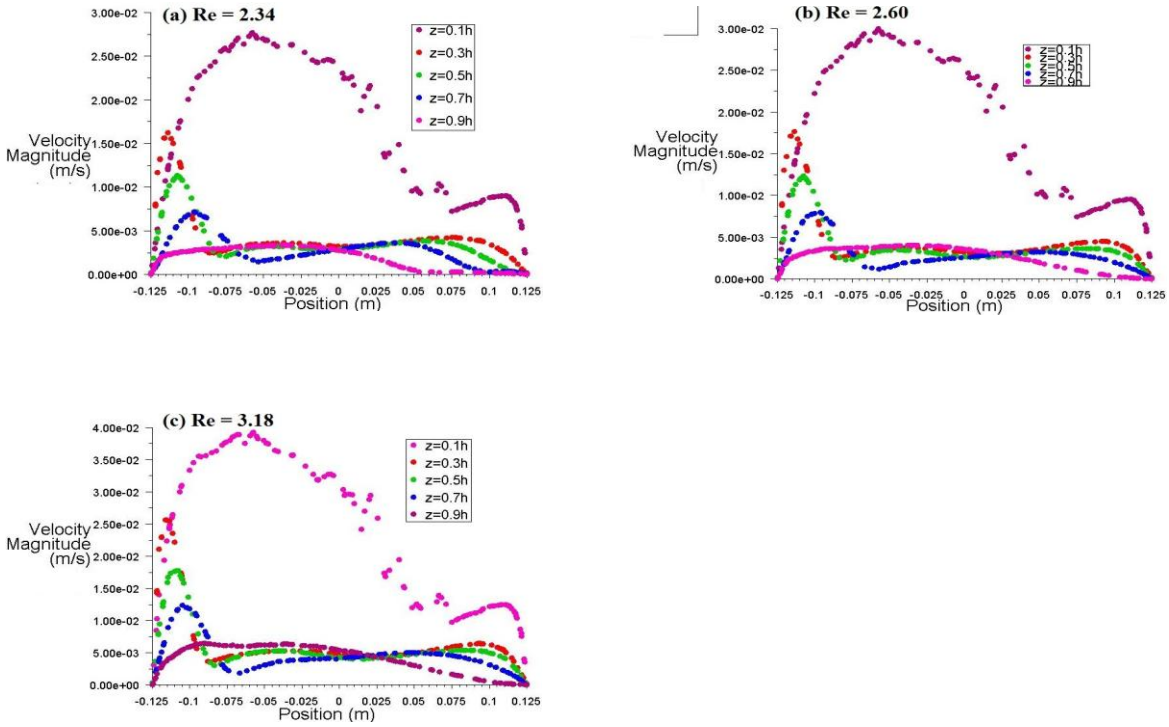

Figure 4.31: Variation of velocity with radial positionn at different axial positons without impeller and baffles for D = 250mm, d = 2mm, μ = 7.75cp and ρ = 1000kg/m^3.

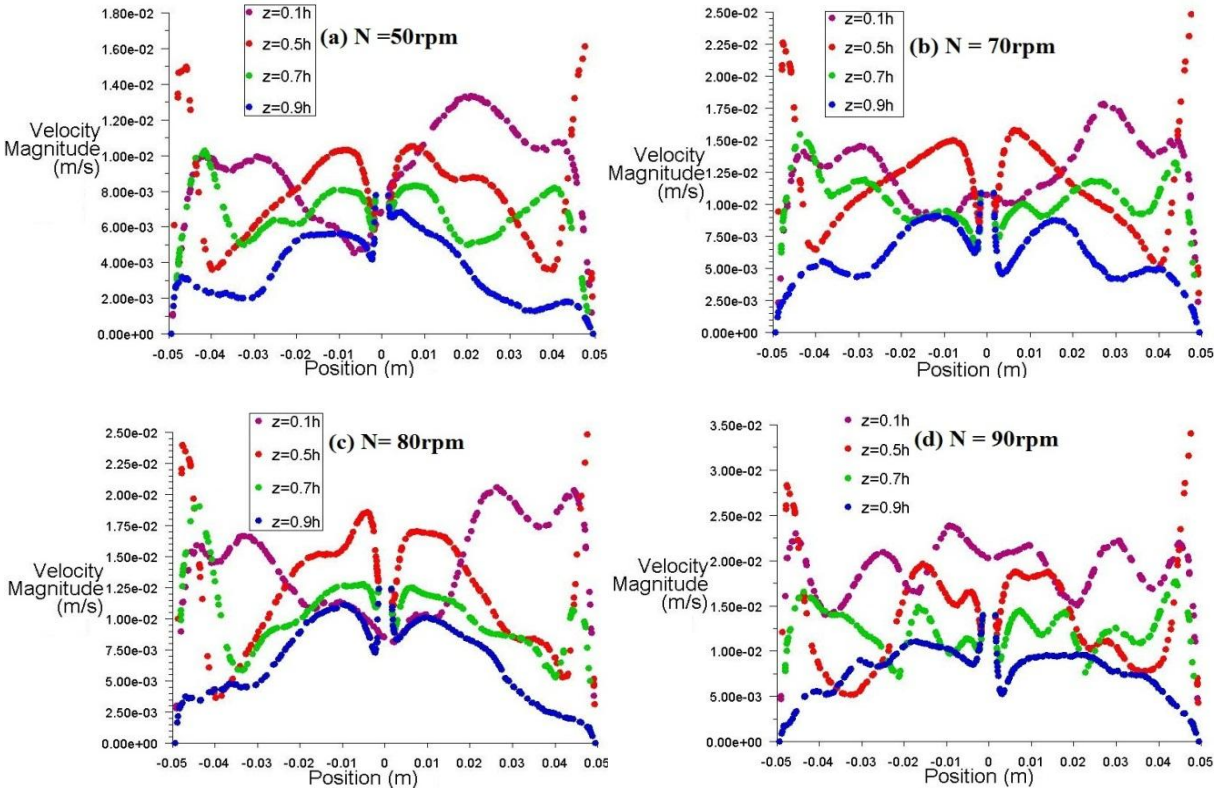

Figure 4.32: Variation of velocity with radial position at different axial positons with moving impeller and baffles for D = 99mm, d = 7.2mm, μ = 9.2cp, N = 0.98 and ρ = 1145kg/m^3.

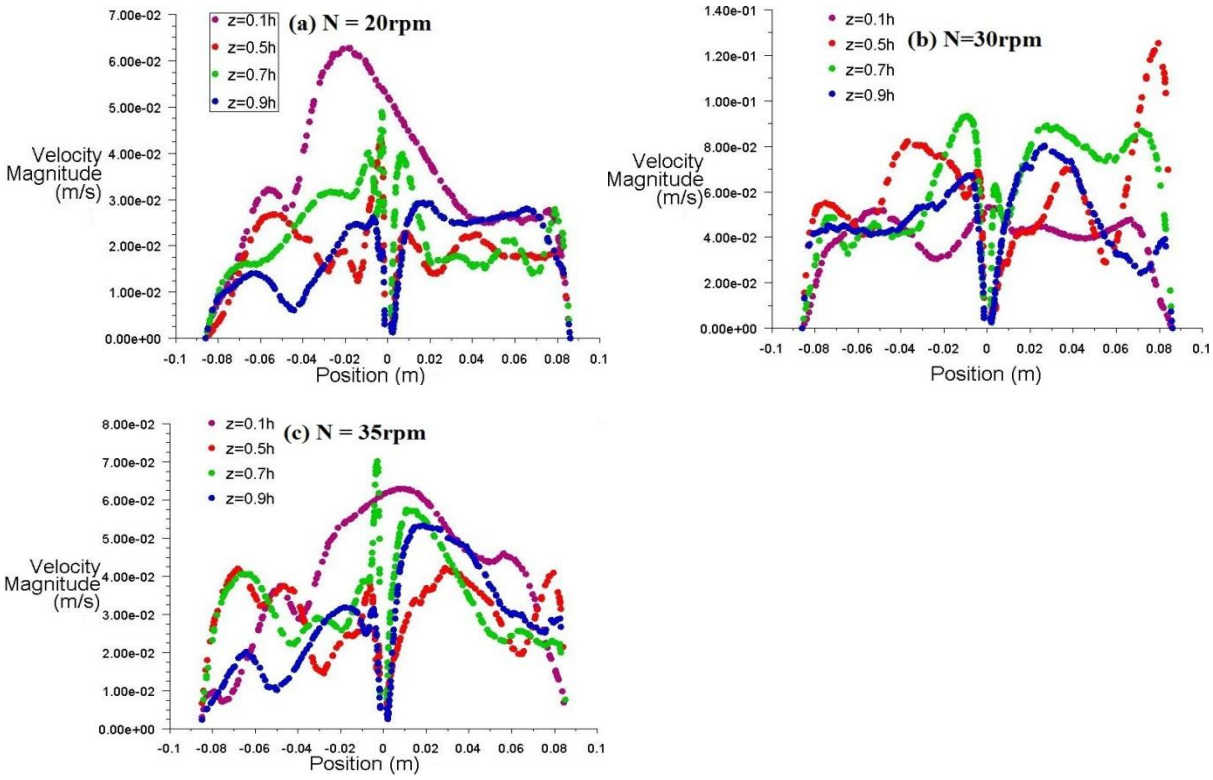

Figure 4.33: Variation of velocity with radial position at different axial positons with moving impeller and baffles for D = 172mm, d = 2mm, μ = 9.8cP, Re = 3.04 and ρ = 1151kg/m^3.

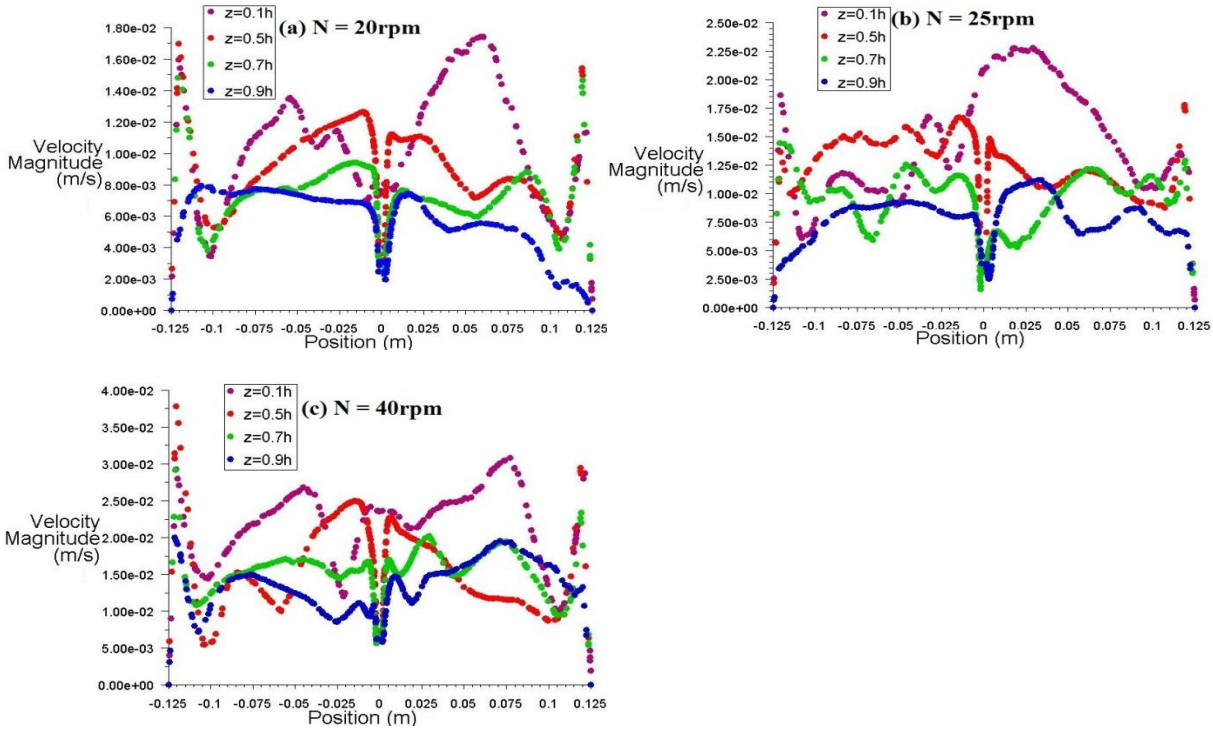

Figure 4.34: Variation of velocity with radial position at different axial positons with moving impeller and baffles for D = 250mm, d = 8.8mm, μ = 19.7cp, Re = 1.37 and ρ = 1179kg/m^3.

The velocity distributions with radial position at different axial position for moving impeller case are shown in Fig. 4.32to 4.34. The effects of impeller speed on velocity profiles at different tank diameter are clearly visible. Fig. 4.32 shows the distribution at relatively high impeller speed for 99mm diameter tank. It shows the occurrence of maximum nearer to right wall for the plane closer to the impeller. The impeller throws out the liquid on the wall and hence maximum velocities are obtained closer to the wall surface. For larger diameter (172mm and 250mm) CSTR, the velocity profiles are found similar to without moving case at relatively lower values of rpm. But as rpm of the impeller increases it shows the velocity trend similar to Fig. 4.32. The comparison of velocity profiles for moving and nonmoving stirrer cases reveals relatively more symmetrical flow pattern in case of rotating impeller CSTR. It happens due to superseding of mechanical energy of the impeller compared to the inlet flow energy.

4.6.9 Variation of Power Number and Flow Number with Reynolds Number

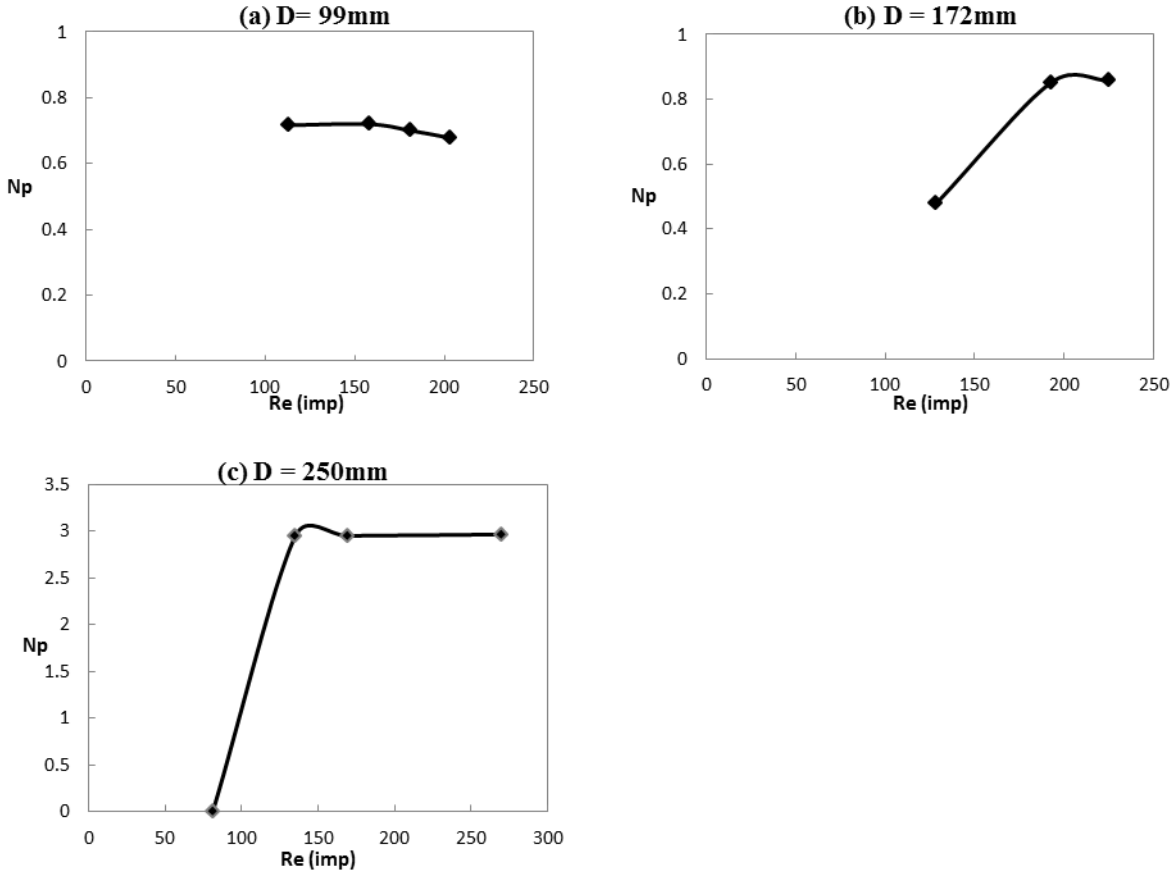

Figure 4.35: Power number vs. impeller Reynolds number for CSTR with different tank diameters having (a) d = 7.2mm, μ = 9.2cP, Re = 0.98 and ρ = 1145kg/m^3 (b) d = 2mm, μ = 9.8cP, Re = 3.04 and ρ = 1145kg/m^3 (c) d = 8.8mm, μ = 19.7cP, Re = 1.37 and ρ = 1151kg/m^3.

Fig 4.35 represents that as impeller Reynolds number ($\mathrm{Re}_m = \rho N^2 D/\mu$) increases power number remains constant for 99mm diameter CSTR and it decreases with increase in Re_m for 172mm and 250mm diameter CSTRs. The increase of power number with diameter of CSTR happens due to increase in liquid capacity of the tank and also due to increase in used liquid's viscosity, which is mentioned in the caption of the figure.

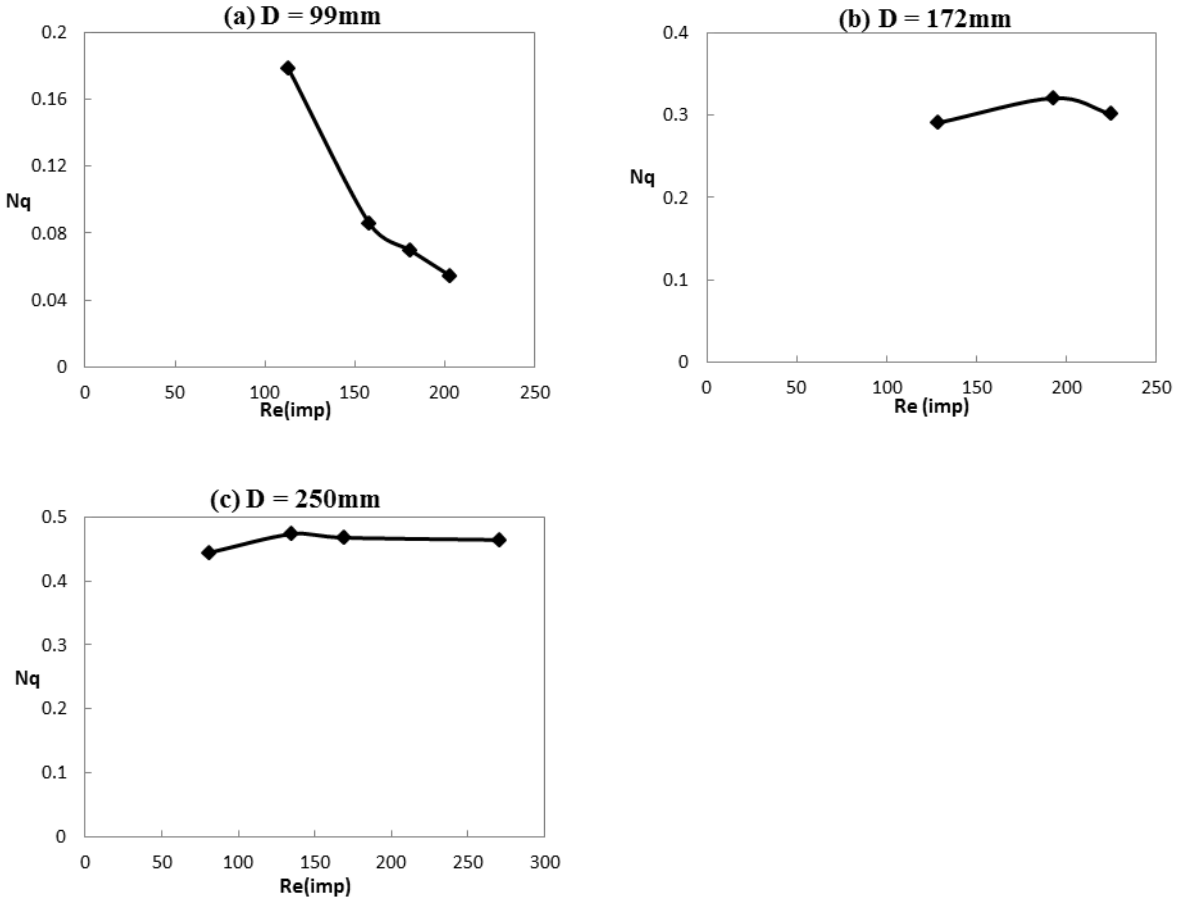

Figure 4.36: Variation of Flow number with Reynolds number for different tank diameters having (a) d = 7.2mm, μ = 9.2cp and ρ = 1145kg/m^3 (b) d = 2mm, μ = 9.8cp and ρ = 1145kg/m^3 (c) d = 8.8mm, μ = 19.7cp and ρ = 1151kg/m^3.

The variation of flow number with impeller Reynolds number is shown in Fig. 4.36. It shows that as Re_m increases, the flow number decreases for 99mm diameter CSTR and it is found independent of Re_m for larger diameter tank with 170mm and 250mm diameters.

4.7 CONCLUSIONS

A CFD study of CSTR by ANSYS Fluent was carried to understand its mixing behaviour. The tracer injection method was used to simulate the CSTR with stationary impeller, and rotating impeller is simulated for finding swept volume by the impeller, Q which is used to calculate the age distribution function $I(\theta)$. The CFD simulated results were found in good agreement with the experimental data. The laminar flow MRF model could capture the initial transient variation of *Q*, which latter becomes constant and follows the relation given for it in open literature. The effect of RPM of the impeller, tank Reynolds number, Viscosity and density of the liquid on the mixing efficiency was found. The mixing behaviour changed from dispersion to ideal mixing state as *N* and tank Re increases. The increase of viscosity helped to approach ideal mixing condition at higher *N*, but at lower *N* flow changes to dispersion state. The velocity vectors confirmed the formation four loops at higher Re, and the phenomena also depends on tank diameter. This also was confirmed through velocity distribution curves. The vorticity and pressure contours successfully resembled the hydrodynamic behavior of the system. The power number and flow numbers were found to be dependent on impeller Reynolds number, tank diameter and viscosity of CSTR liquid.

Chapter 5

STUDY OF RTD OF CSTR USING TRACER INJECTION METHOD

The importance of mixing phenomena in continuous stirred tank reactor (CSTR) is discussed in Chapter 4. There, using computational fluid dynamics (CFD) tools, the mixing performance of the CSTR in absence of moving stirrer and baffles was carried out by KCl injection method. But due to lack input potassium chloride (KCl) concentration in the feed, the same study was studied for moving stirrer and baffles stirrer by calculating swept volume of impeller using ANSYS Fluent. Burghardt and Lipowska, 1972 have studied the mixing behaviour of CSTR using a step change of KCl as tracer in the feed for both moving stirrer with baffles and without stirrer cases. Water and water-glycerin solutions were used as liquid in the CSTR. In their work, the relative density difference of the solutions caused by the content of KCl was not greater than

$$\frac{\Delta\rho}{\rho} = 1.7 \times 10^{-3} \qquad 5.1$$

The purpose of the non-stirrer case study of Burghardt and Lipowska, 1972 was to find out the inlet flow rate where liquid is in a state of ideal mixing. They also have found the RPM of the impeller required to reach the state of ideal mixing specially for high viscous fluid. For both the study a series of experimental run was taken.

For ideal mixing of the liquid solely by the inlet energy, the following relations must be fulfilled (Burghardt and Lipowska, 1972)

$$\mathrm{Re} = \frac{4V^{*}\rho}{\pi D\mu} \geq 13.5 \qquad 5.2$$

Where Re is the tank Reynolds number based on the tank diameter, ρ and μ are the liquid density and viscosities respectively, $V^{*} = A_i u_i$ is the inlet volumetric flow rate with A_i as the inlet cross-sectional area and u_i as inlet velocity. Eq. 5.2 was developed for a fixed inlet (6.6 mm) and tank diameter (170 mm).

The purpose of the present work in this chapter is to predict the experimental internal age distribution function, $I(\theta)$ by using computational fluid dynamics (CFD) model available in

the commercial software ANSYS Fluent. The work covered in this chapter also finds holdback, segregation, mean residence time, number of ideal CSTR in series equivalent to single actual CSTR etc. The effect of parameters like tank Reynolds number, impeller rotation, viscosity and density on the performance of the reactors in terms of transformation of behaviour from dispersion to ideal mixing flow state are also studied.

5.1 SPECIFICATION OF PROBLEM

A schematic representation of a CSTR with a single inlet and outlet streams is shown in Fig. 5.1 (Burghardt and Lipowska, 1972), which is same to Fig. 4.1. The dimension of the reactor and its accessories are given in Table 5.1.

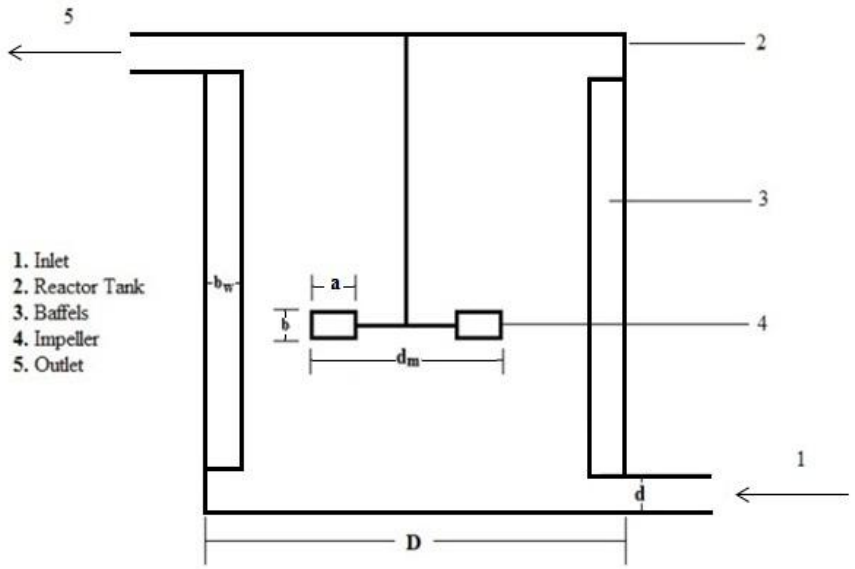

Figure 5.1: Schematic diagram of CSTR (Burghardt and Lipowska, 1972)

Table 5.1: Dimensions of the reactor

S.No		
1	Tank diameter, D	170mm
2	Inlet diameter, *d*	6.6mm
3	No of baffles	4
4	Baffles width (b_w)	$D/12$
5	Type of stirrer	Turbine disc impeller
6	Number of blades in impeller	6
7	Ratio of impeller to the tank diameter	$(d_m/D)=1/3$
8	Length of the impeller blade, *a*	$(d_m/4)$
9	Height of the impeller blade, *b*	$d_m/5$
10	Clearance, *C*	d_m
11	Height of liquid in CSTR, *H*	*H*

Burghardt and Lipowska, 1972 have found the RTD of the reactor without and with baffles and moving stirrer. The purpose of their work was to find out the tank Reynolds number, which accounts the inlet energy, sufficient for ideal mixing condition. They also have found the minimum number of impeller rotation sufficient to reach ideal mixing in moving stirrer case. In mixing process for step tracer input the function, *F(t)* or $F(\theta)$ can be evaluated from the following equation

$$F(t) = F(\theta) = \frac{C(t) - C_0^-}{C_0^+ - C_0^-} \tag{5.3}$$

The age distribution function $I(\theta)$ (Burghardt and Lipowska, 1972) for the step change of tracer concentration can be evaluated using the following expression.

$$I(\theta) = 1 - F(\theta) = \frac{C_0^+ - C(t)}{C_0^+ - C_0^-} \tag{5.4}$$

The residence time distribution function, $E(t)$ is calculated by

$$E(t) = \frac{1}{C_0^+ - C_0^-} \frac{dC(t)}{dt} \tag{5.5}$$

Where KCl concentration in the inlet changes by step from C_0^- to C_0^+, and $C(t)$ is the concentration of KCl in the outlet at any time, t. In the present work C_0^- is taken as zero. And $\theta = t/\tau$. The residence time or holdup time, τ is defined as

$$\tau = \frac{V}{V^*} \tag{5.6}$$

Where, V is volume of liquid inside the reactor.The diffusivity of KCl in the solution is taken as 1.95 X 10^{-9} m^2/s (Harned and Nuttal, 1949).

Dispersion coefficient is an important parameter in mixing process and can be calculated from the following equation,

$$\frac{D_{Coeff}}{uL} = \frac{1}{2}\left(\frac{\sigma}{\tau_m}\right)^2 \tag{5.7}$$

Where the mean residence time, τ_m is

$$\tau_m = \int_0^\infty tE(t)dt \tag{5.8}$$

and the variance, σ is

$$\sigma^2 = \int_0^\infty (t - \tau_m)E(t)dt \tag{5.9}$$

and u is the inlet velocity; L is the diameter of the tank.

The number of ideal CSTR in series giving equivalent performance of the actual CSTR is calculated by

$$N_{CSTR} = \frac{\tau_m^2}{\sigma^2} \tag{5.10}$$

The holdback is defined as the average spending time of the fluid inside the reactor compared to the hydraulic residence time, τ. Mathematically, it can be defined as

$$Holdback = \frac{1}{\tau}\int_0^{\tau} F(t)dt \tag{5.11}$$

$Holdback$ vary from 0 for piston–flow to 1 when most of the space in the vessel is dead water. For completely mixed flow,

$Holdback = 1/e$.

The efficiency of mixing in a vessel can be given by a single quantity, S called "segregation". Mathematically segregation, S is

$$S = \int_0^{\tau} \left(F_{Ideal}(t) - F(t)\right)dt \tag{5.12}$$

S Varies from $+1/e$ for piston flow to values approaching -1 when most of space in the system is dead water.

Where

$$F_{Ideal}(t) = 1 - e^{-V^* t/V} \tag{5.13}$$

In this chapter, the computed values of $I(\theta)$ using Eq. 5.3 are compared with the experimentally found data using tracer injection method (Burghardt and Lipowska, 1972). The effects of number of rotation of the impeller and the viscosity of water-glycerine solution on the nature of mixing are studied theoretically. The behaviour of mixing in CSTR is also studied in terms of Dispersion coefficient, N_{CSTR} etc.

5.2 MATERIAL AND FLOW PROPERTIES

The liquid used in the present work is water–glycerine solution. The properties of the solution are given in Table 5.2.

Table 5.2: Parameters for non-moving case [Burghardt and Lipowska, 1972]

S. N	μ (cP)	ρ (kg/m^3)	V* (l/hr)	τ (min)	Re_t	Type of Flow
1	1	1000	105	1.85	218.4	Ideal Flow
2	1	1000	75	2.66	156.0	- do -
3	1	1000	55	3.74	114.4	- do -
4	1	1000	14.3	13.75	29.3	- do -
5	1	1000	10	19.32	20.8	- do -
6	1.0	1141	8	87.40	4.7	Dispersion Flow
7	4.2	1110	20.25	10.64	11.1	- do -
8	6.2	1130	24.75	8.62	9.5	- do -
9	8	1144	41.40	5.14	12.2	- do -

Table 5.3: Parameters for CSTR with stirrer & baffles [Burghardt and Lipowska, 1972]

S. No.	μ (cP)	ρ (kg/m^3)	V* (l/hr)	τ (min)	N (RPM)	Type of flow
1	11	1152	3.50	60.43	10	Dispersion flow
2	11	1152	3.45	63.30	20	-do-
3	11	1152	3.45	60.70	30	-do-
4	11	1152	3.45	63.91	40	Ideal flow
5	21	1180	4.42	53.76	12	Dispersion flow
6	21	1180	4.34	54.74	25	-do-
7	21	1180	4.46	53.27	50	-do-
8	21	1180	4.35	54.64	70	Ideal flow
9	43	1200	13.95	16.12	25	Dispersion flow
10	43	1200	12.75	16.52	50	-do-
11	43	1200	13.50	15.60	80	-do-
12	43	1200	16.80	12.54	100	-do-
13	43	1200	13.95	15.10	150	Ideal flow
14	43	1200	13.65	15.40	200	Ideal flow

5.3 GEOMETRY AND MESHING OF THE REACTOR

The geometry of the CSTR with four baffles and a single stirrer (six blades) was shown in Fig. 4.2a in chapter 4. It is prepared in ANSYS Workbench. Like previous chapter, here also the CSTR is divided into two parts: stationary and moving zones. The moving zone includes stirrer and cylindrical disk volume around the impeller. Both the zones are connected by interface. Also the same unstructured tetrahedral mesh shown in Fig. 4.2b is also used in the simulation work of this chapter. The meshed CSTR is shown in Fig. 4.2b. The fine unstructured tetrahedral mesh is used with cell count 623089. The quality of mesh depends on the skewness of mesh and it should be less than 0.95. In this case, the skewness of mesh is 0.889. For connecting moving part with stationary part the interface is used and it is meshed with unmapped unstructured tetrahedral cell.

5.4 MODEL EQUATIONS AND SOLUTION ALGORITHM

The model equations and simulation algorithms are discussed in section 4.4 of the chapter 4. In short, laminar flow model with multiple reference frame models are used. In species transport KCl is defined as the tracer by giving the same properties as water(except molecular weight). Water/water-glycerin solution is filled in the tank. KCl is introduced in the tank when hydrodynamically CSTR reaches at steady condition. The system is simulated with hydrodynamics model equations till steady state reaches and then KCl mass equations are solved using transient method. The SIMPLE algorithm is used with UPWIND scheme. The values of under relaxation factors are 0.3, 0.7, 1.0, 1.0 and 1.0 respectively for pressure, momentum, density, body forces and KCl mass equations. The used convergence criterion is of the order of 10^{-3}. The CFD simulation gives transient outlet KCl concentration, which is used in Eq. 5.3 to calculate $I(\theta)$. The mean residence time, variance, $N_{cstr,}$ holdback, segregation etc. are calculated by their respective equations.

5.5 BOUNDARY CONDITIONS

The boundary conditions used are of similar in type to those discussed in chapter 4. The mixture of water-glycerin solution is considered as a single phase. The operating condition is 273K temperature and 101 325 Pa pressure. Inlet velocity is specified and at the outlet pressure is specified. The RPM of the impeller is used for rotating impeller body.

5.6 RESULTS AND DISCUSSIONS

5.6.1 Study on Mixing Without Stirrer and Baffles

Potassium chloride is injected in the tank as tracer and the concentration of it is noted with time at the outlet. $I(\theta)$ is calculated using Eq. 5.3. The mixing line represents ideal mixing condition with $I(\theta) = \exp(-\theta)$. Using the parameters given in Table 5.2, the computations are carried with very low concentration of KCl at the inlet. The inlet flow transmits its energy to the liquid in the tank and causes generation of convective streams and turbulent eddies, which give rise to the mixing of the contents of the tank. The comparative presentations of simulation and experimental (Burghardt and Lipowska, 1972) results are shown in Fig. 5.2 and Fig. 5.3.

Figure 5.2 shows that for Reynolds numbers ranging between 218.4-20.8, computational values follow experimental data as well as ideal mixing line. Figure 5.3 shows that for

relatively low Reynolds number the computational values are following experimental data but they are not on the ideal mixing line. The computed values in both the figures follow the flow conditions as given in Table 5.2. The results in Fig 5.2 resembles that as Reynolds number decreases and viscosity increases the $I(\theta)$ curve moves away from the ideal mixing line i.e. it becomes dispersed flow.

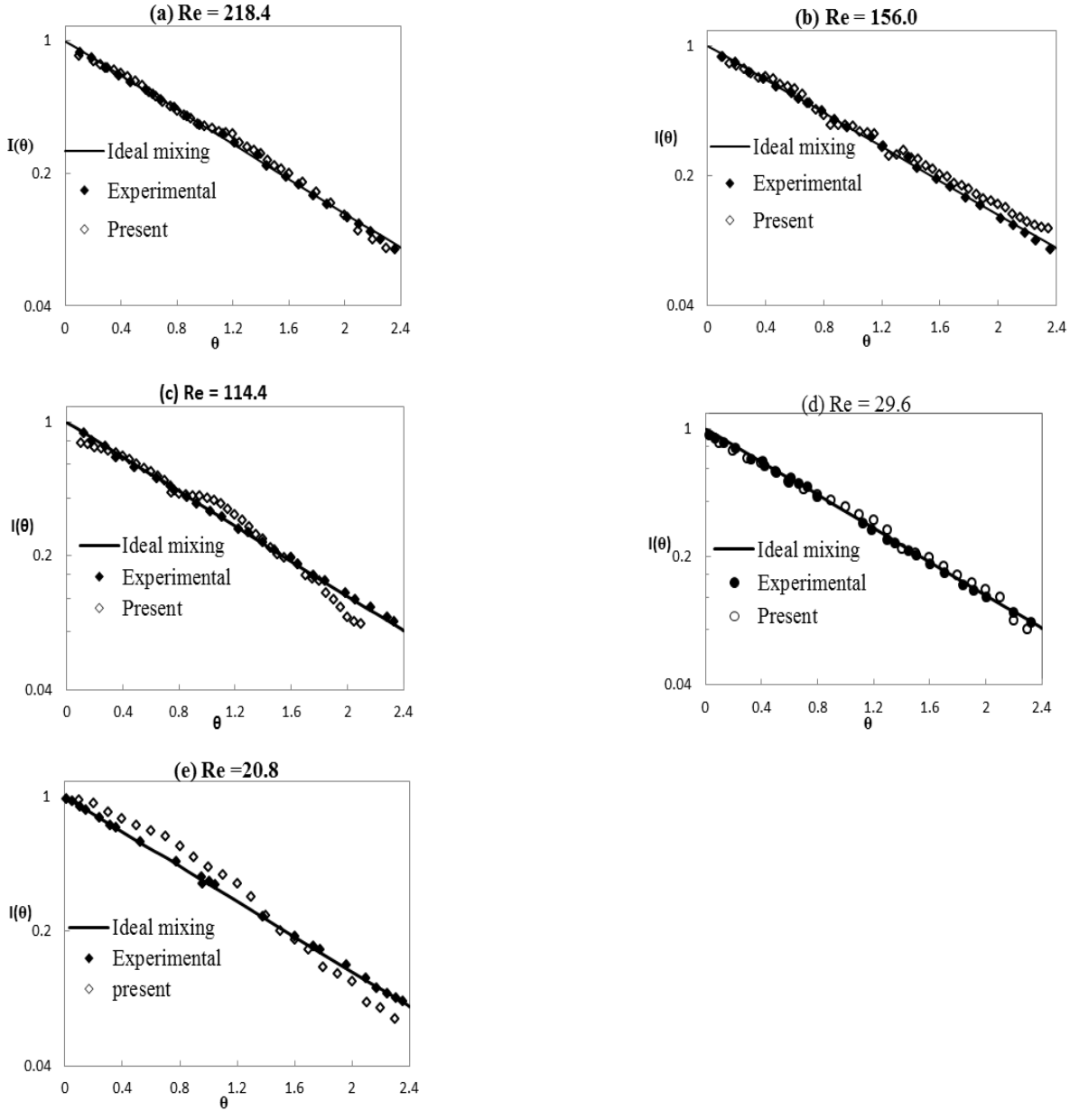

Figure 5.2 Plot of *I(θ)* vs. *θ* for a CSTR without stirrer and baffles and with D = 170mm, d = 6.6mm, μ = 1cp and ρ = 1000Kg/m^3. Inlet KCl concentration is 0.00177 mass fraction.

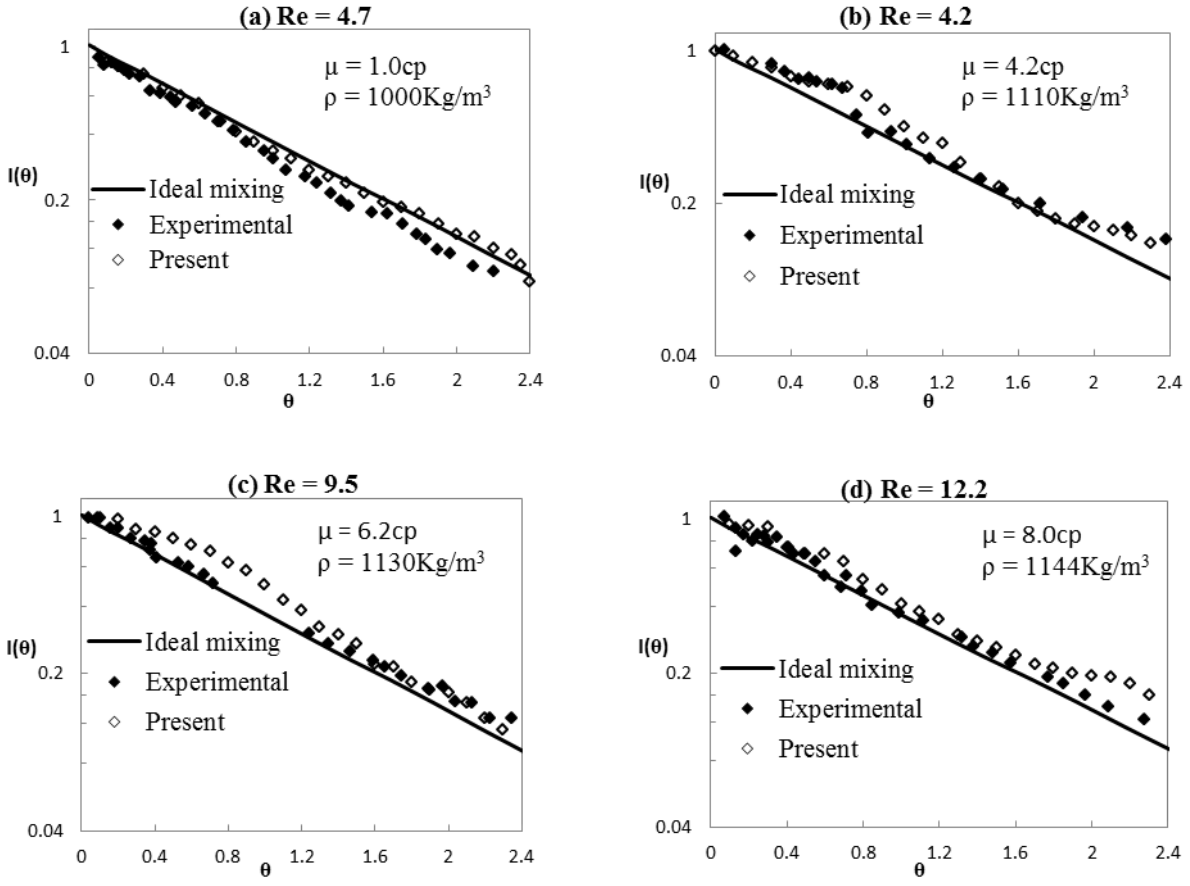

Figure 5.3 Plot of *I(θ)* vs. *θ* for a CSTR without stirrer and baffles and with D = 170mm, d = 6.6mm. Inlet KCl concentration is 0.00177 mass fraction.

5.6.2 Study on Mixing with Stirrer and Baffles

Burghardt and Lipowska, 1972 had conducted mixing experiments for CSTR in the presence of moving stirrer and baffles, and with different liquid density and viscosities as shown in Table 5.3. For given values of *D*, *d* and μ the liquid flow rates and the number of impeller revolutions were varied.

The internal age distribution $I(\theta)$ is calculated by Eq. 5.3. The comparative study between experimental results (Burghardt and Lipowska, 1972) and the present computed values for moving stirrer case are presented in Fig. 5.4, 5.5 and Fig. 5.6. The conditions are mentioned along each graph. In all the figures, both the experimental and computed $I(\theta)$ values are obtained from tracer, KCl injection method. The observation finds that the computed values can predict in excellent the experimental data. The visible fluid mixing sate is perfectly matching with the experimental mixing state as mentioned in Table 5.3. All the figures depict that the computed $I(\theta)$ approaches the ideal mixing line with increase in impeller rotation, *N*. It happens because of the increase of rate of mixing with increase in impeller rotation, which

accounts the amount of mechanical energy given to the liquid. The nature of mixing depends on viscosity. As viscosity increases tank Reynolds number decreases, and hence, more amount of mechanical force will be required for mixing. The figures show that the required RPM of the impeller to reach ideal mixing state increases with increase in viscosity of the liquid.

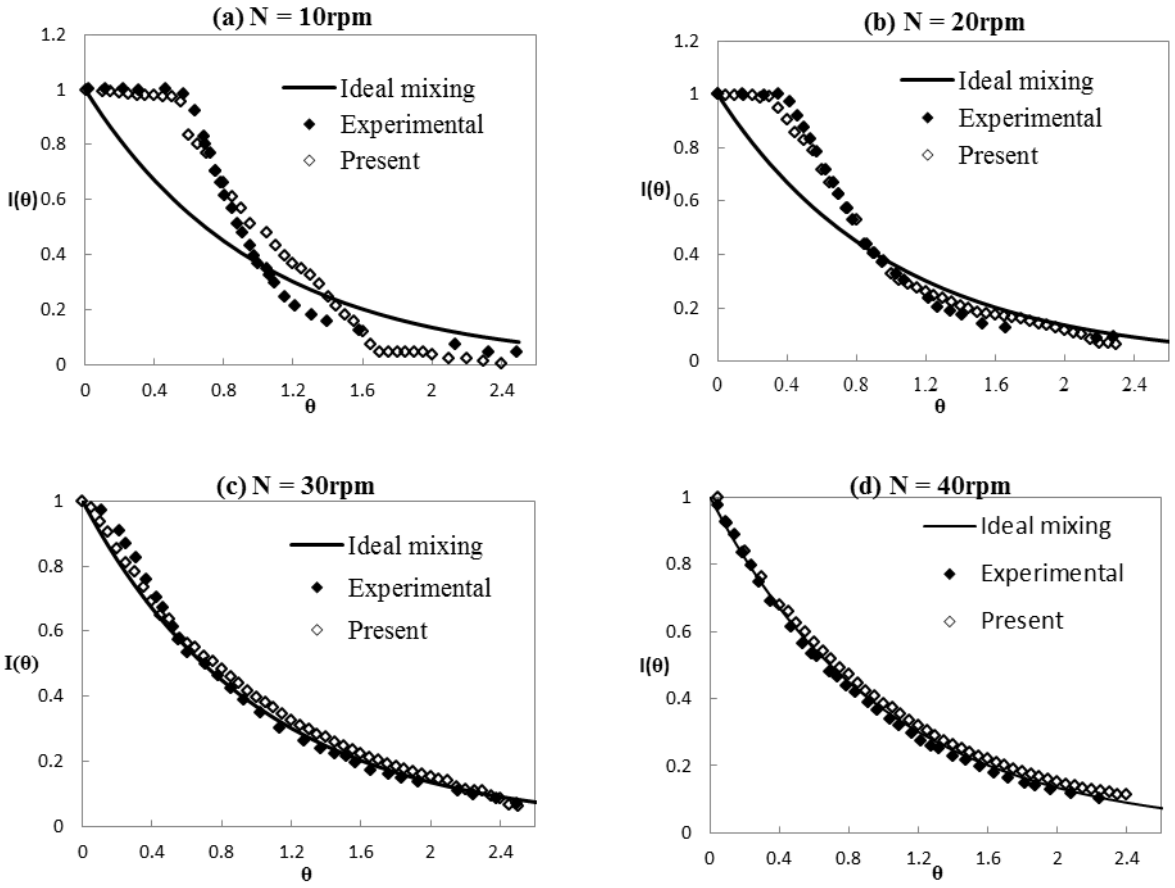

Figure 5.4: Plot of $I(\theta)$ vs. θ for a CSTR with stirrer and baffles and with D = 170mm, d = 6.6 mm, μ = 11cp and ρ = 1152 Kg/m^3. Inlet KCl mass fractions are (a) 0.00169, (b) 0.0019173 (c) 0.00171 (d) 0.00171

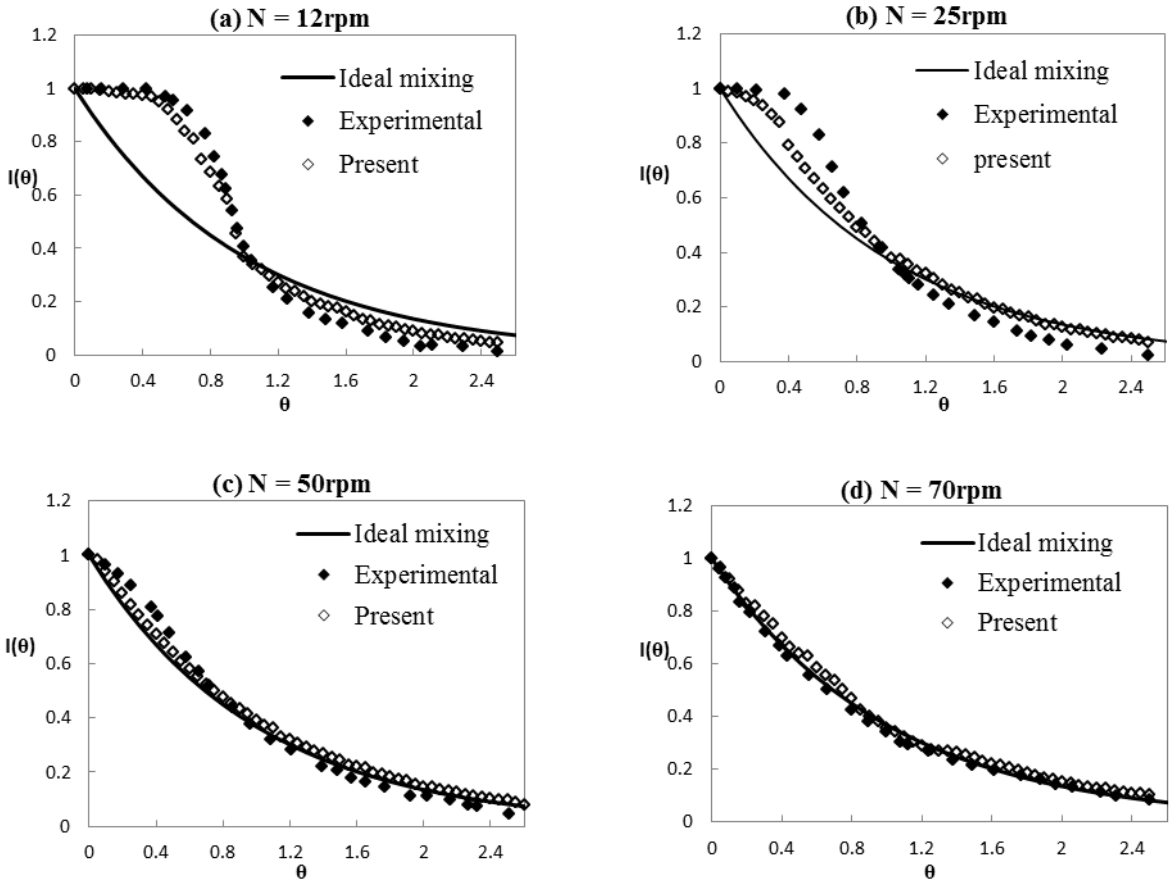

Figure 5.5: Plot of $I(\theta)$ vs. θ for a CSTR with stirrer and baffles and with D = 170mm, d = 6.6 mm, μ = 21cp and ρ = 1180 Kg/m^3. Inlet KCl mass fractions are (a) 0.001513 (b) 0.00168, (c) 0.001705 (d) 0.00171.

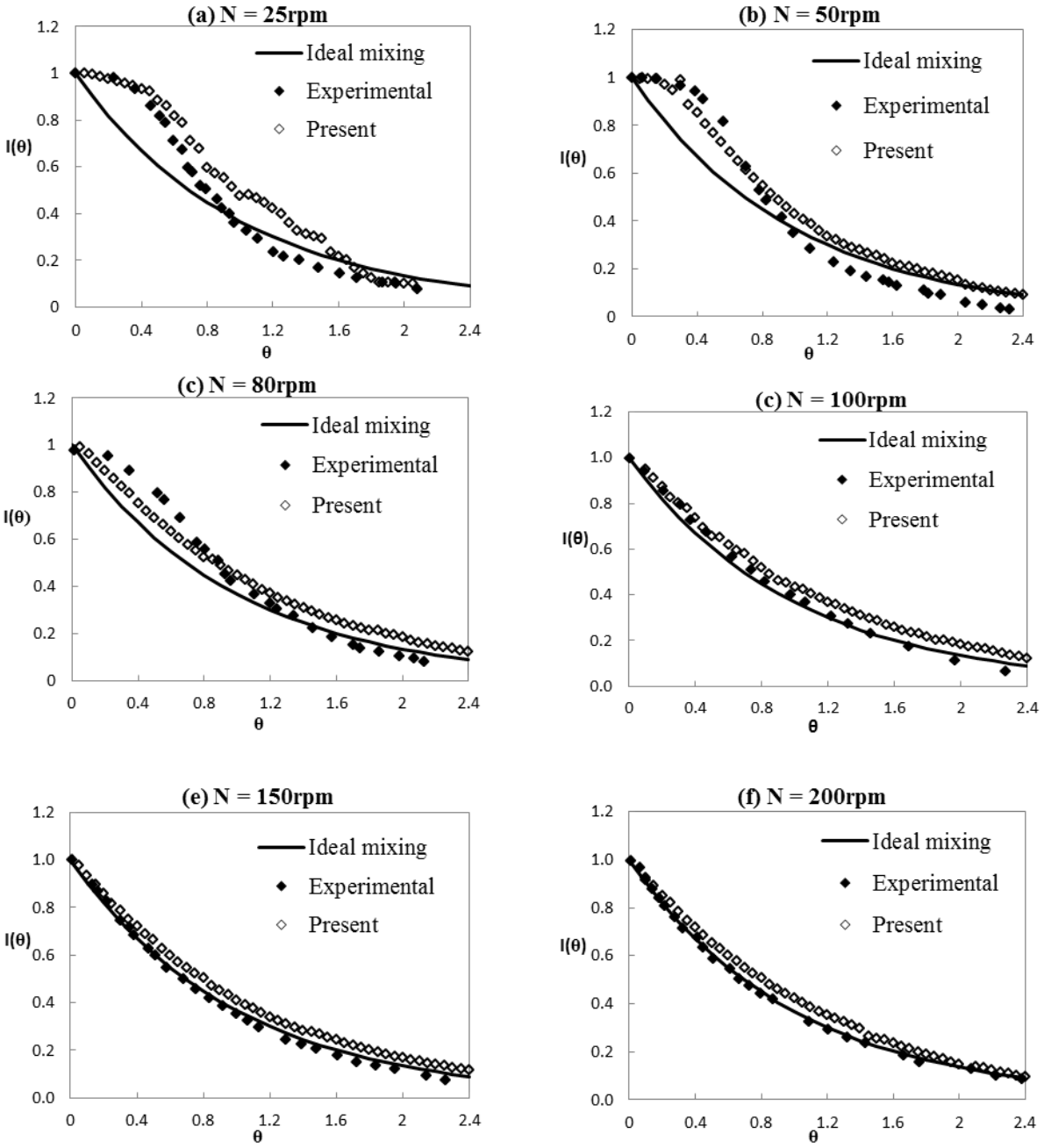

Figure 5.6: Plot of $I(\theta)$ vs. θ for a CSTR with stirrer and baffles and with D = 170mm, d = 6.6 mm, μ = 43cp and ρ = 1200 Kg/m^3. Inlet KCl mass fractions are (a) 0.00169, (b) 0.001664, (c) 0.001668, (d) 0.001664, (e) 0.001603, (f) 0.001664.

5.6.3 Contours of KCl Mass Fraction without Stirrer and Baffles

The contours of mass fraction of KCl for CSTR without impeller and baffles are shown in Fig. 5.7 to 5.11. The graphs are shown in the increasing order of tank Reynolds number, Re at different time θ. KCl enters the reactor at concentration of 0.00177. Initially, the concentration is zero at the outlet. As there is no impeller and baffles, tracer is moving with inlet flow stream. For every time step, there is an increase in the amount of tracer in the

reactor and at some higher time, the tracer sent is completely mixed with water. At high Reynolds number, the tracer movies radially to and follows the trajectory of the opposite wall surface of the inlet port (Fig. 5.7 and 5.8). Due to less amount of inlet energy with lower Re flow, the inlet water moves axially up and then mixes with water until leaves through the outlet (Fig. 5.9, 5.10 and 5.11). Especially at Re, 19.32, the inflow energy is so low that the inlet fluid along with KCl follows the wall surface where inlet line is attached. Thus at lower Re, KCl needs more time to reach the outlet. The comparison shows that at θ, 0.4, KCl reaches closer to the outlet with increase in Re. It happens due to movement of KCl with inlet fluid like jet radially towards the opposite wall, and then movement of it up along the wall surface. Due to increase in inlet energy with Re, the homogeneity of the liquid inside the CSTR increases with increase in Re. The figure also reveals that at lower Re, KCl disperses in the solution at early time compare to higher Re flow.

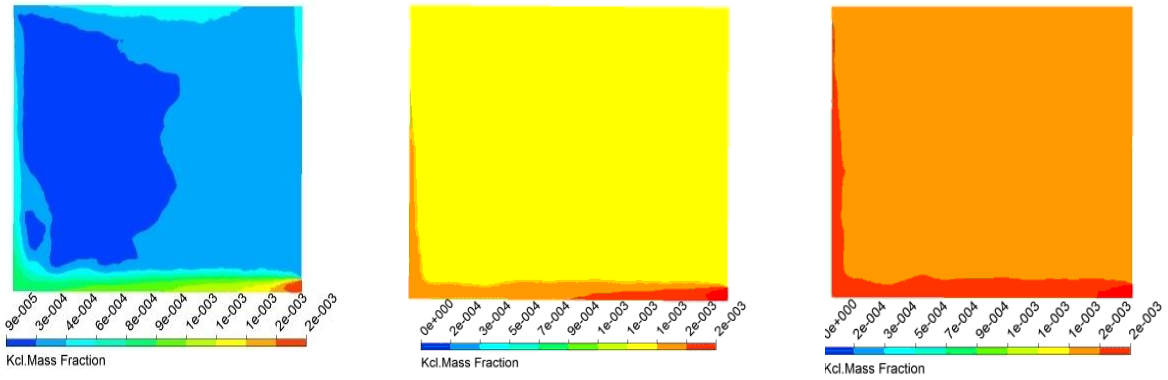

(a) θ = 0.4 (b) θ = 1.0 (c) θ = 2.0

Figure 5.7: The contours of tracer mass fraction without stirrer and baffles for Re = 218.4, D = 170mm, d =6.6mm, μ = 1cp and ρ = 1000Kg/m^3 at different time steps.

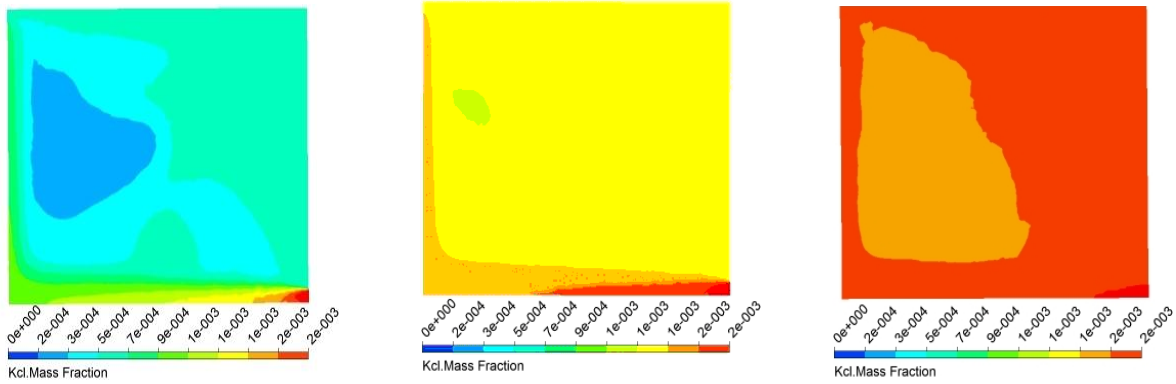

(a) θ = 0.4 (b) θ = 1.0 (c) θ = 2.0

Figure 5.8: The contours of tracer mass fraction without stirrer and baffles for Re = 156.0, D = 170mm, d =6.6mm, μ = 1cp and ρ = 1000kg/m^3 at different time steps.

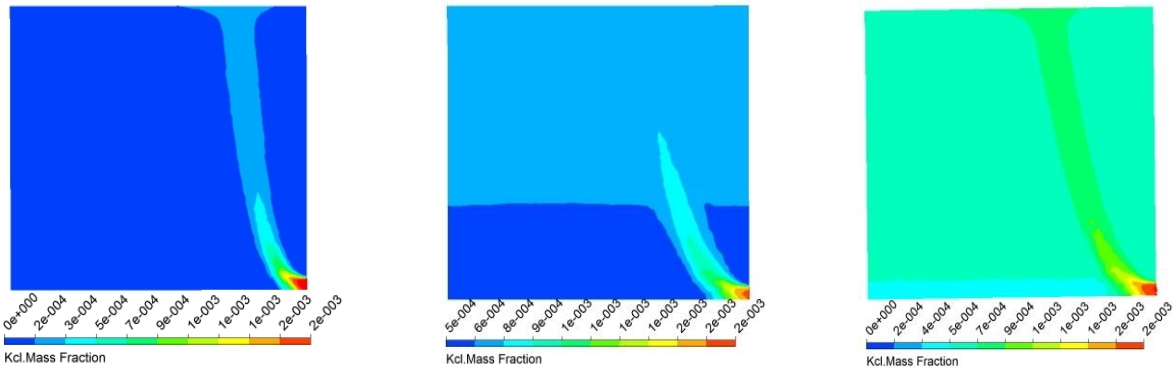

(a) θ = 0.4 (b) θ = 1.0 (c) θ = 2.0

Figure 5.9: The contours of tracer mass fraction without stirrer and baffles for Re = 114.4, D = 170mm, d =6.6mm,μ = 1cp and ρ = 1000kg/m^3 at different time steps.

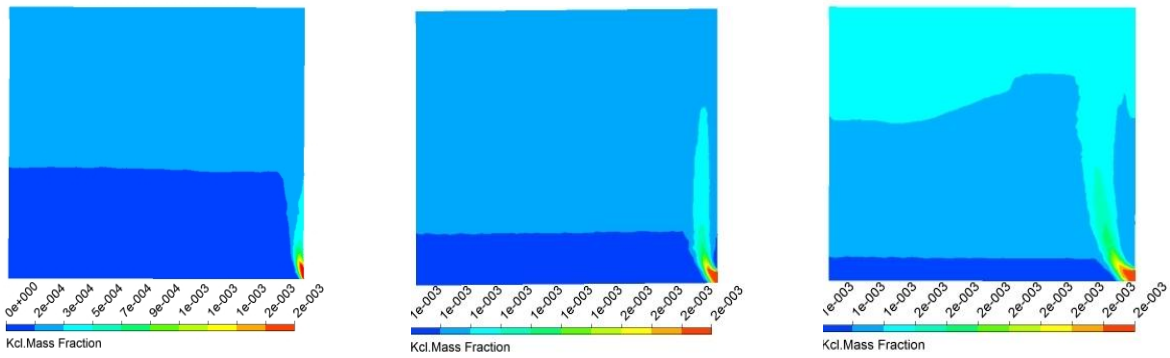

(a) θ = 0.4 (b) θ = 1.0 (c) θ = 2.0

Figure 5.10: The contours of tracer mass fraction without stirrer and baffles for Re = 29.6, D = 170mm, d =6.6mm, μ = 1cp and ρ = 1000kg/m^3 at different time steps.

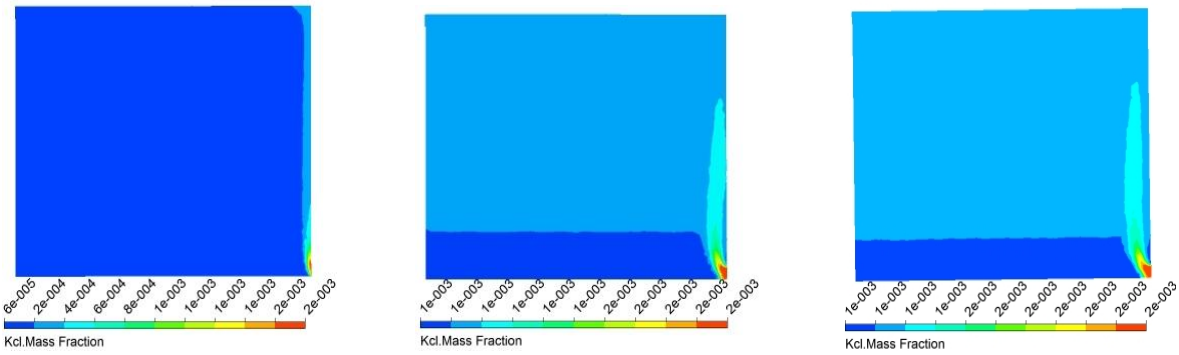

(a) θ = 0.4 (b) θ = 1.0 (c) θ = 2.0

Figure 5.11: The contours of tracer mass fraction without stirrer and baffles for Re = 19.32, D = 170mm, d =6.6mm,μ = 1cp and ρ = 1000kg/m^3 at different time steps.

5.6.4 Contours of KCl Massfraction With Stirrer and Baffles

Mechanical stirrer is used in CSTR to enhance the mixing rate. The contours of KCl mass fraction in the CSTR with stirrer and baffles are shown in Fig. 5.12 to 5.19. It depicts that the sent KCl in the reactor is dispersed in radial direction, and then moves axially up with increase in time. The contours prove the advantage of use of stirrer for getting the ideal

mixing condition even at very low inlet Reynolds number. The study shows that as impeller revolution increases the tracer moves to the bottom of the impeller and slowly it spreads throughout the reactor depending upon the impeller speed. As impeller revolution increases the tracer gets distributed better without dead spaces or channeling.

Figure 5.12 shows that intialy KCl ocupies the bootom part of the reactor and then it moves up slowly with time. But as the RPM of the impeller icreases (Fig. 5.13-5.15), KCl is mixed quicly with water-glycerine solution, and the liquid in the CSTR reaches at homogeneous state comapartively at lesser time. Another imporant observation can be made in Fig. 5.12-5.15 that reactor liquid with inlet KCl concentrtion covers less area as RPM of the impeller increases from 10 to 40. It happens due to increase in mixing efficieny of the CSTR with the rotational speed of the reactor.

The tank Reynolds number decreases with increase in viscosity of liquid. Thus, mean residence time increases with increase in the viscosity of the liquid. Fig. 5.16 with 21cp liquid in CSTR shows that at a particular time (say $\theta = 1$), the distribution of KCl in water-glycerine solution is much less compared to Fig. 5.12 with 11cp solution. Therefore, more viscous solution needs more RPM of the impeller to reach ideal mixing condition as depicted in the figures.

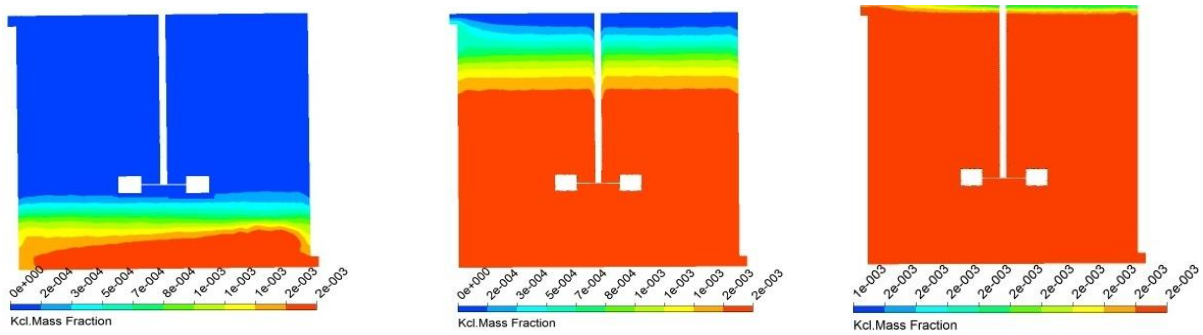

(a) θ = 0.4 (b) θ = 1.0 (c) θ = 2.0

Figure 5.12: The contours of tracer mass fraction with stirrer and baffles for D = 170mm, d =6.6mm, μ = 11cp, N = 10rpm and ρ = 1152kg/m^3 at different time steps.

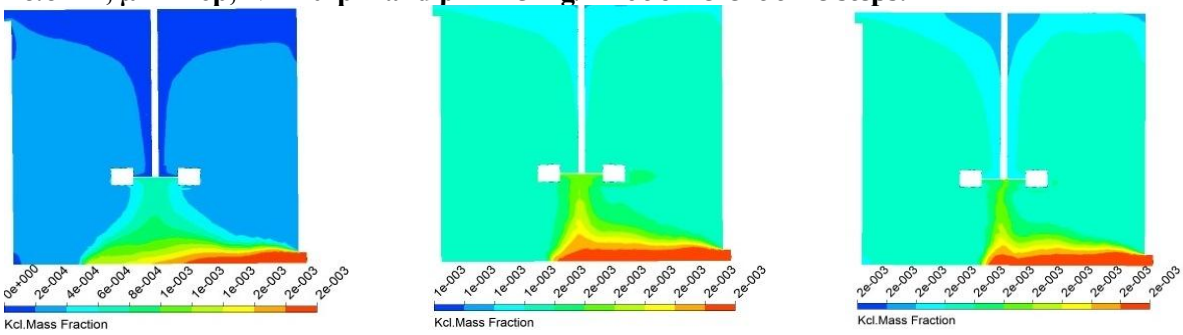

(a) θ = 0.4 (b) θ = 1.0 (c) θ = 2.0

Figure 5.13: The contours of tracer mass fractionwith stirrer and baffles for D = 170mm, d =6.6mm, μ = 11cp, N = 20rpm and ρ = 1152kg/m^3 at different time steps.

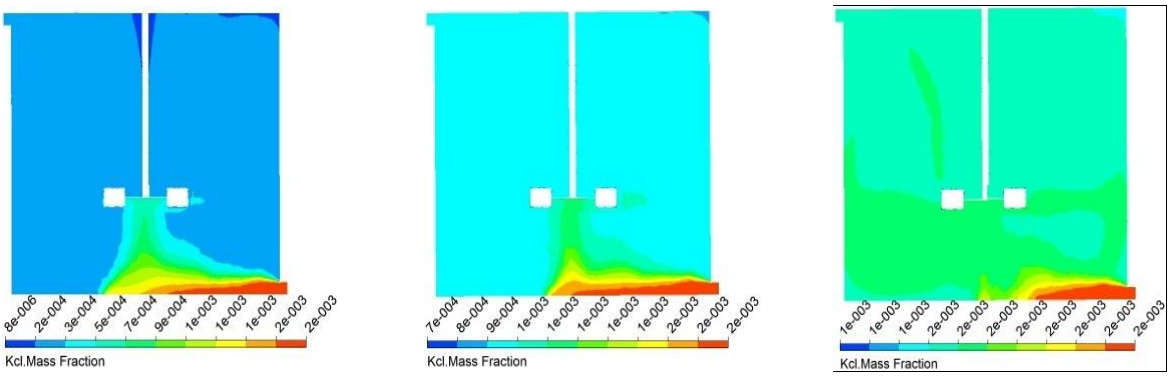

(a) θ = 0.4 (b) θ = 1.0 (c) θ = 2.0

Figure 5.14: The contours of tracer mass fractionwith stirrer and baffles for D = 170mm, d =6.6mm, μ = 11cp, N = 30rpm, Re = 0.753 and ρ = 1152kg/m^3 at different time steps.

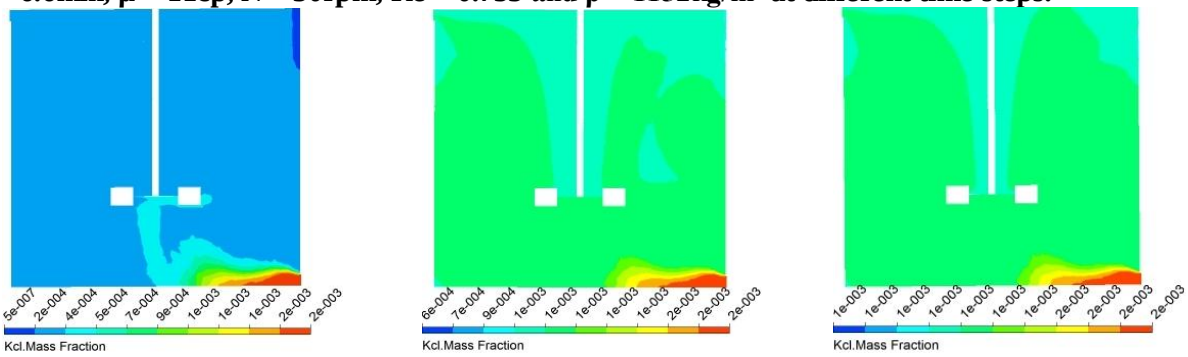

(a) θ = 0.4 (b) θ = 1.0 (c) θ = 2.0

Figure 5.15: The contours of tracer mass fractionwith stirrer and baffles for D = 170mm, d =6.6mm, μ = 11cp, N = 40rpm, Re = 0.753 and ρ = 1152kg/m^3 at different time steps.

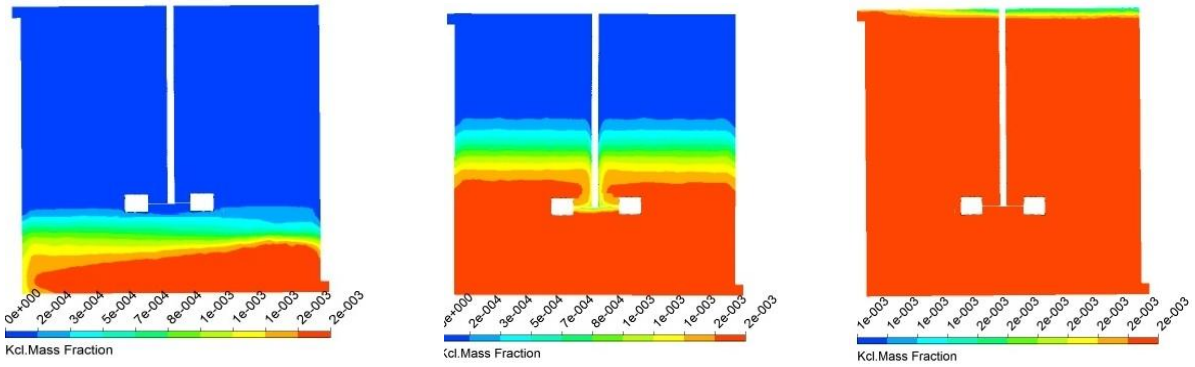

(a) θ = 0.4 (b) θ = 1.0 (c) θ = 2.0

Figure 5.16: The contours of tracer mass fractionwith stirrer and baffles for D = 170mm, d =6.6mm, μ = 21cp, N = 12rpm, Re = 0.516 and ρ = 1180kg/m^3 at different time steps.

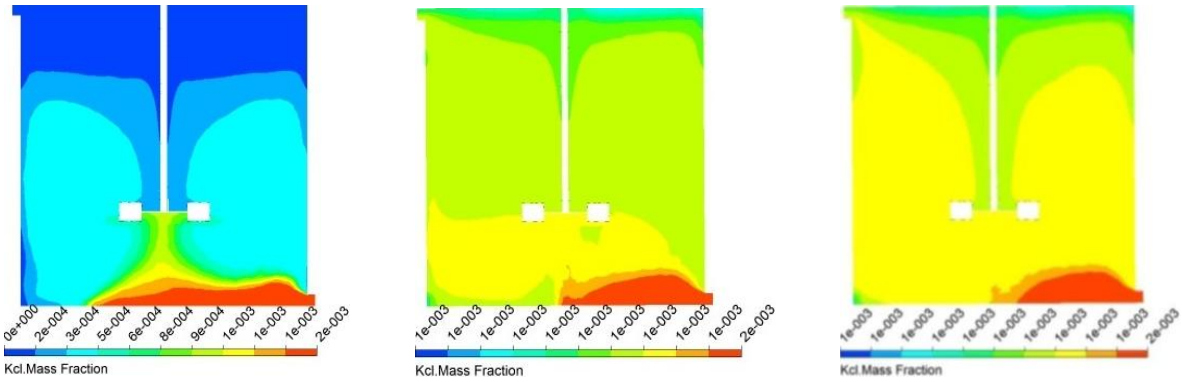

(a) θ = 0.4 (b) θ = 1.0 (c) θ = 2.0

Figure 5.17: The contours of tracer mass fractionwith stirrer and baffles for D = 170mm, d =6.6mm, μ = 21cp, N = 25rpm, Re = 0.508 and ρ = 1180kg/m^3 at different time steps.

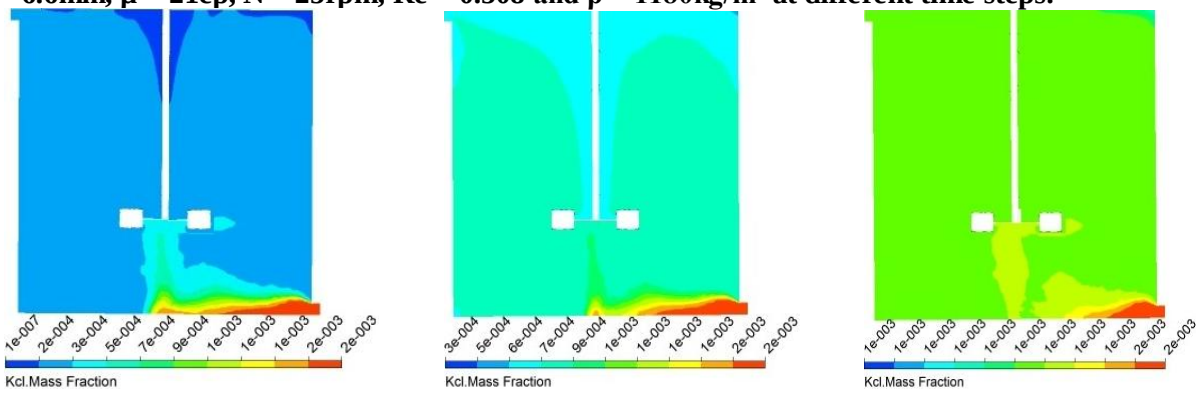

(a) θ = 0.4 (b) θ = 1.0 (c) θ = 2.0

Figure 5.18: The contours of tracer mass fractionwith stirrer and baffles for D = 170mm, d =6.6mm, μ = 21cp, N = 50rpm, Re = 0.520 and ρ = 1180kg/m^3 at different time steps.

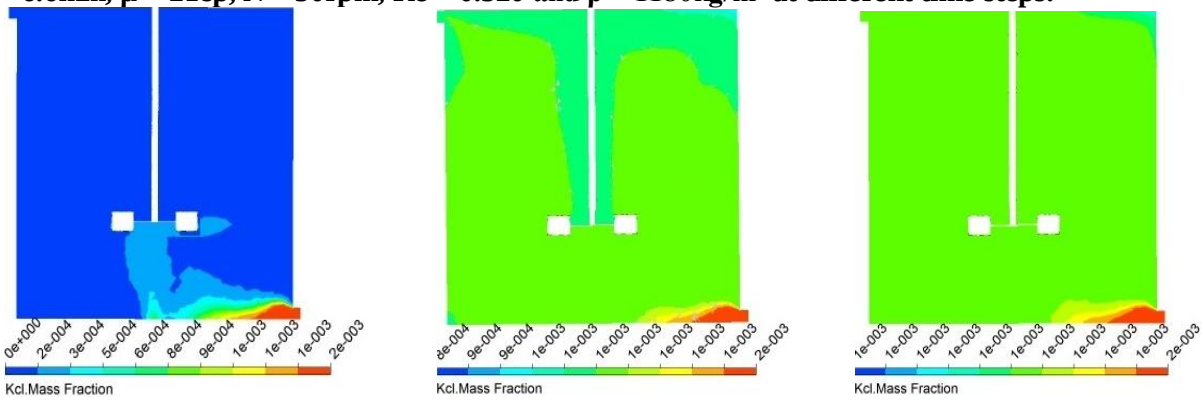

(a) θ = 0.4 (b) θ = 1.0 (c) θ = 2.0

Figure 5.19: The contours of tracer mass fractionwith stirrer and baffles for D = 170mm, d =6.6mm, μ = 21cp, N = 70rpm, Re = 0.508 and ρ = 1180kg/m^3 at different time steps.

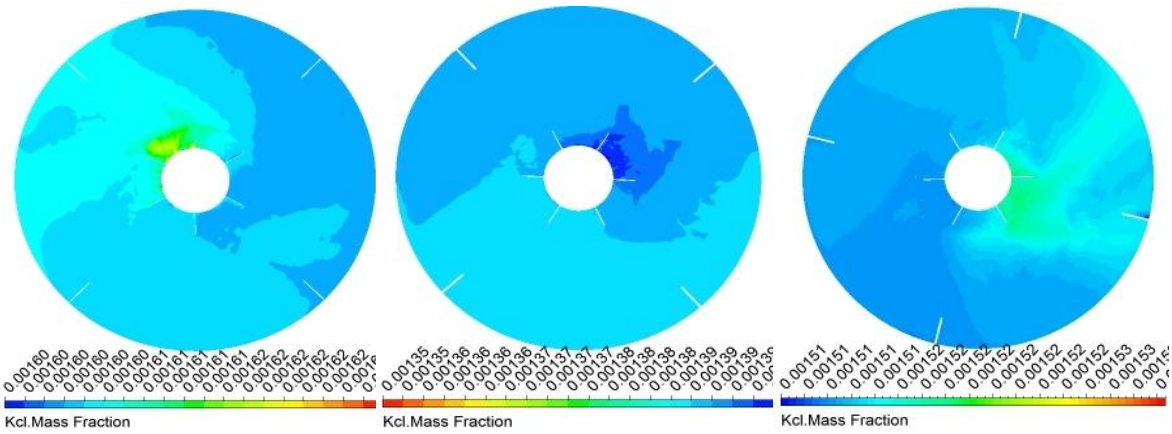

(a) (b) (c)

Figure 5.20: Contours of KCl mass fraction for a CSTR with moving impellers and baffles with D = 170mm, d = 6.6 mm, (a) μ = 11cP, ρ = 1152kg/m^3, N = 40rpm, Re = 0.753; (b) μ = 21cP, ρ = 1180kg/m^3, N = 70rpm, Re = 0.508; (c) μ = 43cp, ρ = 1200kg/m^3, N = 200rpm, Re = 1.64 at θ = 2.0

The contours of KCl around the impeller is shown in Fig. 5.20. It shows a non-uniform distribution of KCl around it.

5.6.5 Contours of Pressure

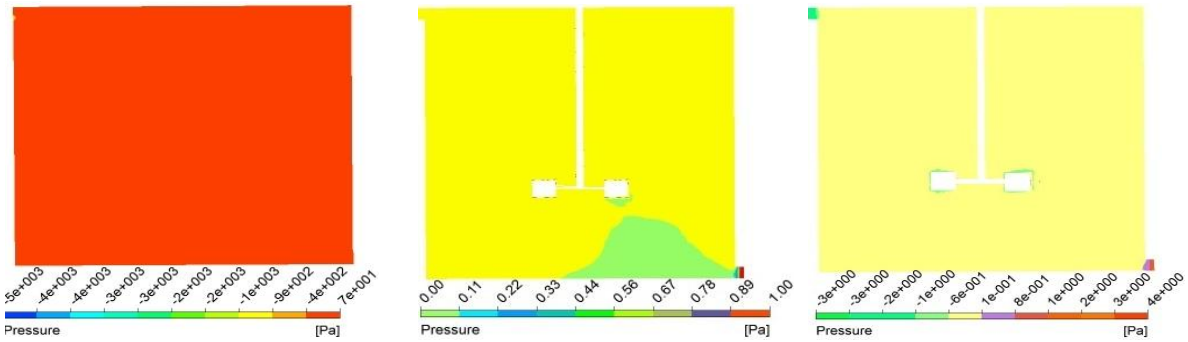

(a) without stirrer and baffles (b) N =10rpm (c) N = 20rpm

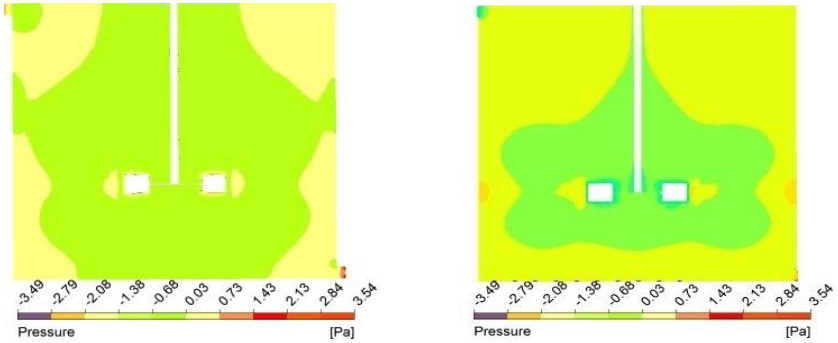

(d) N = 30rpm (e) N = 40rpm

Figure 5.21: The contours of pressure for D = 170 mm, d = 6.6mm (a) Re = 218.4, μ = 1cp, ρ = 1000kg/m^3 and (b) Re = 0.760, μ = 11cp, ρ= 1152kg/m^3, (c-e) Tank Re = 0.753, μ = 11cp, ρ = 1152kg/m^3.

The pressure contours reflects that the distribution of pressure in the reactor depends on the impeller speed, inlet Reynolds number and fluid properties. Figure 5.21a shows the contours of pressure for CSTR without mechanical mixing. As there is no impeller and baffles the pressure is constant throuhout the reactor. Fig. 5.21b-e show contours of pressure at viscosity 11cP and different impeller rotations. The pressure difference is negligible in the reactor at low impeller speed. As impeller speed increases, the pressure change near the impellers and baffles are observed. As viscosity increases from 11cP to 21cP, Fig. 5.22 reveals that there is more variance in pressure magnitude near impellers compared to Figure 5.21. Here also low pressure area is observed around the impeller blades and the area increases with increase in impellers speed and viscosity of CSTR liquid.

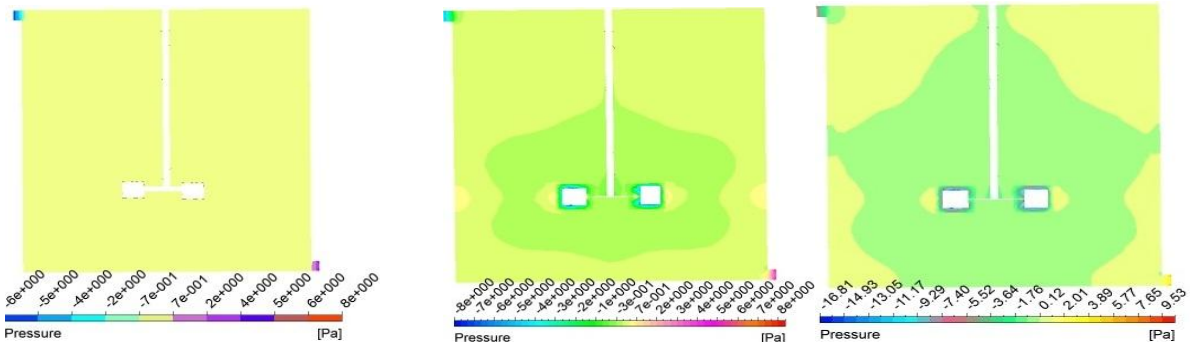

(a) N = 12rpm (c) N = 50rpm (c) N = 70rpm

Figure 5.22: The contours of pressure for D = 170 mm, d = 6.6mm, μ = 21cp, ρ = 1180kg/m^3 (a) Re = 0.516; (b & d) Re = 0.508; (c) Re = 0.520

5.6.6 Velocity Vectors

The velocity vectors for the CSTR are shown in Fig. 5.23to 5.24. The flow path of KCl is cleary viscible in the vector plot for CSTR withot stirrer as shown in Fig. 5.23, and it supports the KCl contours shown in Fig. 5.7-5.11. The figures show that the flow stream issued from the impeller are discharged in the radial direction, with part of the flow recirculating along the vessel wall moves towards the bottom and rest part moves towards top surface, and it results in four circulation loops around the impeller specially at high impeller speeds. The velocity of liquid nearer to the impeller is found maximum at higher RPM of impeller. But at lower RPM, the inlet velocity is found more than the velocity around the impeller (Fig. 5.24a and Fig. 5.25a). Thus, the velocty ditribution at lower impeller speed is almost similar to the without moving case shown in Fig. 5.23. In Fig 5.24-5.25, the flow direction is found unstable, varying from radial to axial. It is also observed in the figures that the size of the loops increases with increase in impeller speed and also the loop moves more

towards the baffels as rpm inmcreases. Fig. 5.24 and 5.25 confirms the formation of loops only at higher rpm.

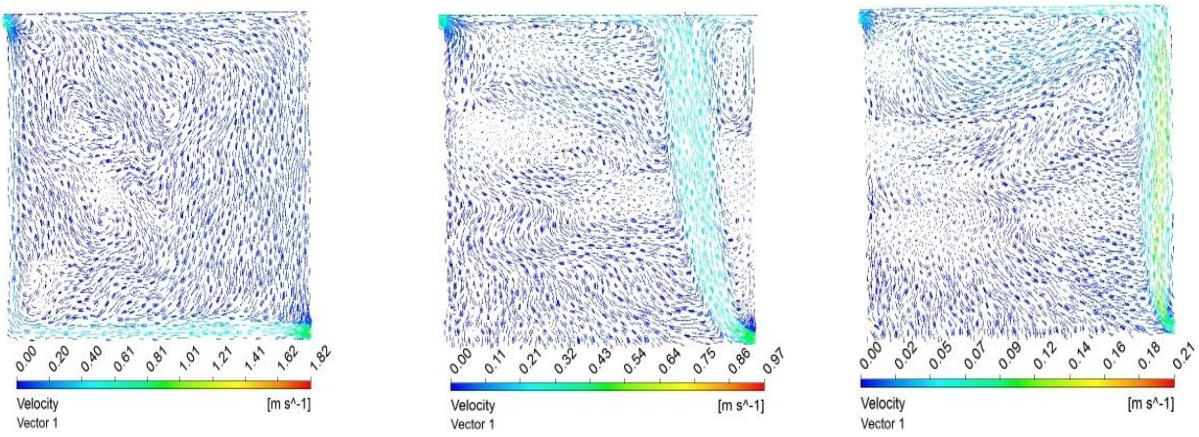

(a) Re = 218. (b) Re = 114.4 (c) Re = 20.8

Figure 5.23: Velocity vectors of CSTR without impeller and baffles with D = 170 mm, d = 6.6mm, μ = 1cp and ρ = 1000kg/m^3.

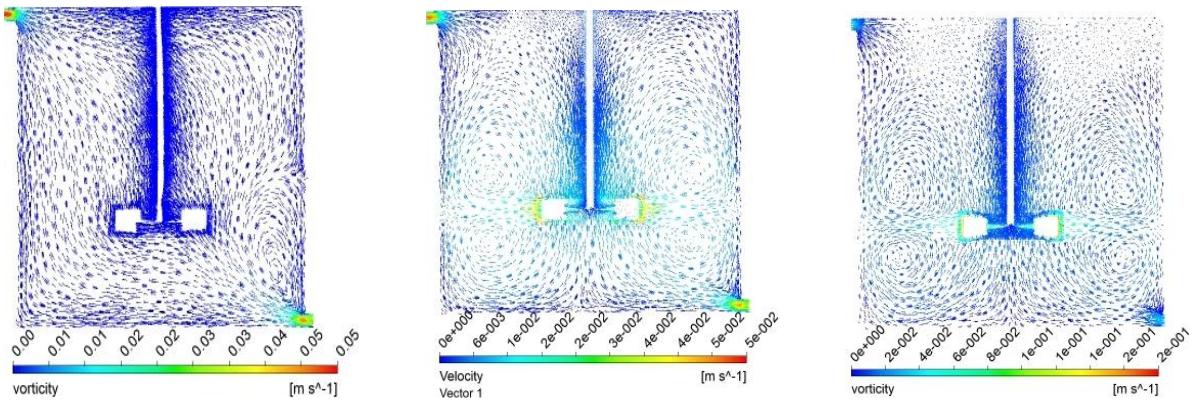

(a) N = 10rpm (b) N = 20rpm (c) N = 40rpm

Figure 5.24: Velocity vectors with moving impeller having D = 170mm, d = 6.6mm, μ = 11cp and ρ = 1152kg/m^3, Re = 0.753.

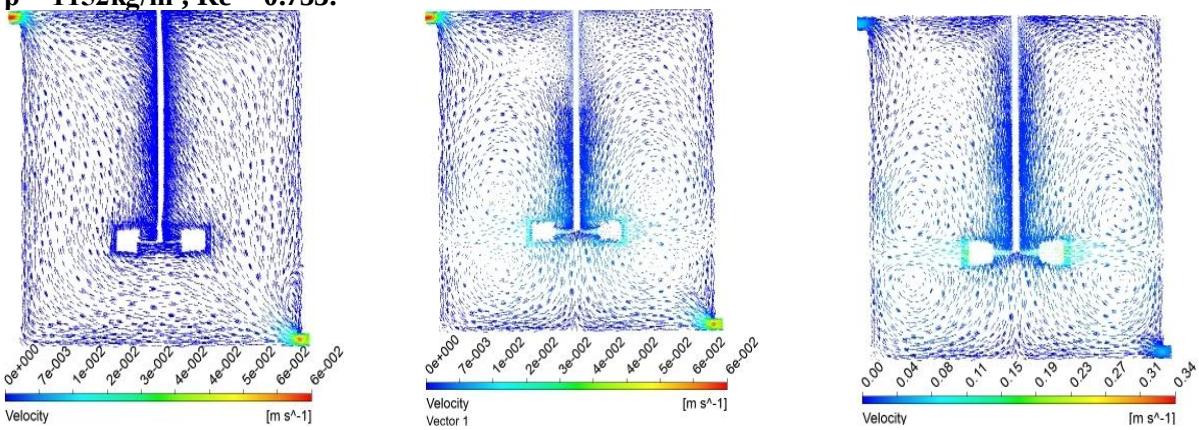

(a) N = 12rpm (b) N = 25rpm (c) N = 70rpm

Figure 5.25: Velocity vectors with moving impeller having D = 170mm, d = 6.6mm, μ = 21cp and ρ = 1180kg/m^3, (a) Re = 0.516, (b) & (c) Re = 0.508.

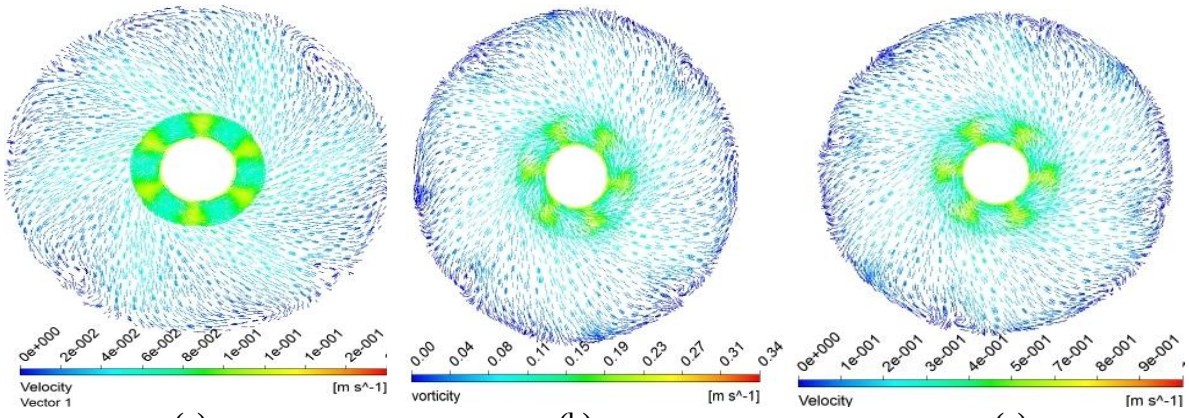

(a) (b) (c)

Figure 5.26: Velocity vectors around the impeller for a CSTR with D = 170mm, d = 6.6 mm, (a) μ = 11cp, ρ = 1152kg/m^3, N = 40rpm, Re = 0.753; (b) μ = 21cp, ρ = 1180kg/m^3, N = 70rpm, Re = 0.508; (c) μ = 43cp, ρ = 1200kg/m^3, N = 200rpm, Re = 1.64.

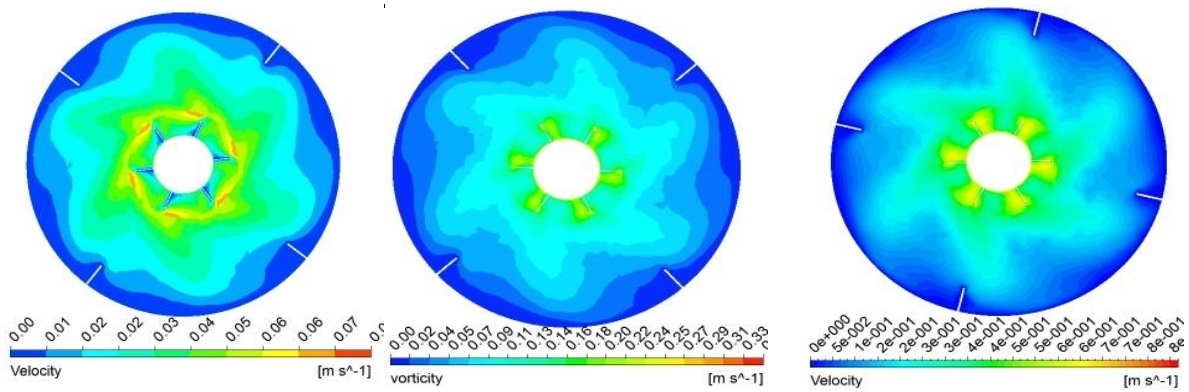

(a) (b) (c)

Figure 5.27: Velocity contours around the impeller for a CSTR with D = 170mm, d = 6.6 mm, (a) μ = 11cp, ρ = 1152kg/m^3, N = 40rpm, Re = 0.753; (b) μ = 21cp, ρ = 1180kg/m^3, N = 70rpm, Re = 0.508; (c) μ = 43cp, ρ = 1200kg/m^3, N = 200rpm, Re = 1.64

The velocity vectors and contours around the impeller are shown in Fig.5.26 and 5.27. The entire plots show the maximum on the impeller surface, and an outward flow from impeller to the CSTR wall.

5.6.7 Contours of Vorticity

The contours of voticities for moving and non-moving stirrer case are discussed in Fig. 5.28 to 5.30. Fig. 5.28 shows that the vorticity is high near the inlet and outlet. The vorticity penetrates more in the radial direction with increase in Re of the tank, and hence, inlet fluid stream moves horizontally at higher Re, whereas at lower Re, the vorticity moves vertically

up and inlet stream also follow the same path. Therefore, the vorticity trajectories support the velocity vector plots. In the central zone of the CSTR more uncertainty in the flow direction is observed. The vortex formation is observed less near the walls and almost absent in certain regions. As Reynolds number increases, the vortices are found less distributed throughout the reactor. In absence of impeller; the vortex moves like a jet horizontally to the opposite wall and then moves vertically parallel to the walls. The length of the jet increases with increase in Re due to decrease in viscous loss of vorticity.

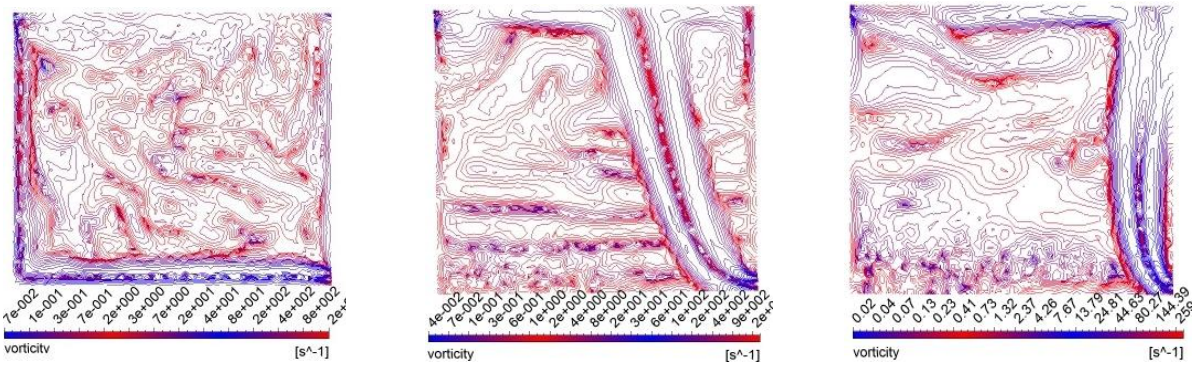

(a) Re-218.4 (b) Re-114.4 (c) Re-29.6

Figure 5.28: Vorticity contours without stirrer and baffles for D = 170mm, d = 6.6mm, μ = 1cp and ρ = 1000kg/m^3.

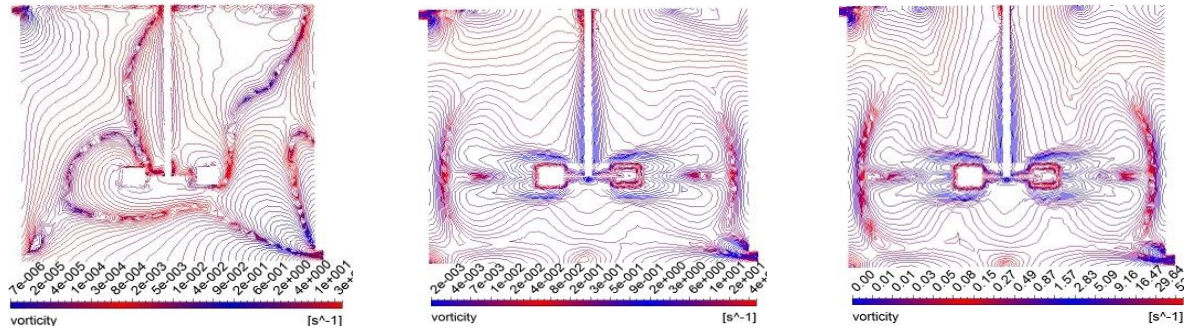

(a) N = 10rpm (b) N = 20rpm (c) N = 30rpm

Figure 5.29: Vorticity contours with stirrer and baffles for D = 170mm, d = 6.6mm, μ = 11cp and ρ = 1152kg/m^3, (a) Re = 0.760; (b-c) Re = 0.753.

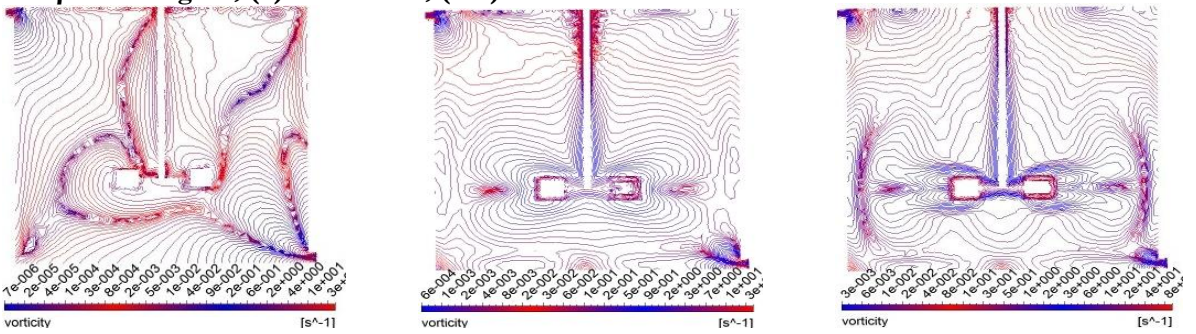

(a) N = 12rpm (b) N = 25rpm (c) N = 50rpm

Figure 5.30: Vorticity contours with stirrer and baffles for D = 170mm, d = 6.6mm, μ = 21cp and ρ = 1180kg/m^3, (a) Re = 0.516; (b) Re = 0.508; (c) Re = 0.508.

To understand the hydrodynamics behaviour of CSTR in presence of moving impellers and baffles, the vorticity contours are presented in Fig. 5.29 to 5.30. All the figures show that the effect of inlet flow on CSTR vorticity is suppressed by rotating impeller.

At low RPM of the impeller (10 RPM in Fig. 5.29 and 12 RPM in Fig. 5.30), the inlet flow energy and the mechanical energy contributed by the impeller are comparable. Hence the fluid moves like a thread around the impeller. As the contribution of inlet flow energy becomes negligible compared to mechanical energy of the impeller at higher Re, the hydrodynamics of the CSTR is controlled by centrifugal force. Hence, a symmetrical flow field is generated as depicted in Fig. 5.29 and 5.30 b & c in terms of vorticity contours. In presence of stirrer and at lower Re, vorticity is found maximum at the inlet (Fig. 5.29a and Fig. 5.30b)) and at higher Re, it becomes maximum around the impeller (Fig. 5.29 and 5.30 b &c).

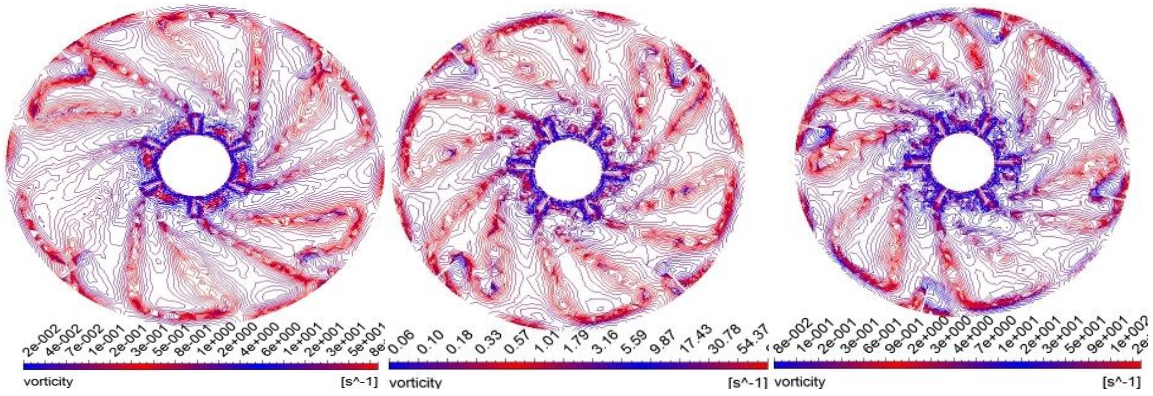

(a) (b) (c)

Figure 5.31: Vorticity contours for a CSTR with moving stirrer and baffles with D = 170mm, d = 6.6 mm, (a) μ = 11cp, ρ = 1152kg/m^3, N = 40rpm, Re = 0.763; (b) μ = 21cp, ρ = 1180kg/m^3, N = 70rpm, Re = 0.508; (c) μ = 43cp, ρ = 1200kg/m^3, N = 200rpm, Re = 1.64.

The contours of vorticity around the impeller are represented in Fig. 5.31. It shows that there is an outward flow from the impeller, and six individual vortex loops are moving with the impeller blades in the angular direction.

5.6.8 Velocity Profiles

The velocity distributions of fluid with radial position at different axial positions are presentenced in the following figures.

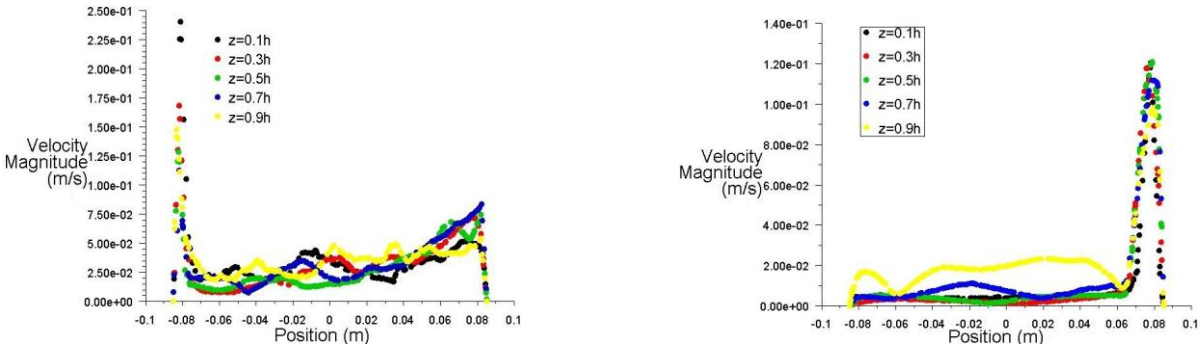

(a) (b)

Figure 5.32: Variation of velocity with radial positionn at different axial positons without impeller and baffles for D = 170mm, d = 6.6mm, μ = 1cp and ρ = 1000kg/m^3, (a) Re = 218.4, (b) 20.8.

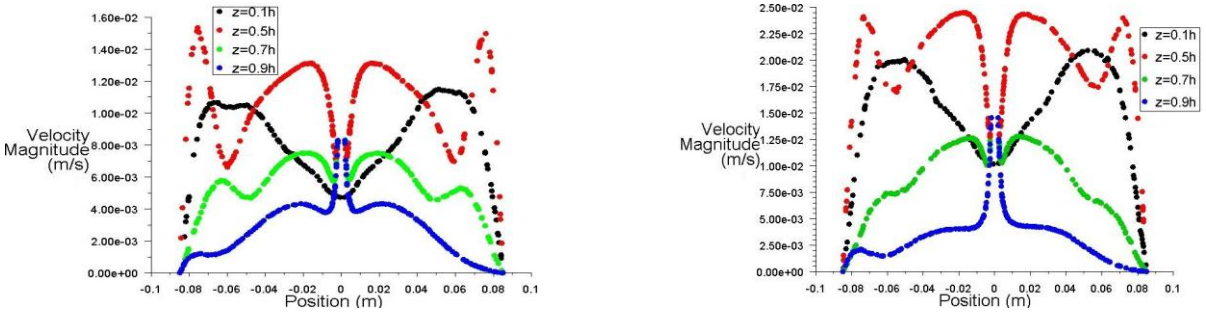

(a) (b)

Figure 5.33: Variation of velocity with radial positionn at different axial positons with impeller and baffles for D = 170mm, d = 6.6mm,(a) μ = 11cp, N = 40rpm and ρ = 1152kg/m^3, Re = 0.753; (b) μ = 21cp, N = 70rpm and ρ = 1180kg/m^3, Re = 0.508.

Fig. 5.32 shows the velocity distributions for non-moving impeller case. The bottom surface of the cylinder is represented by $z = 0$.the figure depicts that among all the profiles velocity passes through the maximum at $z = 0.1H$ and it occurs very close to the left wall surface. It happens due to pass of inlet fluid along the horizontal plane at $z = 0.1H$ and then striking on the left wall and followed by the upward movement along the wall. It is observed in Fig. 5.32a at Re, 218.4. At the lower Re, 20.8 the reverse phenomena is observed. Because of the lower energy capacity of the inlet fluid at Re, 20.8 the fluid moves predominantly in upward direction and hence the maximum velocity is observed near to the right wall surface (Fig 5.32b).

The effects of impeller speed on velocity profiles are clearly visible in Fig. 5.33a and b. Both the figures shown here at relatively higher Re, and hence they have the same kind velocity profiles. The magnitude of velocity at any particular position is found more at higher values of Re. Both the figures also reveal the presence of symmetric velocity profiles.

5.6.9 Effect of Tank Reynolds Number, RPM of Impeller, Viscosity and Density of Liquid on the Mixing Of CSTR with Stirrer and Baffles

The effect of Re, *N*, fluid viscosity and density on the mixing behaviour of the liquid in CSTR is studied. Fig. 5.34 represents the effect of Re on $I(\theta)$. At Re 0.5, dispersion flow occurs, at Re 0.75 the mixing line goes relatively closer to ideal mixing line, and further increase in Re to 1.0 result in the mixing line to follow ideal mixing line. The energy with the inlet flow increases with increase in V^*, which increases proportionately with Re. This inlet energy helps to mix-up the liquid mixture. Therefore, $I(\theta)$ approaches ideal mixing line with increase in Re.

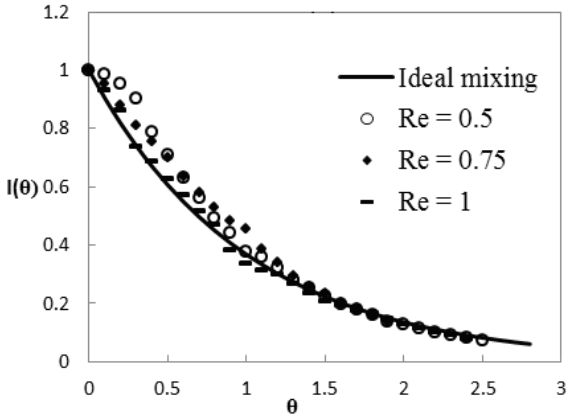

Figure 5.34: Effect of tank Reynolds number on $I(\theta)$ for a CSTR with stirrer and baffles with D =170mm, d = 6.6 mm, μ = 11cp, ρ = 1152 Kg/m^3, N = 20 rpm.

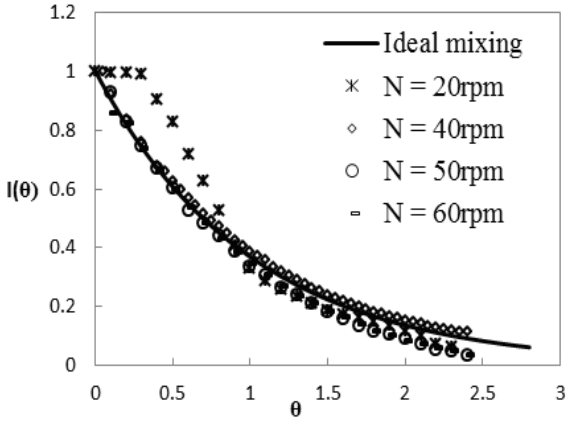

Figure 5.35: Effect of impeller RPM on $I(\theta)$ for a CSTR with stirrer and baffles and with D = 170mm, d = 6.6 mm, μ = 11cp, ρ = 1152 Kg/m^3, Re= 0.753.

The effect of impeller rpm on the mixing efficiency is demonstrated in Fig. 5.31. It can be observed in the figure that the nature of the flow changes from dispersion to ideal mixing state with increase in *N*. A distinct dispersion flow happens at *N* equal to 20, whereas at *N*, 40 to 60, the mixing is very near to ideal mixing condition. This is happening naturally as it is

well known that the amount of mechanical energy imparted on fluid increase with increase in *N*, and hence more mixing.

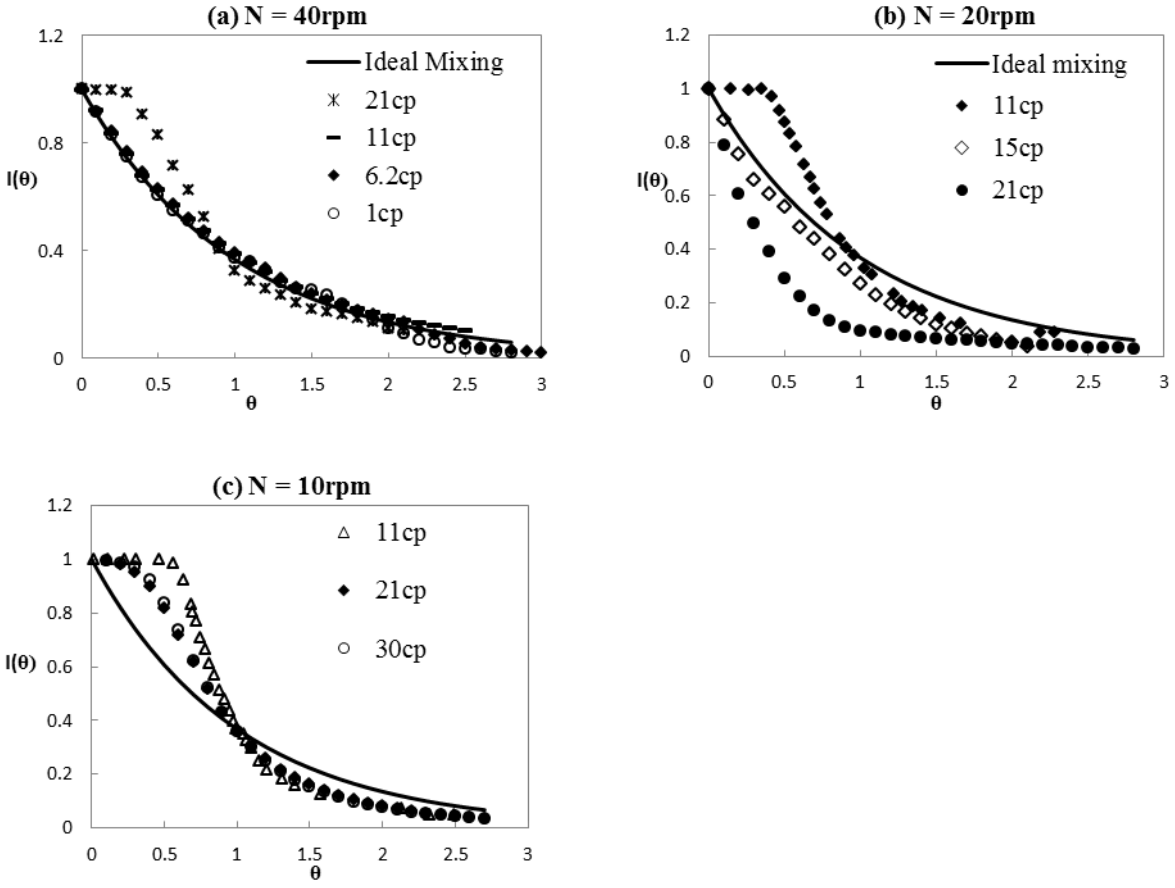

Figure 5.36: Effect of viscosity on $I(\theta)$ for a CSTR with stirrer and baffles and with D = 170mm, d = 6.6 mm, for μ = 1cp, ρ =1000kg/m^3, Re = 218.4; for μ = 6.2cp, ρ = 1130kg/m^3, Re =0.703; for μ = 11cp ρ = 1152kg/m^3, Re = 0.508; for μ = 21cp, ρ is 1180kg/m^3, Re = 0.508; and for μ = 30cp, ρ is 1190kg/m^3, Re = 1.64.

Viscosity of fluid has certain effect on the hydrodynamic behaviour of it and in turn on the mixing behaviour. The effect of viscosity of liquid on $I(\theta)$ at different impeller speeds is shown in Fig. 5.36. The effect at high *N* is just reverse of lower values of it. The figure shows that the mixing line moves towards ideal mixing state with decrease in viscosity at Re 40, whereas it moves away from ideal mixing line for *N* equal to10. For a particular Re, V^* increases with increase in viscosity. The viscous force also increases with viscosity. The impeller does more mechanical work at higher values of *N*, and it makes viscous force negligible at high *N*. At impeller RPM 40, the contribution of inlet energy becomes negligible compared to mechanical energy. Hence mixing is better for low viscous fluid and it is also reflected in Fig. 5.36a. At *N*, 10 the contribution of mechanical energy for mixing is less and

it may in the order or less than the inlet energy. The mixing at *N* equal to 10 is controlled by inlet flow rate V^* which increases with increase in viscosity of the liquid. Therefore, the mixing efficiency at *N*, 10 increases with increase in viscosity and it is observed in Fig. 5.36c. Some peculiar observation is made in Fig. 5.36b, which shows the $I(\theta)$ curve moves towards the ideal mixing line with increase in viscosity from 11cp to 15 cP, but further increase of viscosity to 21cp makes the curve move away from the ideal mixing line in the opposite direction. *N* equal 20 is not sufficient for uniform mixing of fluid inside the tank, but it has relatively more mixing power than *N* equal to 10 RPM. There might be some short-circuit in the CSTR at *N* equal 20 RPM. The increase of viscosity helps to reach KCl to impeller quickly due to increase in V^*. Thus, impeller pushes KCl out of the tank through the short-circuit and the concentration, *C(t)* increase more with time for more viscous fluid. Hence, $I(\theta)$ moves away from ideal mixing line at 21cp in the reverse direction.

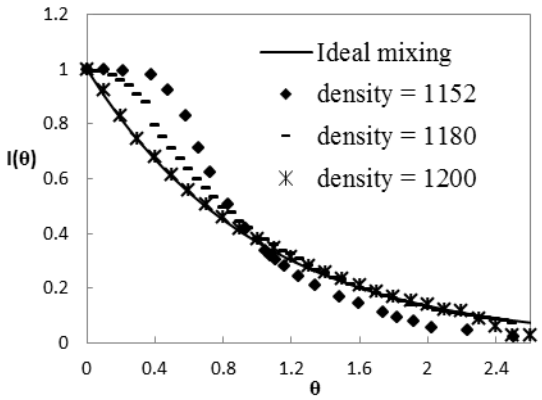

Figure 5.37: Effect of density of liquid on $I(\theta)$ for CSTR with stirrer and baffles and with D = 170mm, d = 6.6 mm, μ = 11cp, ρ = 1152 Kg/m^3, N = 20rpm, Re = 0.763.

The effect of density on the mixing behaviour is depicted in Fig. 5.37. The figure shows that the mixing behaviour changes from dispersion to ideal mixing state as density of the liquid increases. In this study the chosen densities are varying within small range. Probably due to increase in density the centrifugal force applied by impeller on liquid increases at a particular rotational speed of it. Thus the mixing efficiency increases and mixing line approaches the ideal mixing line with increase in density of liquid.

5.6.10 Mean Residence Time, Variance, Hold Back and Segregation

In case of ideal plug flow the value of variance, σ and mean residence time, τ_m should be same. The variation of σ and τ_m with tank Reynolds number is presented in Fig. 5.38a for the

CSTR without stirrer and baffles. The figure shows that at low Re (say 20), there is a substantial difference between the σ and τ_m. It means the mixing is non-ideal for Re equal to 20. As Re makes greater than 20, the mixing process becomes ideal. This is also supported by the profiles in Fig. 5.2. As Re increases, the lateral mixing in the flow direction increases which results in the increase of the dispersion coefficient value. This can be seen in Fig. 5.38b.

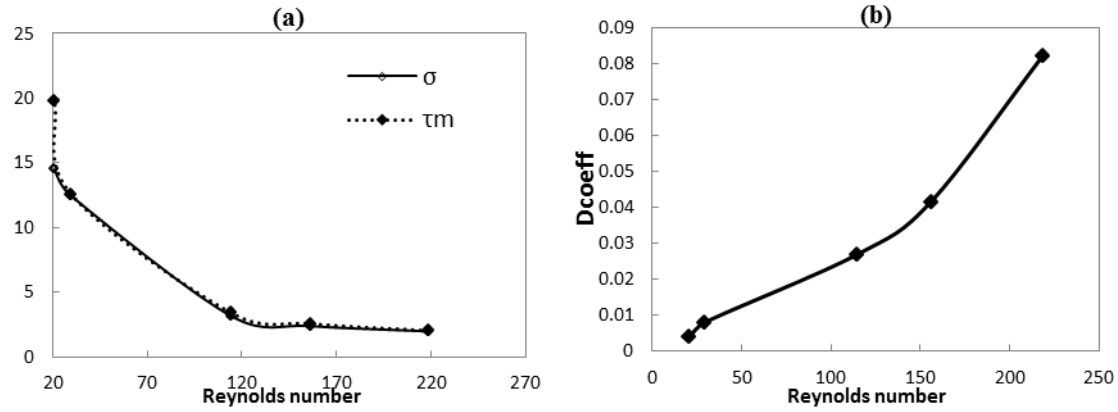

Figure 5.38: Distribution of σ and τ_m and dispersion coefficient for CSTR without impeller and baffles for D = 170mm, d = 6.6mm μ = 1cp and ρ = 1000kg/m^{3}at different Reynolds number.

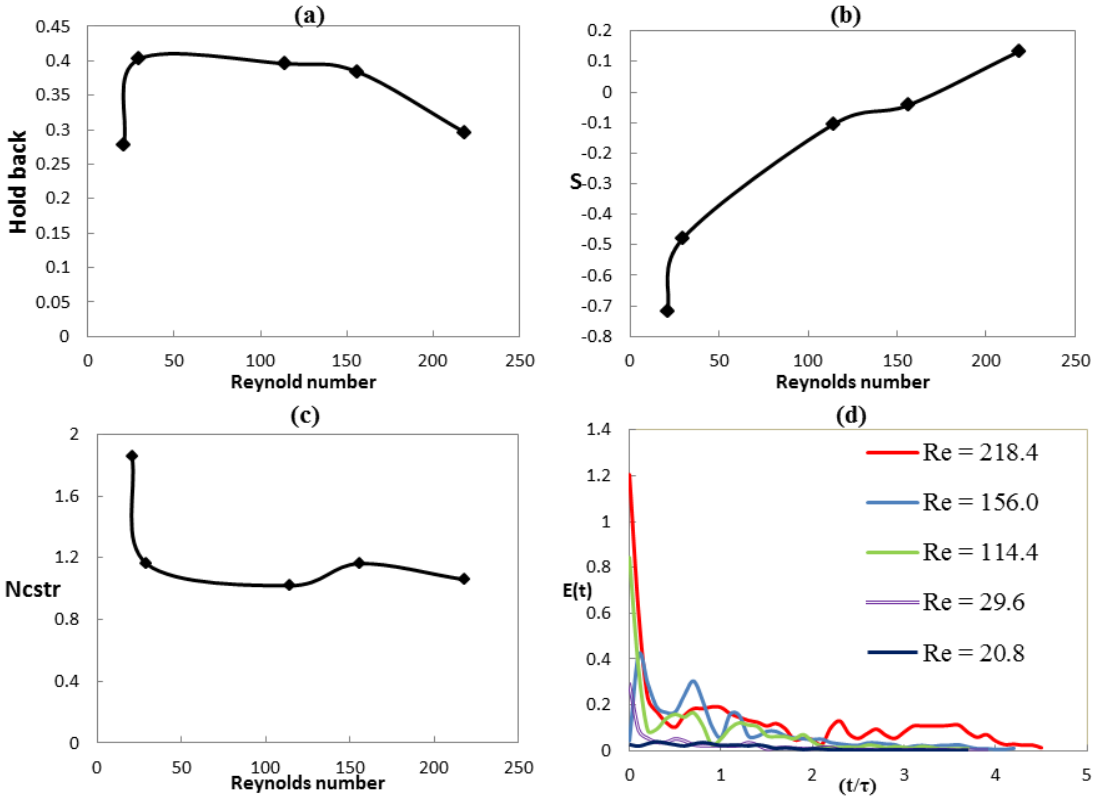

Figure 5.39: Plot of Holdback, Segregation, S, N_{cstr} vs. tank Reynolds number and *E(t)* vs. *t* curves for CSTR without impeller and baffles for D = 170mm, d = 6.6mm μ = 1cp and ρ = 1000kg/m^3.

The distribution holdback and Segregation with tank Reynolds number for CSTR without stirrer is shown in Fig. 5.39a and b respectively. The liquid is completely mixed when holdback is equal to 0.36 (*1/e*). The figure shows that the value of holdback is close to 0.36 for the whole range of Re. Hence based on the holdback distribution, it can be concluded that the mixing is complete at all the used Re values. But the segregation plot as shown in Fig. 5.39b represents that *S* is negative at lower Re values and it increases and tends to 0.36 as Re increases. It can be concluded therefore from the segregation curve that the mixing becomes complete at only higher Re values and at lower Re values the liquid in CSTR is mostly dead fluid. Thus the observation from hold back distribution contradicts the observation from segregation distribution. The value of N_{cstr} is equal to 1.0 for an ideal reactor. Fig. 5.39a shows the effect of Re on N_{cstr}. It is observed in the figure that the value of N_{cstr} decreases and then tends to 1.0 with increase in Re. Therefore, it can be concluded that the CSTR behaves as ideal mixer as Re increases. The residence time function, *E(t)* is plotted against time in Fig. 5.39b for CSTR without stirrer. It shows that maximum peak is obtained at the maximum Re. The time required for the peak tends zero as Re tends to infinite. It happens due to decrease in holdup time, τ with increase in Re.

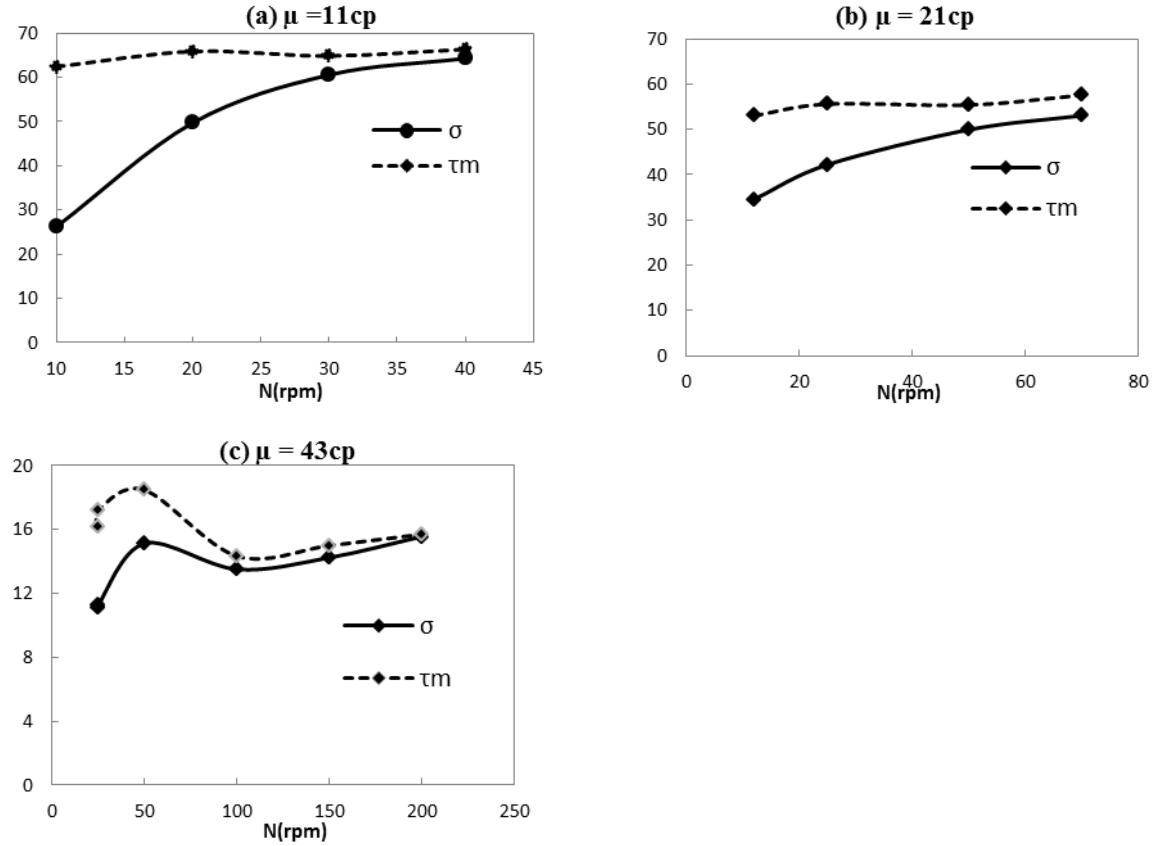

Figure 5.40: Distribution of σ and τ_m for CSTR with impeller and baffles for D = 170mm, d = 6.6mm and (a) Re = 0.753, ρ = 1152kg/m^3, (b) Re = 0.508, ρ = 1180kg/m^3, (c) Re = 0.784, ρ = 1200kg/m^3,

The distribution of σ and τ_m with impeller RPM for CSTR with stirrer and baffles are shown in Fig. 5.40 at different fluid viscosity and tank Reynolds number. All figurers depict that σ and τ_m approach each other with increase in RPM of the impeller. Hence, the mixing of approaches ideal mixing condition with the increase of speed of rotation of the impeller. The figure also reveals that as viscosity increases the magnitude of both σ and τ_m decreases at any particular *N*. It happens because of increase in V^* of the inlet fluid with increase in viscosity of it, which in turn reduces the holdup time, τ. The figure also reveals that the ideal mixing state with equality of σ and τ_m is achieved at higher *N* as the viscosity of fluid increases. This happens naturally as the more viscous fluid needs more mechanical energy for mixing.

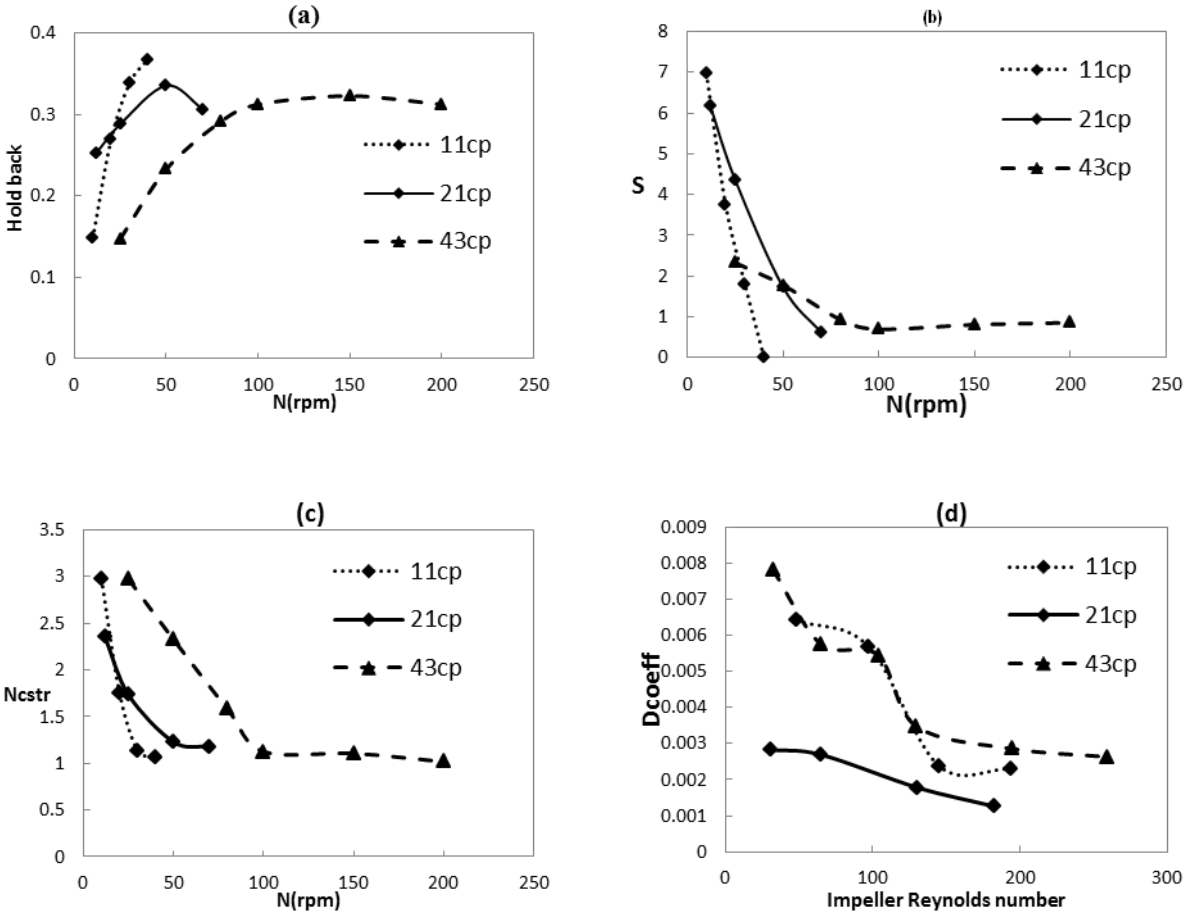

Figure 5.41: Plot of Holdback, Segregation, S, D_{coeff} and N_{cstr} for CSTR with impeller and baffles for D = 170mm, d = 6.6mm, and for μ = 11cp, Re = 0.753, ρ = 1152kg/m^3; for μ = 21cp, Re = 0.508, ρ = 1180kg/m^3; for μ = 43cp, Re = 0.784, ρ = 1200kg/m^3.

The holdback distribution curve as shown in Fig. 5.41a shows that it increases and reaches near about 0.36 value with increase in impeller RPM. Thus the mixing efficiency increases with increase in RPM of the impeller. The values of segregation with moving impeller and baffles are found out of theoretical range (-1 to 0.36) for most of values of *N*. The

dependency of N_{cstr} at different viscosity of the liquid on RPM of the impeller is presented in Fig. 5.42a. It shows that N_{cstr} tends to 1.0 with increase in speed of impeller. Thus mixing tends to ideal mixing state with increase of *N*. It is also observed in Fig. 5.41a that the required RPM of the impeller increases to reach N_{cstr} 1.0 with increase in viscosity. Fig. 5.41b shows that irrespective of fluid viscosity, the dispersion coefficient decreases with increase in impeller Reynolds number ($\mathrm{Re}_m = \rho N d_m^2 / \mu$). Thus the effect of lateral diffusional mass transfer in the flow direction decreases with increase in impeller speed.

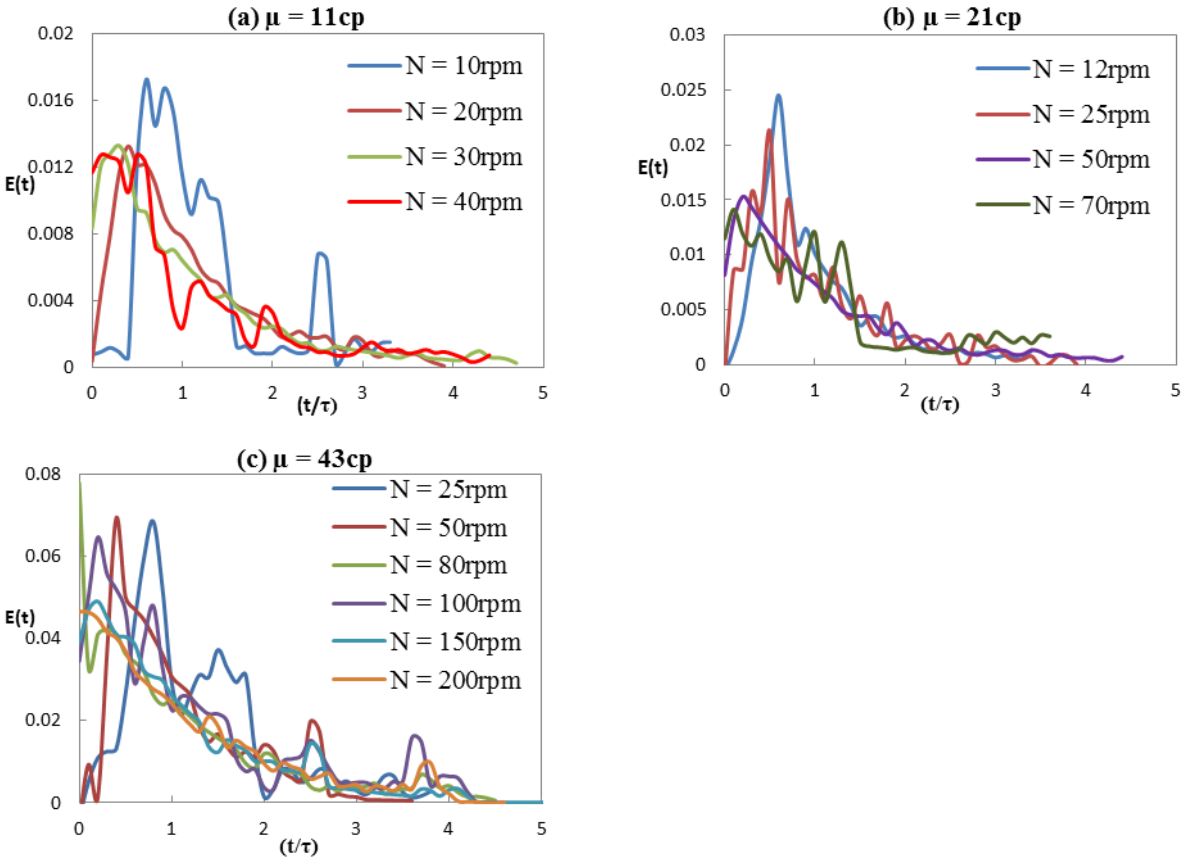

Figure 5.42: Plot of E (t) vs. t for CSTR with impeller and baffles for D = 170mm, d = 6.6mm, (a) Re = 0.753, ρ = 1152kg/m^3; (b) Re = 0.508, ρ = 1180kg/m^3; (c) Re = 0.784, ρ = 1200kg/m^3.

The distribution of residence time distribution function, *E(t)* with time is shown in Fig. 5.42. The figures show that as viscosity increase the peak value of *E(t)* increases at a particular *N* of the impeller. It happens due to decrease in hold up time of the reactor with increase in viscosity.

5.7 CONCLUSIONS

A CFD study of CSTR by ANSYS Fluent was carried to understand the mixing behaviour of it with tracer injection method. The CSTR was simulated with and without impeller and baffles. The computed values of KCl concentration at the outlet were used to find out the age

distribution function $I(\theta)$. The CFD simulated results were found in good agreement with the experimental data of Burghardt and Lipowska, 1972. The effect of RPM of the impeller, tank Reynolds number, Viscosity and density of the liquid on the mixing efficiency was found. The mixing behaviour were changed from dispersion to ideal mixing state as *N* and tank Re increases. The mixing state became dispersion flow with increase of viscosity at higher *N*, but at lower *N* flow was changed to ideal mixing state. At the intermediate speed of the impeller, some anomalous behaviour was observed. The velocity vectors confirmed the formation four loops at higher *Re*. The vorticity and pressure contours successfully resemble the hydrodynamic behaviour of the system. The mixing characteristics also was studied in terms of number of ideal CSTR in series, N_{cstr}, holdback, segregation, mean residence time, τ_m and second moment, σ^2. All the study showed that CSTR behaves as ideal mixer at higher values of impeller speed and tank Reynolds number.

Chapter 6

STUDY ON VORTEX FORMATION INSIDE A STIRRED TANK

Continuous Stirred Tank Reactors (CSTR) generally contains different types of baffles, like four flat vertical plates which either fixed to or offset from vessel wall to avoid vortex formation and air entrainment in the reactor. The presence of baffles enhances mixing process effectively. However, vessels without baffles are also have importance in many applications such as crystallisation and precipitation, solid-liquid mass transfer, fermentation, solid suspension and many more. A vast amount of experimental and computational fluid dynamic modelling work on the hydrodynamics and mixing in baffled vessels agitated mostly by Rushton turbines and also other agitators types has been reported in the literature. But, a very limited number of experimental and computational studies have been carried out in unbaffled vessels (Mahmud et al., 2009). Nagata, 1975 has determined velocity profiles in a flat bottomed unbaffled cylindrical vessel with co-axial turbine agitator. The Reynolds number used to carry out the experiment was in the order of 10^5. In most experimental studies, the liquid surface was covered with lid to prevent vortex formation and air entrainment.

The objective of this chapter is to simulate mixing tank with different types of impellers at different axial position, and capture the interface between gas and liquid phase. The computed values of the vortex height are compared with the theoretically computed values. The simulation of vortex formation study in continuous stirred tank reactor is also carried out to see the evolution of vortex height with time.

6.1 EMPERICAL MODEL EQUATIONS

In unbaffeled vessels, the formation of vortex depends on the impeller speed. At high impeller speed, the gas-liquid may reach the impeller surface. It is called the critical impeller speed. This critical impeller speed gives a good condition for mass transfer between gas-liquid heterogeneous systems. While, mixing below the critical impeller speed is often desired to avoid aeration and strong vibration of the rotating impeller shaft that may lead to mechanical failure (Rieger et al., 1979).

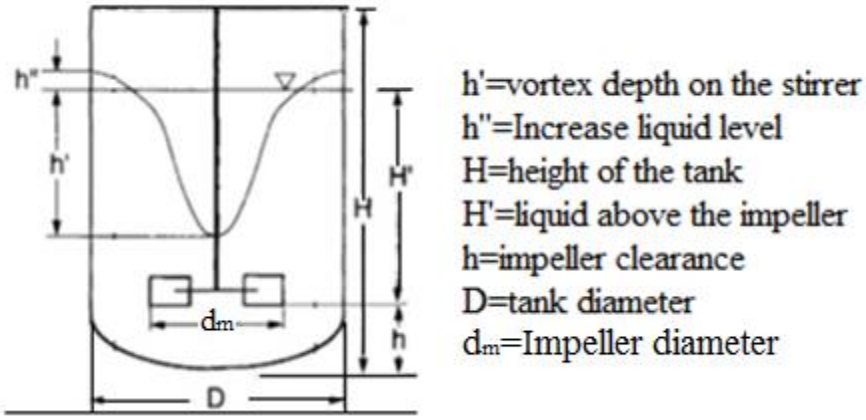

Figure 6.1: Formation of vortex in stirred vessel (Zlokurnik, 2001).

In general, vortex formation as shown in Fig. 6.1 involves with the lowering of the liquid level i.e. vortex depth h' and increasing the liquid level, h'' on the vessel wall. The vortex depthh' depends upon the stirrer type and vessel geometry, which includes stirrer diameter d_m, stirrer speed N, liquid height H' above the stirrer at rest, the physical properties of the liquid like density, kinematic viscosity and also on the gravitational constant, g.

Mathematically h' can be given as

$$h' = f_1(d_m, H', \rho, \nu, N, g) \qquad 6.1$$

The dimensional analysis gives,

$$\frac{h'}{d_m} = f_2\left(Fr, Re_m, \frac{H'}{d_m}\right) = f_3\left(Fr, Ga, \frac{H'}{d_m}\right) \qquad 6.2$$

where $Fr = \frac{N^2 d_m}{g}$, is the Froude number; $Re_m = \frac{\rho N d_m^2}{\mu}$ is the Reynolds number;

$Ga \equiv \frac{Re_m^2}{Fr} \equiv \frac{d_m^3 g}{\nu^2}$, is the Galileo number

Van de Vusse, 1955 investigated the mixing conditions under which the vortex reaches the impeller surface i.e.$h' = H'$, and at critical speed Eq. 6.2 reduces to

$$\frac{h'}{d_m} = f_2(Fr, Re_m) \qquad 6.3$$

The empirical relations developed by Van de Vusse is

$\mathrm{Re}_m \le 3\times10^3$ $\quad \frac{h'}{d_m} = 24 \cdot Fr \cdot Re_m^{-0.8}$ 6.4

$\mathrm{Re}_m \ge 10^4$ $\quad \frac{h'}{d_m} = 2 \cdot Fr$ 6.5

Zlokarnik, 1971 has done experimental investigation to find vortex depth of a gate agitator, six-blade disc turbine and propeller in CSTR. The experiments was carried out for three different sized vessels (D= 300; 400; 600 mm). In the work, the following h'/d_m relation was developed for turbine impeller.

$$\frac{h'}{d_m} = 62 \cdot Fr \cdot (0.1 - Ga^{-0.18}) \cdot \left(\frac{H'}{d_m}\right)^{-0.16} \quad 6.6$$

Le Lan and Angelino, 1972had reported a semi-theoretical equation for the depth of vortex created by using six flat-blade disc turbine. The semi-empirical relation is

$$\frac{h'}{d_m} = \pi^2 \cdot \left(\frac{Re_m}{3.27 \cdot Re_m + 4400} - 0.05 \cdot \frac{D}{d_m}\right) \cdot Fr \cdot \frac{D}{d_m} \quad 6.7$$

For the range of $\frac{D}{d_m} = 1.39 \; to \; 4.55$, $\frac{h}{d_m} = {}^1/_2 \; to \; {}^2/_3$ and $Re_m = 5000 \; to \; 7\times10^4$

Rieger et al., 1979 carried out an experimental investigation of vortex depth in an unbaffled cylindrical vessel with co-axial turbine. Five different types of impellers: Six standard-blade disc turbines, six flat -blade turbine, six pitched-blade turbine, and three pitched -blade turbine and anchor agitator were used in the work. Two different impeller positions with h = d_m and h= d_m/3.On the basis of theoretical analysis, the dimensionless vortex depth was correlated as a function of Froude and Galileo numbers and relative impeller size. For high and low Galileo number range, the following equations are recommended for the prediction of the vortex depth respectively,

$$\frac{h'}{d_m} = B_1 \cdot Ga^{0.069} \cdot \left(\frac{D}{d_m}\right)^{-0.38} \cdot Fr^{1.14 \cdot Ga^{-0.008} \cdot \left(\frac{D}{d_m}\right)^{0.008}} \quad 6.8$$

$$\frac{h'}{d_m} = \bar{B}_1 \cdot Ga^{0.33} \cdot \left(\frac{D}{d_m}\right)^{-1.18} \cdot Fr^{3.38 \cdot Ga^{-0.074} \cdot \left(\frac{D}{d_m}\right)^{0.14}} \quad 6.9$$

Where B_1 and $\bar{B}_1$ are to be determined experimentally by fitting Eq. 6.8 and 6.9 respectively. They have found that the deepest vortex is created by a six flat-blade turbine, which is

followed by a six-blade disc turbine, six pitched -blade turbine and pitched three-blade turbine. They also have concluded that a decrease in impeller clearance caused decrease in the vortex depth for all agitators expect for a six flat-blade turbine where the effect of impeller clearance was found insignificant.

6.2 BACKGROUND OF COMPUTATIONAL WORK

Numerical simulations of turbulent free surface flows in unbaffled vessels are scant. Ciofalo et al., 1996 developed an iterative method to determine the vortex shape. The technique involved with an initial guess of the free surface profile, which is assumed as flat. The free surface profile was used to generate body fitted computational mesh. The flow field and surface pressure using different RANS turbulence models were calculated on the generated body fitted mesh. The surface pressure was used to compute the new shape of liquid surface. The method is computationally inexpedient as it requires generation of new mesh for the next iteration. Hence the use of VOF method for capturing gas-liquid interface is more convenient option. The VOF method for CFD was first applied by Serra et al., 2001 to simulate flows with wavy free surface in baffled vessels.

Haque et al., 2006 has coupled VOF method with a homogeneous multiphase CFD model. It was used first time to simulate turbulent flows with liquid surface in an unbaffled vessel, which is agitated by a paddle impeller and Rushton turbine. The predicted vortex profiles generated by both impellers using the free surface models were compared with the experimentally determined profiles by Nagata, 1975 and Ciofalo et al. 1996.

Torre et al., 2007 have used Eulerian-Eulerian multiphase approach with VOF method along with $k-\varepsilon$ and Reynolds Stress Transport (RST) turbulence models to capture the vortex shape and air entrainment. The simulation was done in a partially baffled vessel agitated by a retreat curve blade impeller. The numerical prediction of the free surface shape was in good agreement with experimental data.

Lamarque et al., 2010 have simulated a complex turbulent free surface flow in an unbaffled mixing tank using Large-eddy Simulation. The free surface vortex generation was captured using a front tracking method. The fluid was stirred by a magnetic rod instead of a classical mixing device such as paddle or propeller impellers.

6.3 DEFINITION OF THE PROBLEM &COMPUTATIONAL ALGORITHMS

A flat bottom unbaffled stirred vessel is taken for the computational simulation of air-water multiphase system. The density and viscosity of water used for simulation is 998.2 kg/m^3 and 0.001 kg/m-s respectively. Similarly for air the density is 1.225 kg/m3 and viscosity is 1.7894×10^{-5} kg/m-s. The diameter (D) of vessel is 0.2 meter. The height of vessel is extended to 1.5D in order to give sufficient space for the elevation of water along the wall surface. Two different types of impeller, Rushton turbine and paddle impeller are used for stirring liquid water. The diameter of both the impellers (d_m) is 0.33D.Two different positions of 0.33D and 0.25$D$are used to mount the impellers above the bottom surface of stirred vessel. The computational domain is discretised using an unstructured mesh consisting of near about2, 00,000 tetrahedral elements (Fig. 6.2). At rest position the height of liquid is maintained at 0.2m above the bottom of vessel.

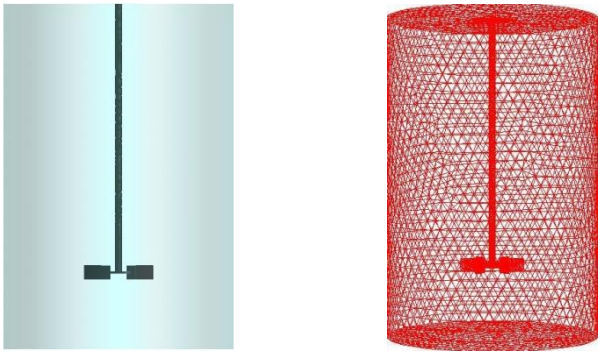

(a) (b)

Figure 6.2: (a) computational vessel domain, (b) computational mesh

The unbaffled stirred vessel is modelled using a moving reference frame (MRF) and VOF method for capturing air-water interface. In MRF approach, the stirrer and shaft are kept stationary while the vessel wall and bottom surface are assigned an angular velocity which is equal and opposite of the stirrer rotational speed. No-slip boundary condition is applied to all solid walls. At the top surface of the cylinder (computational domain in gas phase) zero-shear boundary condition is used. The Reynolds Averaged Navier-Stokes (RANS) equations are solved to obtained velocity field inside the vessel. The realizable $k-\varepsilon$ turbulence model with standard wall function is used to resolve the turbulence created by moving stirrer. The PISO algorithm is used for coupling the pressure and velocity. All the simulations are carried out using transient solver with first order implicit scheme in time and first order upwind

difference scheme for convective and turbulent term. The convergence criteria for all discretised terms are set to the order of 10^{-3}.

6.4 RESULTS AND DISCUSSIONS

The simulation is carried out at four different stirrer rotating speed, 100, 200, 300 and 400 rpm. The stirrer Reynolds number ($\rho N d_m^2/\mu$) for each rotating speed is in the turbulent region. The contours of water phase in Fig.6.3 and 6.4 show the predicted profiles of air-water interface obtained using VOF method in the stirred vessels for both Rushton turbine and paddle impeller with bottom clearance of 1/3*D*.

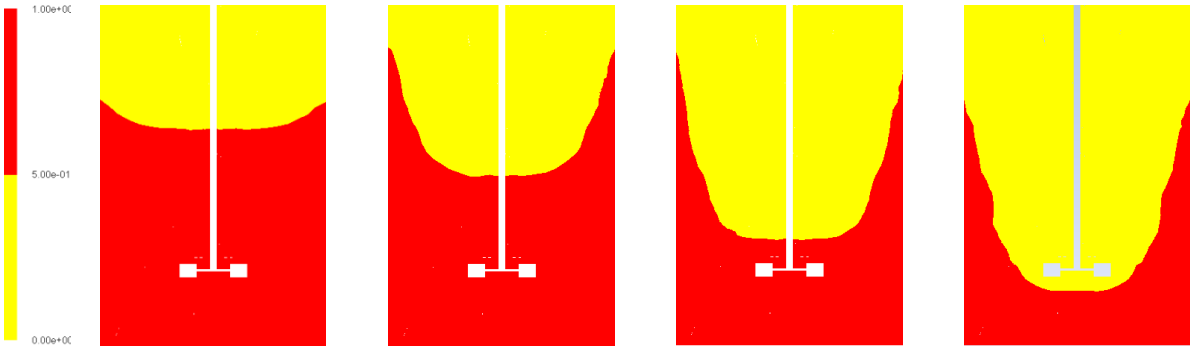

(a) 100 rpm (b) 200 rpm (c) 300 rpm (d) 400 rpm

Figure 6.3: Predicted air-water interface in stirred vessel agitated by Rushton turbine with bottom clearance of 1/3*D*

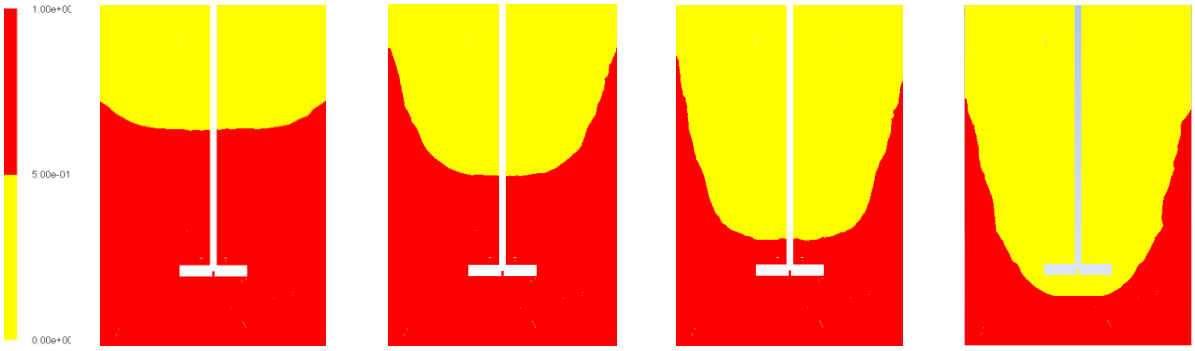

(a) 100 rpm (b) 200rpm (c) 300 rpm (d) 400 rpm

Figure 6.4: Predicted air-water interface in stirred tank agitated by Paddle impeller at bottom clearance of 1/3*D*

The figures show that as the rotating speed of stirrer increases the depth of air-water interface also increases. At stirrer rotating speed of 400 rpm, the air-water interface level is well below

the stirrer mounting height. Table 6.1 draws the comparison of theoretical vortex height with predicted air- water interface from the simulation. The theoretical vortex height is calculated using Eq. 6.6. The predicted air-water interface is calculated by subtracting the final position of interface from the initial position that is 0.2m.

Table 6.1: Comparison of air-water interface height between theoretical and predicted values with impeller clearance 1/3D

Impeller Rotation (RPM)	Theoretical vortex height value Eq. 6.6	Predicted air-water interface value at clearance 1/3*D* of impeller (in mm)	
		Rushton turbine	Paddle impeller
100	4.12	9.1	10.1
200	16.48	50.4	50.85
300	37.083	106.3	106.3
400	65.925	152.7	156.71

Fig 6.5 and 6.6 shows the predicted profiles of air-water interface for both types of stirrer Rushton turbine and paddle impeller with bottom clearance of 1/4*D* for stirrer rotating speed ranging from 100 to 400 rpm.

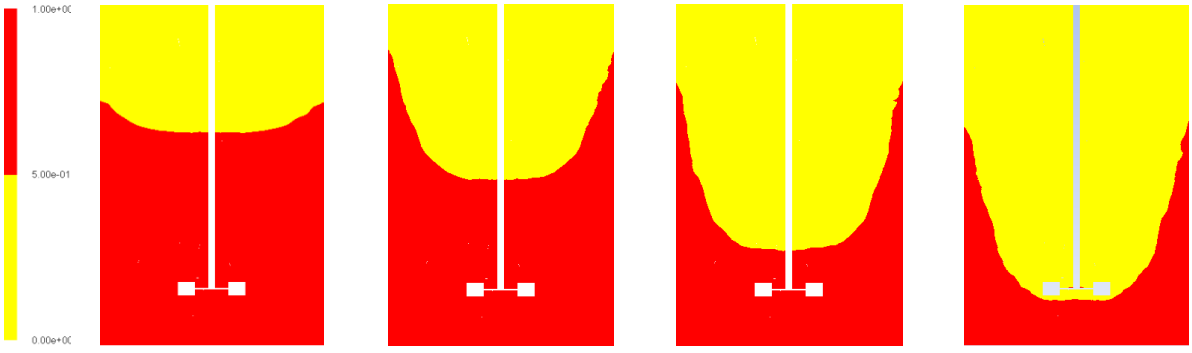

(a) 100 rpm (b) 200 rpm (c) 300 rpm (d) 400 rpm

Figure 6.5: predicted air-water interface in stirred vessel agitated by Rushton turbine at bottom clearance of 1/4*D*

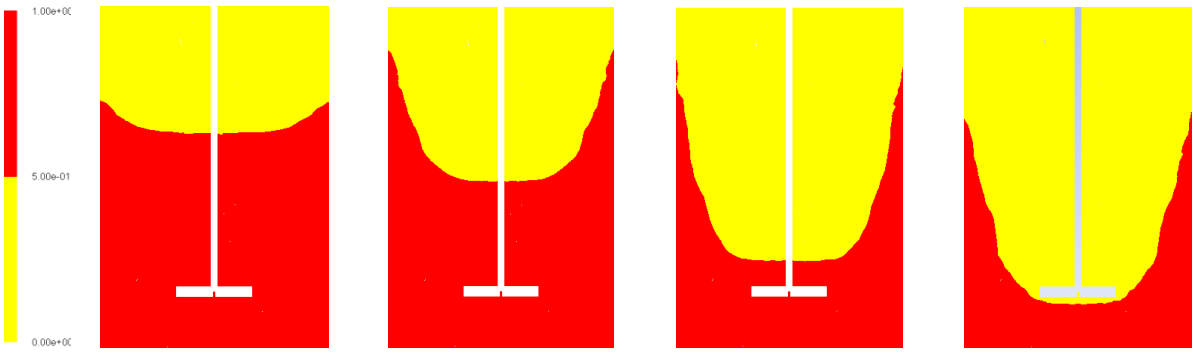

(a) 100 rpm (b) 200 rpm (c) 300 rpm (d) 400 rpm

Figure 6.6: Predicted air-water interface in stirred tank agitated by Paddle impeller at bottom clearance of 1/4*D*

The comparison of theoretical vortex height with predicted air- water interface for the stirrer with bottom clearance of 1/4*D* can be seen in table 6.2.

Table 6.2: Comparison of air-water interface height between theoretical and predicted values with impeller clearance 1/4D

Impeller Rotation (RPM)	Theoretical vortex height value From Zlokarnik (in mm)	Predicted air-water interface value at clearance 1/4D of impeller (in mm)	
		Rushton turbine	Paddle impeller
100	4.36	12.74	11.9
200	17.44	54.31	53.5
300	39.26	116.16	122.7
400	69.79	148.67	161.4

From both the tables 6.1 and 6.2 it is clear that the predicted values of air-water interface by VOF method is found very large compared to the theoretical values of it. The values predicted are almost double the theoretical values.

The velocity vector plots for both Rushton and paddle impellers at different rotating speed of stirrer with bottom clearance of 1/3*D* are shown in Figs 6.7 and 6.8. The vectors are shown on a plane which is at 1/3*D* distance from the bottom surface. The same natures of velocity vector profiles are obtained for the stirrer with off bottom clearance of 1/4*D*. It is observed inFigs6.7 and 6.8 that water is set to circulatory motion due to rotation of stirrer in the

absence of baffles in vessel. The velocity magnitude increases with increase in rotating speed of impeller. The maximum magnitude of velocity is found near to the wall of the vessel. This is due to the simulation strategy adapted to solve the problem where the stirrer and shaft are kept constant and the wall of the vessel is assigned to angular rotation speed.

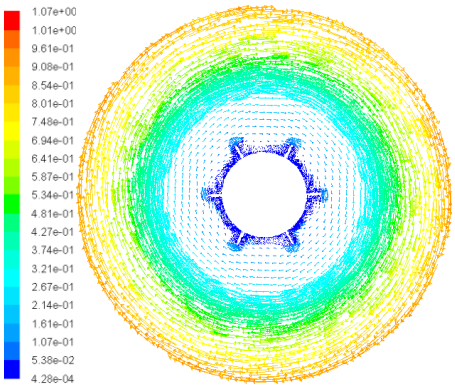

a) 100 rpm

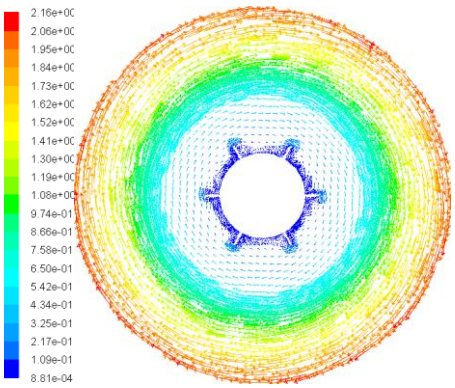

b) 200 rpm

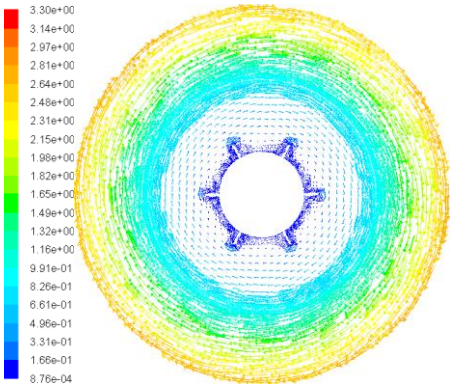

c) 300 rpm

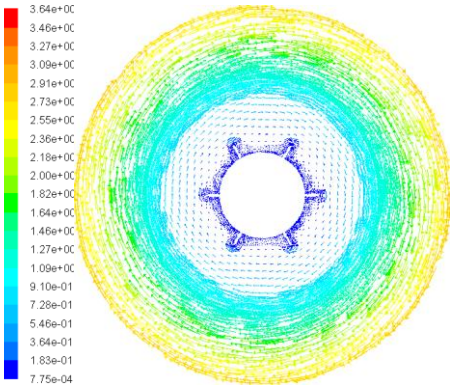

d) 400 rpm

Figure 6.7: Velocity vector plots for Rushton turbine mounted at clearance of 1/3D

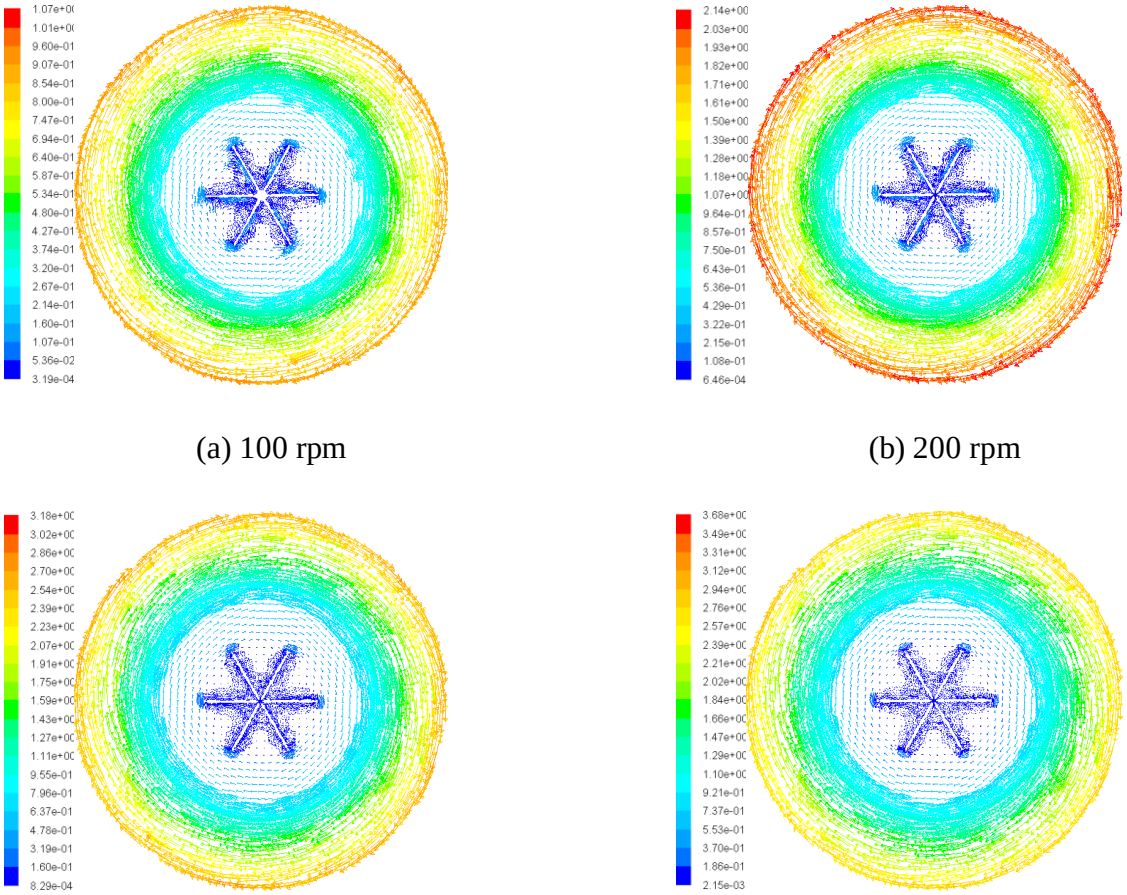

(a) 100 rpm

(b) 200 rpm

(c) 300 rpm

(d) 400 rpm

Figure 6.8: Velocity vector plots for paddle impeller mounted at clearance of 1/3D

Figs 6.9 and 6.10, shows the counter plots of vorticity near the stirrer region for Rushton and paddle impeller respectively. The formation of trailing vortices behind each blades of Rushton turbine and paddle impeller can be clearly seen in Fig6.9 (b) and 6.10 (b).

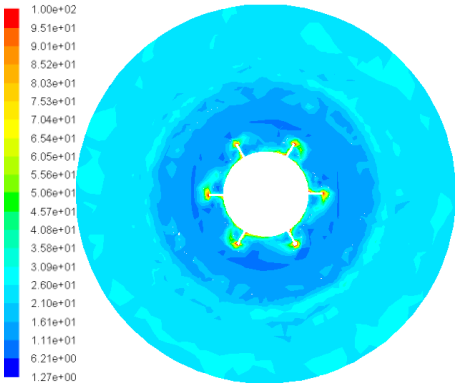

(a) 100 rpm

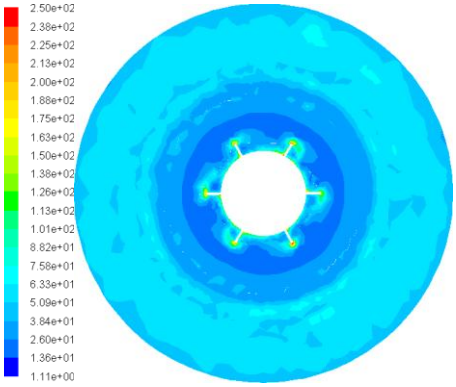

(b) 200 rpm

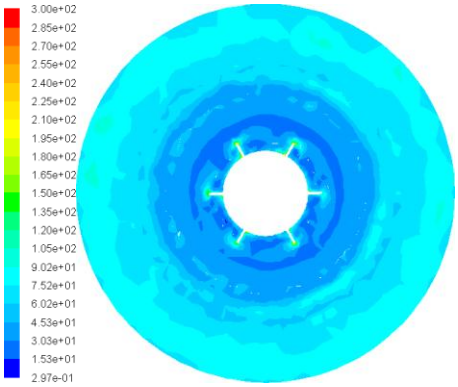

(c) 300 rpm

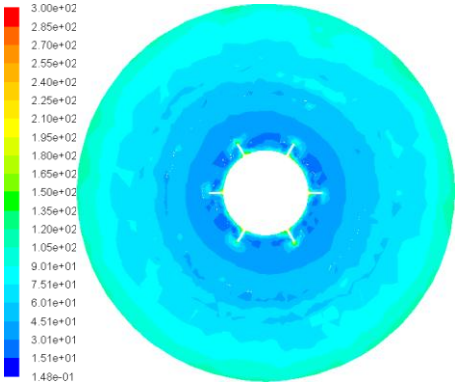

(d) 400 rpm

Figure 6.9: Contour plots of vorticity near Rushton turbine mounted at clearance of 1/3D

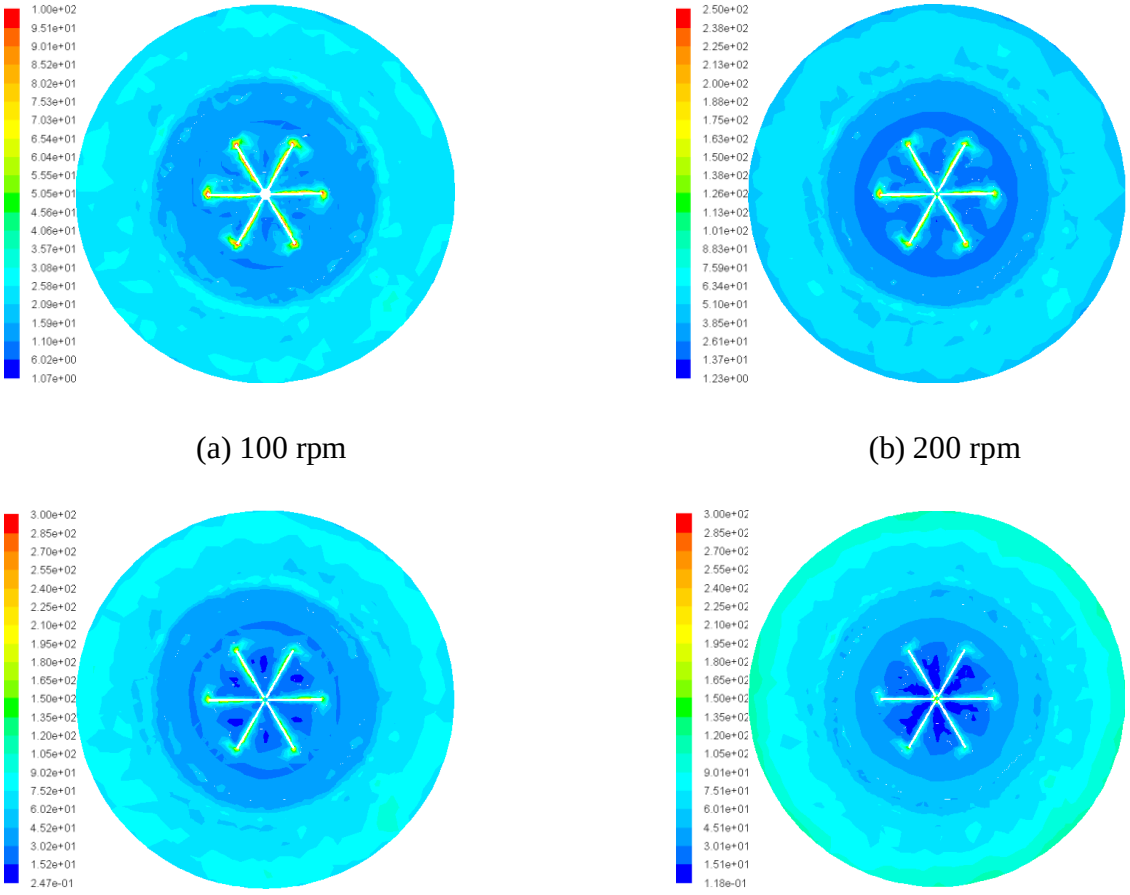

(a) 100 rpm

(b) 200 rpm

(c) 300 rpm

(d) 400 rpm

Figure 6.10: Contour plots of vortices near paddle impeller mounted at clearance of 1/3D

The air-water interface in continuous unbaffeled stirred vessel is also shown in Fig.6.11. It represents the effect of inlet flow on the air-water interface. The diameter of inlet and outlet pipe is taken as 0.01m. The inlet pipe is mounted at height of 0.22m above the bottom surface of the CSTR, and outlet pipe is taken near the bottom of the vessel. The CSTR is simulated till steady state with inlet and outlet flow equal to zero. It is the time equal to zero. The vortex is formed at steady state, and then inlet flow rate with 0.5 m/s velocity starts to flow. Fig 6.11 (b) and (c) show the effect of inlet flow on interface at time 5 sec and 10 sec after the water starts to flow continuously in the vessel. The smooth shape of interface is interrupted by inlet flow. At 10 sec the interface is completely destroyed and the water level is observed to increase with time.

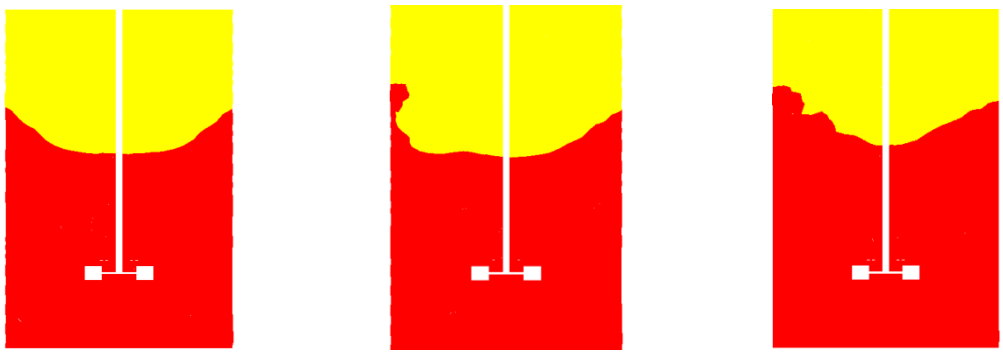

(a) At 0 sec (b) at 5 sec (c) at10 sec

Figure 6.11: Effect of inlet flow on air-water interface in continuous stirred vessel

The air-water interface study is also carried out for baffled stirred vessel. The simulation is carried out using the same strategy as in case of unbaffled stirred vessel. Fig. 6.12 shows the comparison between air-water interfaces (in terms of water phase fraction) formed in stirred vessel in absence and presence of baffles with sitter rotating at 100 rpm. Fig. 6.13 shows the iso-surface of interface in both stirred vessel. The interface formed in unbaffled vessel is smooth and uniformed in nature. While the interface formed in baffled vessel showed the little deep level of interface behind each baffle (Fig. 6.13c). This might be due to the formation of secondary circulation behind the baffles. The simulation for higher rotating speed of stirrer in baffled vessel has also carried out but it showed physically unrealistic results.

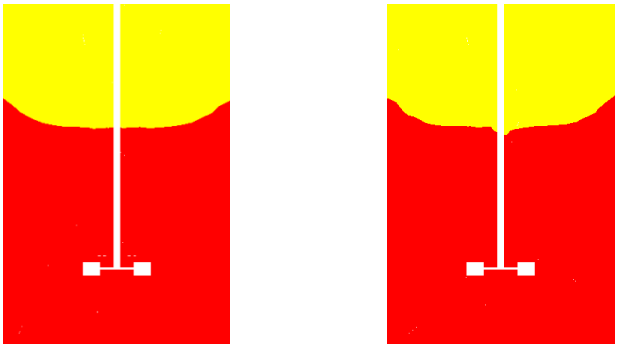

(a) Unbaffled vessel (b) Baffled vessel

Figure 6.12: Comparison of air-water interface in unbaffled and baffled stirred vessel

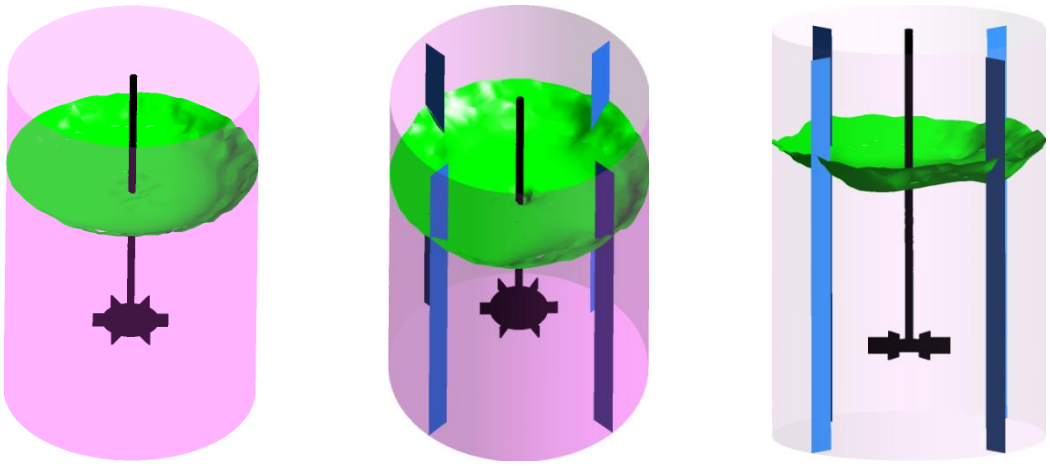

(a) C

Figure 6.13: Iso-surface comparison of interface in (a) unbaffled vessel, (b) baffled stirred vessel and (c) baffled vessel showing deep level of interface behind baffle

6.5 CONCLUSIONS

The simulation of stirred vessel with air-water multiphase system was done. The air-water interface was captured using Volume of Fluid (VOF) method. The simulation results was found able to capture the interface in unbaffeled vessel, but in baffled case with high rotating speed it showed unrealistic results As the rotation speed of stirrer increased, the level of air-water interface moved towards the stirrer. For stirrer speed of 400 rpm, the air-water interface level has reached well below the stirrer and air was entrained into the stirrer region. In CSTR, the air-water interface was disturbed by the inflow and level of water was also increased with time.

Chapter 7

CONCLUSIONS AND FUTURE SCOPE

In this chapter the salient accomplishments and major conclusions of this work are summarized and recommendations for the future are made.

7.1 CONCLUSIONS

In this work the mixing and hydrodynamic behaviour of CSTR was studied. The CFD model equations were solved by ANSYS Fluent 12.0 software. The effect of tank Reynolds number and impeller rpm on the mixing efficiency was found. The effect of impeller rpm on vortex height was carried out.

Based on the analysis of the residence time distribution (RTD) of CSTR with swept volume method, the following conclusions can be drawn

- Computed internal age distributions were found in good agreement with the experimental data.
- The laminar flow MRF model could capture the initial transient variation of *Q*, which latter becomes constant.
- The mixing efficiency was found to be dependent on the RPM of the impeller, tank Reynolds number, Viscosity and density of the liquid.
- The mixing behaviour was changed from dispersion to ideal mixing state as rpm of the impeller and tank Reynolds number increases.
- The increase of viscosity had helped to approach ideal mixing condition at higher rpm of the impeller, but at lower value of it the flow changes to dispersion state.
- The velocity vectors had confirmed the formation four loops at higher *Re* and the phenomena also were found to depend on tank diameter.
- The power number and flow numbers were found to be dependent on impeller Reynolds number, tank diameter and viscosity of CSTR liquid.
- The velocity profiles were found to be a function of tank Reynolds number and impeller rotational speed.
- At higher rpm of the impeller, more symmetrical velocity profiles were observed.

- The six blades of the impeller had produced six vortex loops which rotate with the impeller.
- The velocity vectors, vorticity had successfully represented the hydrodynamics behaviour of the CSTR.
- The rotation of the impeller had become responsible for the formation of low pressure and high pressure zones

Based on the analysis of RTD study of CSTR using tracer injection method, the following conclusions can be made

- The simulated internal age distribution function was found in excellent agreement with the experimental data.
- The internal age distribution function was found to vary with tank Reynolds number and impeller speed.
- As tank Reynolds number and impeller rpm increased the mixing behaviour were changed from dispersion to ideal mixing state.
- The tracer, KCl was found to move along the fluid flow path.
- The distribution of KCl mass fraction was found to be dependent on the tank Reynolds number and impeller rpm.
- The rotation of the impeller was responsible for the formation of low pressure and high pressure zones.
- The velocity vectors, vorticity and pressure contours had represented successfully the hydrodynamic behaviour of the CSTR.
- The vorticity contours around the impeller showed the formation of six vortex loops which move with the impeller.
- In case of CSTR without stirrer, the maximum velocity was found nearer to the wall of the CSTR.
- Viscosity and density of the liquid had played a crucial in mixing process.
- The variance and mean time were found equal at high tank Reynolds number and impeller rpm, and the equality shows the ideal mixing condition.
- The number of ideal CSTR in series approached 1.0 with increase in tank Reynolds number and impeller rpm.

- The behaviour of mixing of liquid in the CSTR also was studied successfully with the help of holdback calculation.
- The segregation was found out of theoretical range at higher rpm of the impeller.

Based on the analysis of the study of vortex formation inside a stirred tank, the following conclusions can be made

- The simulation of vortex formation using ANSYS Fluent 12.0 was successfully carried out.
- The Fluent's Volume of Fluid (VOF) method was used for predicting the vortex formation for both baffled and unbaffeled stirred tanks.
- The vortex height was compared with the theoretically calculated values. The present computed results were two times of theoretical values.
- The vortex in the continuous reactor was varied with time.

7.2 FUTURE SCOPE OF THE WORK

- Study of the mixing behaviour of CSTR both experimentally and theoretically with gas-liquid interface
- Improvement on the modeling and simulation study of vortex formation in a stirred tank reactor.

REFERENCES

Adeosun, J.T. and Lawal, A., 2010, "Residence-time distribution as a measure of mixing in T-junction and multilaminated/elongational flow micromixers", Chemical Engineering Science, Vol. 65, pp. 1865 – 1874.

Alcamo, R., Micale, G., Grisafi, F., Brucato, A. and Ciofalo, M., 2005, "Large-eddy simulation of turbulent flow in an unbaffled stirred tank driven by a Rushton turbine", Chemical Engineering Science, Vol. 60, pp. 2303–2316.

Anderson, J.D. Jr., 1995, "Computational fluid dynamics: The basics with applications", McGraw-Hill International Editions, New York.

ANSYS, 2009, "ANSYS FLUENT 12.0 theory guide", ANSYS, Inc.

Arratia, P.E., Lacombe, J.P., Shinbrot, T. and Muzzio, F.J., 2004, "Segregated regions in continuous laminar stirred tank reactors", Chemical Engineering Science, Vol. 59, pp. 1481 – 1490.

Aubin, J., Mavros, P., Fletcher, D.F., Bertrand, J. and Xuereb, C., 2006, "Alternative operating methods for improving the performance continuous stirred tank reactors", Chem Eng Des., Vol. 79, No. A, pp. 845-856.

Brucato, A., Ciofalo, M., Grisafi, F. and Micale, G., 1994, "Complete numerical solution of flow fields in baffled stirred vessels: The inner–outer approach", Proceedings of 8th European Conference on Mixing, pp. 155–162.

Bruce, A.E.R., Sai, P.S.T. and Krishnaiah, K., 2004, "Characterization of liquid phase mixing in turbulent bed contactor through RTD studies", Chemical Engineering Journal, Vol. 104, pp. 19 – 26.

Buffham, B.A., 1983, "Internal and external residence-time distributions", Chemical Engineering Communications, Vol.22, pp.105-107.

Buffham, B.A., and. Nauman, E.B, 1984, "Residence-time distributions at higher cycle ratios limiting forms obtained by increasing the recycle and by reducing-the throughput", Chemical Engineering Science, Vol. 39, No. 5, pp. 841 – 849.

Burghardt, A., Lipowska, L., 1972, ‘‘Mixing phenomena in a continuous flow stirred tank reactor’’, Chemical Engineering Science, Vol. 27, 1783-1795.

Cao, Y., Li, P., Zhou, J., Sui, Z. and Zhou, X., 2011, “Pressure drop and residence time distribution in carbon-nanofiber/graphite-felt composite for single liquid-phase flow”, Industrial & Engineering Chemistry Research, Vol. 50, pp. 9431 – 9436.

Ciofalo, M., Brucato, A., Grisafi, F. and Torraca, N., 1996, “Turbulent flow in closed and free-surface unbaffled tanks stirred by radial impeller”, Chemical Engineering Science, Vol. 51, pp. 3557–3573.

Cozewith, C. and Squire, K.R., 2000, “Effect of reactor residence time distribution on polymer functionalization reactions”, Chemical Engineering Science, Vol. 55, pp. 2019 – 2029.

Danckwerts, P.V., 1953, “Continuous flow systems: Distribution of residence times,” Vol.2, No.1, pp. 1-13.

Danckwerts, P.V., 1958, “The Effect of Incomplete Mixing on Homogeneous Reactions”, Chemical Engineering Science, Vol. 8, pp.93-102.

Date, A.W., 2005, “Introduction to computational fluid dynamics”, Cambridge University Press, New York.

Dittrich, C. J., and Mutsersb, S. M. P., 2007, “On the residence time distribution in reactors with non-uniform velocity profiles: The horizontal stirred bed reactor for polypropylene production”, Chemical Engineering Science, Vol. 62, pp. 5777 – 5793.

Dong, L., Johansen, S.T. and Engh, T.A., 1994, “Flow induced by an impeller in an unbaffled tank—II. Numerical modelling,” Chemical Engineering Science, Vol. 49, pp. 3511–3518.

Dudukovic, M.P., 2010, “Reaction engineering: Status and future challenges”, Chemical Engineering Science, Vol. 65, pp.3-11.

Fan, L., Xu, N., Wang, Z., and Shi, H., 2010, "PDA experiments and CFD simulation of a lab scale oxidation ditch with surface aerators", Chemical Engineering Research and Design, Vol. 88, pp. 23-33

Fernandez-Sempere, J., Font-Montesinos, R. and Espejo-Alcaraz, O., 1995, "Residence time distribution for unsteady-statesystems", Chemical Engineering Science, Vol. 50, No. 2, pp. 223 – 230.

Fogler, H. S., 1999, "Elements of Chemical Reaction Engineering", 3rd Ed., Pearson Education, Inc.

Haque, J.N., Mahmud, T., Roberts, K.J. and Rhodes, D., 2006, "Modeling turbulent flows with free-surface in unbaffled agitated vessels," Industrial and Engineering Chemistry Research, Vol. 45, pp. 2881–2891.

Harned, .H.S., and. Nuttall, R.L., 1949, "The Diffusion Coefficient of Potassium Chloride in Aqueous Solution at 25°C", Molecular Interaction, Vol. 51, pp. 781–788.

Harvey, P.S. and Greaves, M.G., 1982, "Turbulent flow in an agitated vessel Part-I: A predictive model," Chemical Engineering Research Design, Vol. 60, pp. 195–200.

Hocine, S., Pibouleau, L., Azzaro-Pantel, C. and Domenech, S., 2008, "Modelling Systems Defined by RTD Curves", Computers & Chemical Engineering, Vol. 32, pp. 3112-3120.

Javed, K.H., Mahmud, T. and Zhu, J.M., 2006, "Numerical simulation of turbulent batch mixing in a vessel agitated by a Rushton turbine", Chemical Engineering Processes, Vol. 45, pp. 99–112.

Kolhapure, N.H., Tilton, J.N. and Pereira, C.J., 2004, "Integration of CFD and condensation polymerization chemistry for acommercial multi-jet tubular reactor", Chemical Engineering Science, Vol. 59, pp. 5177 – 5184.

Kreft, A. and Zuber, A., 1978, "On the physical meaning of the dispersion equation and its solutions for different initial boundary conditions", Chemical Engineering Science, Vol. 33, pp. 1471 – 1480.

Kumar, A., Ganjyal, G.M., Jones, D.D. and Hanna, M.A., 2008, "Modeling residence time distribution in a twin-screw extruder as a series of ideal steady-state flow reactors", Journal of Food Engineering, Vol.84, pp. 441–448.

Kumaresan, T. and Joshi, J.B., 2006, "Effect of impeller design on the flow pattern and mixingin stirred tanks", Chemical Engineering Journal, Vol. 115, No. 3, pp. 173-193.

Kuncewicz, C.Z., 1997, "Modelling of liquid flow in a mixer in the laminar flow", PhD Thesis, pp.766

Lamarque, N., Zoppe, B., Lebaigue, O., Dolias, Y., Bertrand, M. and Ducros, F., 2010, "Large-eddy simulation of the turbulent free-surface flow in an unbaffled stirred tank reactor", Chemical Enginnering Science, Vol. 65, pp. 4307 - 4322.

Le Lan, A. and Angelino, H., 1972, "Etude du vortex dans les cuvesagitées", Chemical Engineering Science, Vol. 27, pp. 1969-1978.

Lee, K.C., Ng, K. and Yianneskis, M., 1996, "Sliding mesh predictions of the flows around Rushton impellers," IChemE. Symposium Series, Vol.140, pp. 1–12.

Levenspiel, O. and Smith, W. A., 1957, "Notes on the diffusion-type model for the longitudinal mixing of inflow", Chemical Engineering Science, Vol. 6, pp. 227 – 233.

Levenspiel, O. and Turner, J.C.R. , 1970, "The interpretation of residence-time experiments", Chemical Engineering Science, Vol. 25, pp. 1605 - 1609.

Levenspiel, O., 1999, "Chemical Reaction Engineering", 3rd Ed., John Wiley & Sons, Inc.

Levenspiel, O., La1, B.W. and Chatlynne, C.Y., 1970, "Tracer curves and the residence time distribution", Chemical Engineering Science, Vol. 25, pp. 1611-1613.

Lintz, H.G. and Weber, W., 1980, "The study of mixing in a continuous stirred tank reactor using an autocatalytic reaction", Chemical Engineering Science, Vol. 35, pp. 203-208.

Lipowska, L., 1974, “The influence of geometric parameters on the ideal mixing range of liquid in a continuous flow stirred tank reactor”, Chemical Engineering Science, Vol. 29, pp. 1901 – 1908.

Luo, J.Y., Gosman, A.D., Issa, R.I., Middleton, J.C. and Fitzgerald, M.K., 1993, “Full flow field computation of mixing in baffled stirred vessels,” Chemical Engineering Research Design, Vol. 71, pp. 342–344.

Madhuranthakam, C.M.R., Pan, Q. and Rempel, G.L., 2009, “Residence time distribution and liquid hold up in Kenics KMX static mixer with hydrogenated nitrile butadiene rubber solution and hydrogen gas system”, Chemical Engineering Science, Vol. 64, pp. 3320 – 3328.

Martin, A. D., 2000, “Interpretation of residence time distribution data”, Chemical Engineering Science, Vol. 55, pp. 5907-5917.

Middleton, J.C., Peirce, F. and Lynch, P.M., 1986, “Computation of flow fields and complex reaction yield in turbulent stirred reactors and comparison with experimental data,” Chemical Engineering Research Design, Vol. 64, pp. 18–22.

Mishra, V.P., Dyster, K.N., Jaworski, Z., Nienow, A.W. and Mckemmie, J., 1998, “A Study of an up and a down-pumping wide blade hydrofoil impeller: Part I. LAD measurements”, Canadian Journal of Chemical Engineering, Vol. 76, No. 3, pp. 577-588.

Montante, G., Lee, K.C., Brucato, A. and Yianneskis, M., 1999, “Double to single loop flow pattern transition in stirred vessels,” Canadian Journal of Chemical Engineering, Vol. 77, pp. 649-659.

Murthy, B.N., Ghadge, R.S., and Joshi, J.B., 2007, “CFD simulations of gas-liquid-solid stirred reactor: Prediction of critical impeller speed for solid suspension”, Chemical Engineering Science, Vol. 62, pp. 7184 - 7915.

Nagata, S., 1975, “Mixing Principles and Applications”, Wiley, New York.

Nauman, E. B. and Collinge, C. N., 1968, “The theory of contact time distributions in gas fluidized beds”, Chemical Engineering Science, Vol. 23, pp. 1309 – 1316.

Nemade, P.D., Dutta, S.M. and Shankar, H.S., 2009, "Residence time distribution and oxygen transfer in a novel constructed soil filter", Journal of Chemical Technology and Biotechnology, Vol. 85, pp. 77 – 84.

Ochieng, A. and Onyango, M.S., 2008, "Mixing in a tank stirred by a Rushton turbine at a low clearance," Chemical Engineering and Processing, Vol. 47, pp. 842-851.

Osorio-Revilla, G., Gallardo-Velazquez, T., Ramırez-Torres, A. and Rivera-Espinoza, Y., 2011, "Residence time distribution in spouted bed drying of Maltodextrin solutions on a bed of inert particles", The Canadian Journal of Chemical Engineering, Vol. 9999, 2011.

Patel, H., Ein-Mozaffari, F. and Dhib, R., 2010, "CFD analysis of mixing in thermal polymerization of styrene", Computers and Chemical Engineering, Vol. 34, pp. 421 – 429.

Patwardhan, A.W. and Joshi, J.B., 1999, "Relation between flow pattern and blending in stirred tanks", Industrial Engineering Chemistry Research, Vol. 38, No. 8, pp. 3131-3143.

Plasari, E., David, R. and Villermaux, J., 1977, "Phenomena in residence time distributions of mechanically and jet-stirred reactors in the liquid phase", Chemical Engineering Science, Vol. 32, pp.1121 – 1124.

Popovic, M. Papalexiou, A. And Reuss, M., 1983, "Gas residence time distribution in stirredtank bioreactors", Chemical Engineering Science, Vol. 12, pp. 2015 – 2025.

Raghuraman, J. and Varma, Y.B.G., 1973, "Model for residence time distribution in multistage systems with cross-flow between active and dead regions", Chemical Engineering Science, Vol. 28, pp. 585 – 591.

Ranade, V.V., 2002, "Computational flow modelling for chemical reactor engineering", Academic Press, Vol. 5, California.

Ranade, V.V. and Joshi, J.B., 1990, "Flow Generated by a Disc Turbine: Part II Mathematical Modelling and Comparison with Experimental Data," Chemical Engineering Research Design, Vol. 68A, pp. 34–43.

Ranade, V.V., Perrard, M., Xuereb, C., Le Sauze, N. and Bertrand, J., 2001, "Trailing vortices of Rushton turbine: PIV measurements and CFD simulations with snapshot approach," Chemical Engineering Research Design, Vol. 79 (1), pp. 3 – 12.

Rieger, F., Ditl, P. and Novak, V., 1979, "Vortex depth in mixed unbaffled vessels", Chemical Engineering Science, Vol.34, pp. 397 - 403.

Rigby, G.D., Evans, G.M. and Jameson, G.J., 1997, "Bubble breakup from ventilated cavities in multiphase reactor," Chemical Engineering Science, Vol. 52, pp. 3677–3684.

Robinson, B.A. and Tester, J.W., 1986, "Characterization of flow maldistribution using inlet-outlet tracer techniques: an application of internal residence time distributions", Chemical Engineering Science, Vol. 41, No. 3, pp. 469 – 483.

Rushton, J.H., Costich, E.W. and Everett, H.J., 1950a, "Power characteristics of mixing impellers: Part I", Chemical Engineering Progress, Vol. 46(8), pp. 395 – 404.

Rushton, J.H., Costich, E.W. and Everett, H.J., 1950b, "Power characteristics of mixing impellers: Part II", Chemical Engineering Progress, Vol. 46(9), pp. 467 – 476.

Sahle-Demessie, E., Bekele, S. and Pillai, U.R., 2003, "Residence time distribution of fluids in stirred annular photoreactor", Catalysis Today, Vol. 88, pp. 61–72.

Saravanathamizhan, R., Paranthamana, R., Balasubramaniana, N., Ahmed Bashab, C., 2008, "Residence time distribution in continuous stirred tank electrochemical reactor", Chemical Engineering Journal, Vol. 142, pp. 209–216.

Scargiali, F., Grisafi, F., Cermakova, J., Machon, V. and Brucato, A., 2004, "Residence time distribution of solid particles in a continuous, high-aspect-ratio

multiple-impeller stirred vessel", Chemical Engineering Science, Vol. 59, pp. 3601 – 3618.

Serra, A., Campolo, M. and Soldati, A., 2001, "Time dependent finite-volume simulation of the turbulent flow in a free-surface CSTR," Chemical Engineering Science, Vol. 56, pp. 2715–2720.

Tabor, A., Gosman, A.D. and Issa, R.A., 1998, "Numerical simulation of the flow in a mixing vessel stirred by a Rushton turbine," IChemE Symposium Series, Vol. 140, pp. 25 – 34.

Tannehill, J.C., Anderson, D.A. and Pletcher, R. H., 1997, "Computational fluid dynamics and heat transfer", Taylor & Francis, Levittown.

Thijert, M.P.G., Oyevaar, M.H., Kuper, W.J. and Westcrterp, K.R., 1992, "Residence time distribution of the gas phase in a mechanically agitated gas-liquid reactor", Chemical Engineering Science, Vol.47, No. 13/14, pp. 3339 – 3346.

Torré, J., Fletcher, D.F., Lasuye, T. and Xuereb, C., 2007, "Transient hydrodynamics and free surface capture of an under-baffled stirred tank during stopping Bully Les Mines, France", Chemical Engineering Research and Design, Vol.85, pp.626-636.

Torré, J., Fletcher, D.F., Lasuye, T. and Xuereb, C., 2007, "Single and multiphase CFD approaches for modelling partial baffled stirred vessels: Comparison of experimental data with numerical predictions", Chemical Engineering science, Vol. 62, pp. 6246-6262.

Trivedi, R.N. and Vasudeva, K. 1974, "RTD for diffusion free laminar flow in helical coils", Chemical Engineering Science, Vol. 29, pp. 2291-2295.

Turner, J.C.R., 1982, "Perspectives in residence-time distributions", Chemical Engineering Science, Vol. 38(1), pp. 1-4.

Van de Vusse, J.G., 1962, "A new model for the stirred tank reactor", Chemical Engineering Science, Vol. 17, pp. 507 – 521.

Van De Vusse., J.G., 1955, “Mixing by agitation of miscible liquids, Parts I. and II”, PhD Thesis TU Delft 1953, S. 44, in Chemical Engineering Science, Vol. 4, pp. 178-200 and 209 - 220.

van der Lans, R. P., Glarborg, P., Dam-Johansen, K. and Larsen, P. S., 1997, “Residence time distributions in a cold, confined swirl flow: Implications for chemical engineering combustion modeling”, Chemical Engineering Science, Vol. 52, No. 16, pp. 2743 – 2756.

Venneker, B. C. H., Derksen, J. J. and Van den Akker, H. E. A., 2010, “Turbulent flow of shear-thinning liquids in stirred tanks—The effects of Reynolds number and flow index”, Chemical Engineering Research and Design, Vol. 88, pp. 827 – 843.

Venneker, B.C.H. and van den Akker, H.E.A., 1997, “CFD Calculations of the Turbulent Flow of Shear-Thinning Fluids in Agitated Tanks”, Proceedings of 9th Euro. Conference on Mixing, Vol. 11, pp.179–186.

Viollet, P.L., and Simonin,O., 1994, “ Modelling dispersed two phase flows: closure, validation and software development”, Applied Mechanical Reviews, Vol. 47, No. 6, pp. S80-S84.

Wilcox, D. C., 1993, “Turbulence modelling for CFD”, DCW Industries, Inc., California.

Wolf, D. and Manning, F. S. 1966, “Impact tube measurement of flow patterns, velocity profiles and pumping capacities in mixing vessels”, The Canadian Journal of Chemical Engineering, June, pp. 137 – 142.

Xiao-chang, C., Ting-an, Z. and Qiu-yue, Z. 2009, “Computational simulation of fluid dynamics in a tubular stirred reactor”, Transactions of Nonferrous Metals Society of China, Vol. 19, pp. 489 – 495.

Yablonskya, G.S.,Constalesb, D. and Marinc, G.B., 2009, “A new approach to diagnostics of ideal and non-ideal flow patterns: I. The concept of reactive-mixing index (REMI) analysis”, Chemical Engineering Science, Vol. 64, pp. 4875 – 4883.

Zheng, W., Zaisha, M.,Chao,Y. and Xiangqian, S., 2006, "Computational fluid dynamcis approach to the effect of mixing and draft tube on the precipitation of Barium Sulfate in a continuous stirred tank", Chinese J. Chem Eng., Vol. 4 No.6, pp. 713-722.

Zlokarnik, M., 1971, "Trombentiefebeimrühren in unbewehrtenbehältern", ChemieIngenieurTechnik, Vol. 43, pp.1028 - 1030.

Zlokarnik, M., 2001, "Stirring theory and practice", Wiley-VCH.

Zwettering, T. N., 1959, "The degree of mixing in continuous flow system", Chemical Engineering Science, Vol. 11, No. 1.